1986

Diffusion-deposition of particles from a continuous line source into a disturbed atmospheric boundary layer

Chin-Shun Lin
Iowa State University

INFORMATION TO USERS

This reproduction was made from a copy of a manuscript sent to us for publication and microfilming. While the most advanced technology has been used to photograph and reproduce this manuscript, the quality of the reproduction is heavily dependent upon the quality of the material submitted. Pages in any manuscript may have indistinct print. In all cases the best available copy has been filmed.

The following explanation of techniques is provided to help clarify notations which may appear on this reproduction.

1. Manuscripts may not always be complete. When it is not possible to obtain missing pages, a note appears to indicate this.

2. When copyrighted materials are removed from the manuscript, a note appears to indicate this.

3. Oversize materials (maps, drawings, and charts) are photographed by sectioning the original, beginning at the upper left hand corner and continuing from left to right in equal sections with small overlaps. Each oversize page is also filmed as one exposure and is available, for an additional charge, as a standard 35mm slide or in black and white paper format.*

4. Most photographs reproduce acceptably on positive microfilm or microfiche but lack clarity on xerographic copies made from the microfilm. For an additional charge, all photographs are available in black and white standard 35mm slide format.*

*For more information about black and white slides or enlarged paper reproductions, please contact the Dissertations Customer Services Department.

U·M·I Dissertation Information Service

University Microfilms International
A Bell & Howell Information Company
300 N. Zeeb Road, Ann Arbor, Michigan 48106

Lin, Chin-Shun

DIFFUSION-DEPOSITION OF PARTICLES FROM A CONTINUOUS LINE SOURCE INTO A DISTURBED ATMOSPHERIC BOUNDARY LAYER

Iowa State University PH.D. 1986

PLEASE NOTE:

In all cases this material has been filmed in the best possible way from the available copy. Problems encountered with this document have been identified here with a check mark ✓.

1. Glossy photographs or pages _____
2. Colored illustrations, paper or print _____
3. Photographs with dark background _____
4. Illustrations are poor copy _____
5. Pages with black marks, not original copy _____
6. Print shows through as there is text on both sides of page _____
7. Indistinct, broken or small print on several pages ✓
8. Print exceeds margin requirements _____
9. Tightly bound copy with print lost in spine _____
10. Computer printout pages with indistinct print _____
11. Page(s) _____ lacking when material received, and not available from school or author.
12. Page(s) _____ seem to be missing in numbering only as text follows.
13. Two pages numbered _____. Text follows.
14. Curling and wrinkled pages _____
15. Dissertation contains pages with print at a slant, filmed as received _____
16. Other _____

_____

_____

University
Microfilms
International

Diffusion-deposition of particles from a continuous line source into a disturbed atmospheric boundary layer

by

Chin-Shun Lin

A Dissertation Submitted to the
Graduate Faculty in Partial Fulfillment of the
Requirements for the Degree of
DOCTOR OF PHILOSOPHY

Major: Aerospace Engineering

Approved:

Signature was redacted for privacy.

In Charge of Major Work

Signature was redacted for privacy.

For the Major Department

Signature was redacted for privacy.

For the Graduate College

Iowa State University
Ames, Iowa

1986

TABLE OF CONTENTS

LIST OF TABLES

LIST OF FIGURES

CHAPTER 1. INTRODUCTION

The wind transport of fine particular matter is of fundamental importance in a broad range of disciplines. Examples include the movement of dust and pollutants in atmospheric flows and various industrial processes such as the piping of suspensions. Due to the fact that air pollution can endanger human health by harming the respiratory system and can create safety hazards by causing visibility reductions, there has been considerable interest in the past decade in the predictions of turbulent particulate diffusion and deposition.

The terminal settling velocity of small particles increases with the diameter. Thus, for sufficiently small particles, the terminal settling velocity is less than the average vertical component of turbulent fluctuation speed, and the turbulent eddies will greatly affect the motion of the particles in the air stream. This phenomenon is called particle diffusion. When the air stream containing such small suspended particles moves past a surface at any inclination to the vertical, deposition may occur on the surface. This removal of particulate material from the flowing turbulent streams to an adjacent surface can occur by several natural processes. Two important removal mechanisms are (1) the dry deposition of the pollutants on the surface, by gravitational settling, eddy impaction,

chemical absorption and other effects, and (2) the chemical transformation in the atmosphere. Only the dry-deposition effect is considered in this study.

Few detailed studies have been reported which aim to investigate diffusion-deposition in real and simulated atmospheric flows over a level surface containing a topographic obstruction. Field and wind tunnel experiments of particle diffusion and deposition are difficult to perform with accuracy. The works herein reported are numerical investigations which utilize the knowledge gained from experimental and analytical investigations under specified conditions.

The purpose of the present study is to simulate the transport, diffusion, and dry deposition of small particle material emitted from an idealized continuous line source into the atmosphere over various complex terrains such as a forward-facing step, a backward-facing step, and a rectangular block. In formulating a mathematical model to describe this complicated flow situation, the complete two-dimensional equations of motion for turbulent flow must be considered. Numerical models use mathematical techniques (with some degree of approximations and necessary assumptions) to predict the actual physical processes governing the disturbed atmospheric flow dynamics and particulate transport.

This research is organized around two components: (1) a description of the atmospheric flow pattern near the obstructions and (2) an estimation of the pollutant concentration and deposition generated by these patterns. The flow section provides means for qualitative and quantitative estimates of the frontal eddy size, the recirculating roof and wake cavities, and the behavior of the far wake. The concentration calculations and the particle deposition are estimated due to line sources located upwind of the obstruction.

In the presence of the varied surface topography of the earth, the atmospheric wind near the surface is practically always fully turbulent. For the purpose of this study, we assume neutral stability in the atmosphere. Therefore, the upstream conditions are purposely selected to simulate a neutrally stable, fully rough turbulent atmospheric boundary layer.

The steady-state Navier-Stokes equations are employed in the vorticity-stream function (ω-ψ) formulation. The k-ε two-equation turbulence model, consisting of transport equations for the mean turbulent kinetic energy (k) and its isotropic dissipation rate (ε), is used for the closure of the conservation equations. Gosman's upwind finite-difference scheme (Gosman et al., 1969), which is developed by using an integral method, is modified as a time-marching

approach and hence used to solve the four coupled non-linear transport equations ($\psi,\omega,k,\varepsilon$). From the ψ distribution, we can find the velocity field and hence solve the diffusion problems.

The steady-state advection-diffusion equation is solved by using an implicit Crank-Nicolson difference scheme. However, in order to solve the finite-difference equation iteratively, we also modify the Crank-Nicolson scheme to be the Gauss-Seidel with Successive-Over-Relaxation (S.O.R.) method (Liu and Karaki, 1972).

Comparisons and analyses are performed based on these numerical predictions of the flow fields and the particulate diffusion and deposition. The result is a better understanding of the physical effects of the atmospheric motion and the fine particles suspended and carried by the atmospheric wind over complex terrains.

CHAPTER 2. THE PLANETARY BOUNDARY LAYER

The planetary or atmospheric boundary layer is that region of the atmospheric surface layer which is directly affected by the friction between the ground and the atmosphere. The thickness of the atmospheric boundary layer varies with local terrain conditions and is typically of the order of 100 to 1000 m. Above that height, ground effects are no longer important. In the atmospheric boundary layer, air motions are induced by the pressure gradient imposed by large-scale atmospheric pressure fields and by the diurnal heating cycle set up by the solar radiation. The resulting temperature and velocity fields represent the natural conditions of the atmosphere in which most human activities take place.

It has been recognized that the structure of the atmospheric boundary layer is quite similar to that in the turbulent boundary layer along a flat plate. We may consider the atmospheric boundary layer as made up of two parts: (1) the upper sublayer, whose characteristics are dominated by the conditions near the edge of the surface layer and whose mechanics are determined by the interactions of pressure gradient and Coriolis force, and (2) the lower sublayer, whose structure is governed by the momentum flux to the surface which depends on the nature of the ground (Plate, 1971).

Variations in both thermal and mechanical turbulence and in wind velocity are greatest in the layer in contact with the earth surface. Turbulence induced by buoyant forces in the atmosphere is closedly related to the vertical temperature structure and turbulence field (Turner, 1970). When temperature decreases with height at a rate of 1 ^{o}C per 100 meters, the atmosphere is in neutral equilibrium (usually at dawn and dusk transition periods and cloudy windy condition). For a larger negative gradient (super-adiabatic lapse rate), the atmosphere is in unstable equilibrium (usually in the daytime) and the vertical motions are enforced. A positive gradient (inversion) or smaller negative gradient leads to stable equilibrium (usually at night) and the vertical motions are damped or reduced.

The transfer of momentum upward or downward in the atmosphere is also related to stability. With neutral stability, the logarithm of height is observed to be directly proportional to velocity at that height. Conversely, a plot of Log. height (ordinate) against velocity (abscissa) is a curve-convex up for a stable equilibrium and concave up for an unstable condition (upward motions transfer the momentum deficiency).

The Generalized Velocity Profile

It is observed that in the lowest part of the atmospheric layer (up to approximately 30 m), the heat and momentum fluxes can be considered to be independent of the height. The surface layer acts as an interface between the solid ground surface below and the well-mixed layer above, with rapid flow adjustments to the surface conditions. Although theoretical efforts to obtain analytical solutions for the mean wind profile have not been successful, it is possible to use the similarity description to obtain semi-empirical relations.

Numerous investigations of the fluid flow have established the following logarithmic relationship between mean horizontal fluid velocity (U) and height (Z) from the surface

$$\frac{U}{U^*} = \frac{1}{\kappa}\ln\left(\frac{Z}{Z_o}\right) \qquad (2.1)$$

where

$U^* = \sqrt{(\tau/\rho)}$ = friction velocity

τ = surface shear stress

ρ = fluid density

Z_o = surface effective roughness height

κ = Von Karman's constant ≈ 0.40

This relationship holds good in the neutral atmospheric layer adjacent to the surface in which the shear stress is effectively constant.

Deacon (1949) investigated the vertical profiles of mean wind velocity in the lowest atmospheric layer and found that the slope of the wind velocity profile has the form

$$\frac{dU}{dZ} = bZ^{-\beta} \tag{2.2}$$

where

$\beta > 1$ for unstable condition

$\beta = 1$ at neutral stability

$\beta < 1$ for stable condition

He also observed that β ranges from 0.75 to 1.25 for the flow over long grass. The profiles of the potential temperature (θ) have an analogous relationship to Eq. (2.2), i.e.,

$$\frac{d\theta}{dZ} = b'Z^{-\beta'}$$

The constants, b and b', are determined by experiment. The difference of the stability parameters β and β' are observed to be not very significant. Integrating Eq. (2.2) and expanding it in a series form, we can compare that with Eq. (2.1) and find

$$b = \frac{U^*}{\kappa Z_o^{1-\beta}}$$

The velocity profile is then obtained by

$$\frac{U}{U^*} = \frac{1}{\kappa}\ln\left(\frac{Z}{Z_o}\right) \qquad \text{for } \beta = 1 \qquad (2.3a)$$

$$\frac{U}{U^*} = \frac{1}{\kappa(1-\beta)}\left\{\left(\frac{Z}{Z_o}\right)^{1-\beta}-1\right\} \qquad \text{for } \beta \neq 1 \qquad (2.3b)$$

Eq. (2.3b) enables β to be found from the measured wind velocities at two heights as

$$U_2/U_1 = \{(Z_2/Z_o)^{1-\beta}-1\}/\{(Z_1/Z_o)^{1-\beta}-1\}$$

The velocity profile given by Eq. (2.3a) was also approximated by Deacon (1949) by the power law

$$\frac{U}{U^*} = q'\left(\frac{Z}{Z_o}\right)^{\alpha} \qquad (2.4)$$

which is fitted to the wind velocity profile to give agreement with the observed velocities at some small height and at a greater height chosen so that the two levels embrace the greater part of the particle diffusion.

The empirical power law has two significant characteristics that make it very useful: The power law is a simple and good average representation of the velocity profile, and the integral relations based on this easily integrated law are not far from correct. Furthermore, the

power law can give the velocity (U) and the skin friction coefficient (C_f) in explicit terms and can yield explicit relations for the boundary-layer thickness (δ_t) in terms of the Reynolds number (Re) and distance (X). For those reasons, the power law has often been applied to the particulate diffusion problems, such as predicting diffusion characteristics (Calder, 1949) or wind tunnel modeling of wind forces (Davenport, 1965).

Businger et al. (1971) expressed the wind shear and potential temperature gradient, based on the AFCRL (Air Force Cambridge Research Laboratories) Kansas observation, in the dimensionless forms, respectively,

$$\phi_m(\zeta) = (\kappa Z/U^*)(\frac{\partial U}{\partial Z}) \qquad (2.5a)$$

$$\phi_n(\zeta) = (\kappa Z/\theta^*)(\frac{\partial \theta}{\partial Z}) \qquad (2.5b)$$

where ϕ_m and ϕ_n are functions of the dimensionless height ζ defined by $\zeta = Z/L$. The quantity Z/L embodies the effect of stratification. The parameter L, based on Businger (1973), is defined as

$$L = \frac{\theta U^{*2}}{\kappa g \theta^*}$$

where the characteristic potential temperature $\theta^* = -\overline{w'\theta'}/U^*$. w' and θ' are the fluctuations of vertical velocity and potential temperature, respectively. This parameter L is the Monin-Obukhov length. The absolute value

of L may be considered a characteristic height which determines the structure of the surface layer. For a stable atmosphere Z/L > 0, for a neutral atmosphere Z/L ≈ 0, and for an unstable atmosphere Z/L < 0. It is obvious that when L is very large or Z is very small, the atmosphere is in neutral stability condition. We can conclude that the lowest portion of the atmospheric layer is near neutral stability.

Based on the empirical observations, the ϕ_m and ϕ_n functions can be written, respectively, as

$$\phi_m = (1-15\zeta)^{-0.25} \qquad \text{for } \zeta \leq 0$$

$$\phi_m = (1+4.7\zeta) \qquad \text{for } \zeta \geq 0$$

and

$$\phi_n = 0.74(1-9\zeta)^{-0.5} \qquad \text{for } \zeta \leq 0$$

$$\phi_n = 0.74+4.7\zeta \qquad \text{for } \zeta \geq 0$$

Eq. (2.5a) and Eq. (2.5b) may be integrated, respectively, to give the following expressions for the wind and potential temperature profiles (Paulson, 1970):

$$\frac{U}{U^*} = \frac{1}{\kappa}\left(\ln\frac{Z}{Z_o} - \Psi_1\right) \tag{2.6a}$$

and

$$\frac{\theta-\theta_o}{\theta^*} = \frac{0.74}{\kappa}\left(\ln\frac{Z}{Z_o} - \Psi_2\right) \tag{2.6b}$$

where

$$\Psi_1 = \begin{cases} 2\ln(0.5+0.5\phi_m^{-1}) + \ln(0.5+0.5\phi_m^{-2}) \\ \qquad - 2\tan^{-1}(\phi_m^{-1}) + 1.570796 & \text{for } \zeta \le 0 \\ -4.7\zeta & \text{for } \zeta \ge 0 \end{cases}$$

and

$$\Psi_2 = \begin{cases} 2\ln(0.5+0.5\sqrt{(1-9\zeta)}) & \text{for } \zeta \le 0 \\ -6.35\zeta & \text{for } \zeta \ge 0 \end{cases}$$

and θ_o is the potential temperature at the surface. It is noted that the value of κ resulting from the work of Businger et al. (1971) is about 0.35 which is fairly low compared to the value of 0.40 derived from wind tunnel experiments.

The friction velocity (U*) and the characteristic potential temperature (θ*) are determined by an iterative process based on Eq. (2.6a) and Eq. (2.6b), respectively (Kemper et al., 1979):

$$U^* = \frac{\kappa\sqrt{(U_1^2 + V_1^2)}}{\ln(Z_1/Z_o)-\Psi_1}$$

$$\theta^* = \frac{k(\theta_1-\theta_o)}{0.74(\ln(Z_1/Z_o)-\Psi_2)}$$

where Z_1 is the height for the first data point above the ground. U_1 and V_1 are the mean horizontal wind components at height Z_1. θ_1 and θ_o are the mean potential temperatures measured at heights Z_1 and Z_o, respectively. Z_1 is typically chosen to be a few meters above the ground. It is obvious that the height Z_1 is very important in getting a representative stability value. It is noted that for a neutral stability $\zeta = 0$ and hence $\Psi_1 = \Psi_2 = 0$, we have $\phi_m = 1$ and $\phi_n = 0.74$.

Momentum Eddy Diffusivity

With the assumption of constant shear stress in the lowest surface layer, we may use two alternative methods for specifying the vertical eddy viscosities.

One method was proposed by Deacon (1949). With the introduction of the friction velocity $U^* = \sqrt{(\tau/\rho)}$, where the turbulent shear stress $\tau_t = \rho K^m(\partial U/\partial Z)$, we obtain that

$$K^m = \kappa U^* \cdot Z_o \cdot (Z/Z_o)^{\beta}$$

The above equation indicates that the momentum eddy diffusivity is proportional to the height raised to a power β.

The second method was developed by O'Brien (1970). In this model, the K^m profile is made up of three parts.

Within the surface layer K^m is a linear function of height. Above the top of the boundary layer, K^m is assumed constant, and interior values are specified by use of Hermite interpolating polynomials. The complete expression of the K^m profile is

$$K_z^m = \begin{cases} \kappa\, u^*\, Z/\phi_m & \text{for } Z_o \le Z \le Z_b \\ K_i + \dfrac{(Z-Z_i)^2}{(Z_i-Z_b)^2}\{K_b - K_i + (Z - Z_b)\{K_b' + \dfrac{2(K_b-K_i)}{(Z_i-Z_b)}\}\} & \text{for } Z_b < Z < Z_i \\ K_i & \text{for } Z_i \le Z \end{cases}$$

where Z_b is the surface layer thickness, Z_i is the boundary layer thickness and $K_b' = \partial K_z^m/\partial Z$ at $Z = Z_b$. It is found that the maximum value of K^m is appearing at a height of .333 Z_i and is given by

$$(K_z^m)_{max} = 0.148(K_b + Z_i K_b')$$

A typical curve for K^m vs. Z is shown in Figure 1. For temperate latitude, the estimate of Z_i (Plate, 1971) in good agreement with field observations is

$$Z_i = (1/5.4)(U^*/f)$$

where f is the Coriolis parameter. For the surface layer thickness Z_b, Chang (1981) assumed that

$$Z_b = 0.01(U^*/f)$$

Thermal Eddy Diffusivity

From Businger (1973) and Tennekes (1982), the inverse of the turbulent Prandtl number, σ, is defined as the ratio of the thermal eddy diffusivity (K^h) to the momentum eddy diffusivity (K^m):

$$K^h/K^m = \sigma$$

From the definitions of K^m and K^h, we have

$$K^h/K^m = \phi_m/\phi_n$$

We then obtain that $K^h/K^m = 1.35$ for a neutral stability condition. This is larger than usually assumed for neutral condition but is in good agreement with laboratory experiments (Hinze, 1959). A plot of K^h/K^m vs. ζ is shown in Figure 2.

Mass Eddy Diffusivity

The profile of the mass eddy diffusivity (K^p) is more questionable. It is stated that all gases as well as suspended particles will diffuse at the same rate, and the mass eddy diffusivity will probably be numerically equal to

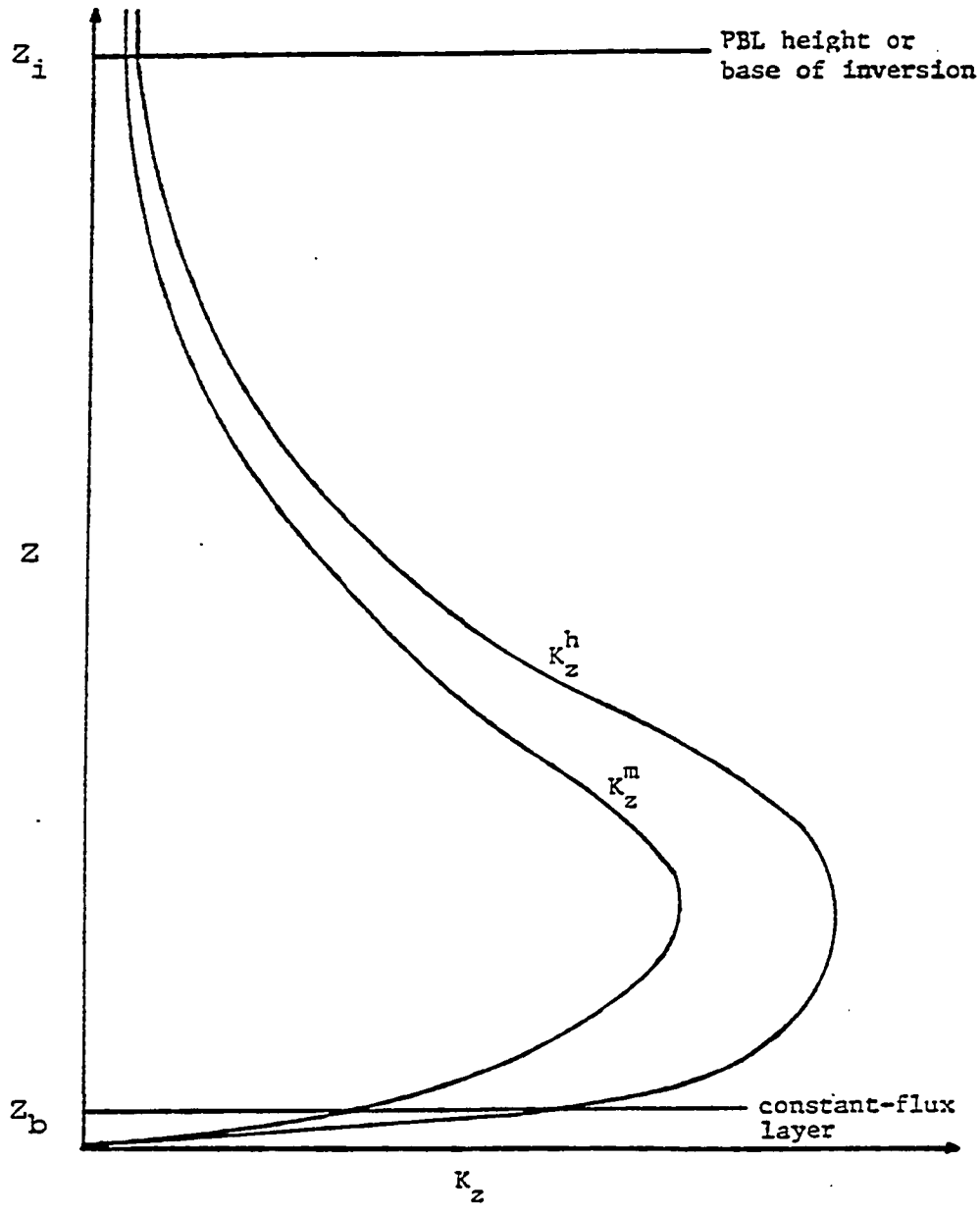

FIGURE 1. The O'Brien profile for the vertical momentum and thermal eddy diffusivities

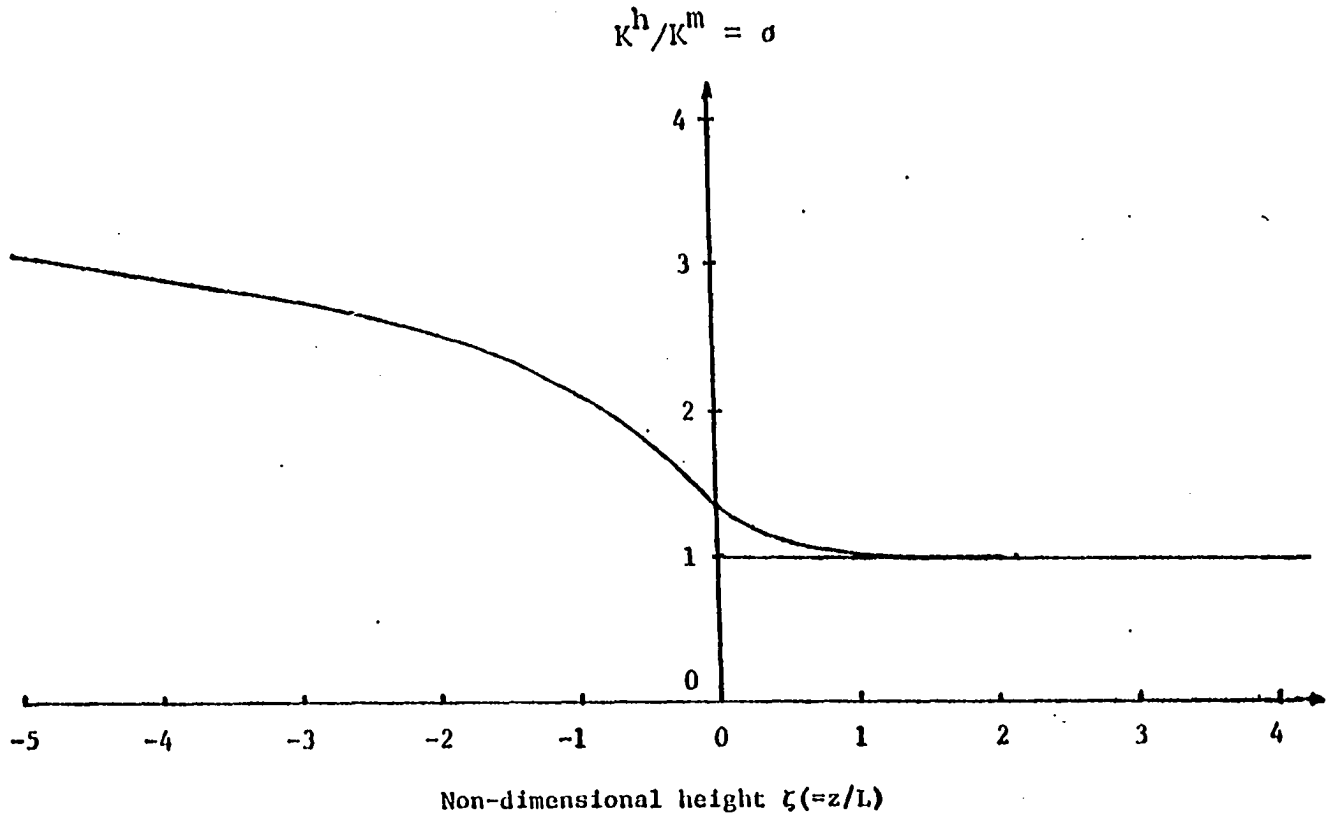

FIGURE 2. A plot of the inverse of the turbulent Prandtl number σ as a function of the non-dimensional height ζ

the momentum eddy diffusity and to the thermal eddy diffusivity (Bosanquet and Pearson, 1936). Many researchers have assumed $K^p = K^m$ in their studies, such as Calder (1949) and Smith (1957). In the present study, however, it will be assumed that the mass eddy diffusivity is equal to the thermal eddy diffusivity, i.e.,

$$K^p = K^h$$

This assumption has been confirmed by the studies of Horst (1979) and Hassid (1983).

CHAPTER 3. THE GRADIENT-TRANSFER DIFFUSION MODEL

The three basic theoretical approaches for investigating atmospheric diffusion problems are the statistical theory, gradient-transfer theory and similarity theory. These approaches are developed to predict the particle diffusion in the atmosphere and can be compared to the wind tunnel data and equivalent field measurements.

The statistical theory of turbulent diffusion, based on the random walk model, was developed by Taylor (1921). This model is normally formulated in a Lagrangian reference frame. With the assumption that the motions of diffused particles have a certain stochastic nature, the history of the motion of an individual particle is described in terms of given statistical properties which are necessary to represent diffusion.

In the gradient-transfer approach, it is assumed that turbulence causes a net movement of material down the gradient of its concentration at a rate which is proportional to the magnitude of the gradient. This approach includes both analytical theory based on the power-law velocity and diffusivity profiles, and numerical prediction which can be based on any form of the velocity and eddy diffusivity profiles. It is noted that the gradient-transfer theory is sometimes called the K-theory and is based on the Eulerian approach.

For the similarity theory, the controlling physical parameters are postulated and laws relating the diffusion to these parameters are then derived on a dimensional basis. It can be shown to be consistent with gradient-transfer theory within the constant stress layer.

We are interested in the numerical investigations, so the gradient-transfer theory will be used as the model for the atmospheric diffusion-deposition.

Advection-Diffusion Equation

Based on the species continuity equation, the three-dimensional atmospheric advection-diffusion equation without any source (or sink) is in the following form:

$$\frac{\partial C}{\partial t} + U\frac{\partial C}{\partial x} + V\frac{\partial C}{\partial y} + (W-W_f)\frac{\partial C}{\partial z} = \frac{\partial}{\partial x}(K_x\frac{\partial C}{\partial x}) + \frac{\partial}{\partial y}(K_y\frac{\partial C}{\partial y}) + \frac{\partial}{\partial z}(K_z\frac{\partial C}{\partial z}) \qquad (3.1)$$

Here, x, y, z are the horizontal downwind, horizontal crosswind and vertical coordinates, respectively; U, V, W are the wind speed in the x, y, and z directions, respectively, and W_f is the gravitational settling velocity taken positive in the negative z-direction. C is the particle concentration at (x, y, z), and K_x, K_y, and K_z are the mass eddy diffusivities in the x, y, z directions, respectively. In Eq. (3.1), several assumptions have been made:

1. The Cartesian coordinate axes coincide with the principal axes of mass eddy diffusivities.
2. The fluid is incompressible.
3. It is a binary mixture system.
4. The wind velocity is the particle velocity.
5. Molecular diffusion is negligible compared with the eddy diffusion.
6. The diffusion process due to the pressure and temperature gradients is neglected and Fick's first law is applied for the mass eddy diffusivities, i.e., $\overline{u'C'}=-K_x(\partial C/\partial x)$, etc.

For the steady-state, two-dimensional flow with the longitudinal diffusion term much smaller than the convective term, Eq. (3.1) becomes

$$U\frac{\partial C}{\partial x} + (W-W_f)\frac{\partial C}{\partial z} = \frac{\partial}{\partial y}(K_y\frac{\partial C}{\partial y}) + \frac{\partial}{\partial z}(K_z\frac{\partial C}{\partial z}) \qquad (3.2)$$

This is the governing equation describing the particle diffusion from a continuous point source located at x = 0, y = 0, z = H. The corresponding initial and boundary conditions are given by

$$C(0,y,z) = Q/U\cdot\delta(y)\cdot\delta(z-H)$$
$$C(x,\pm\infty,z)_{z=0} = 0$$
$$\{K_z(\partial C/\partial z)\}_{z=0} = \{(W_d-W_f)C\}_{z=0}$$
$$C(x,y,\infty) = 0 \qquad (3.3)$$

where Q is the emission rate or the strength of the point source (kg/sec), W_d is the dry deposition velocity (positive in the downward direction), and δ is the Dirac delta function.

It is noted that when deposition occurs, from Eq. (3.3) the turbulent flux at the surface (z=0) is given by

$$K_z \cdot \partial C/\partial z = (W_d - W_f) \cdot C$$

This requires that $W_d > W_f > 0$. If $0 < W_d < W_f$, then re-entrainment of the particles from the surface into the atmosphere occurs. The corresponding continuity condition is given by

$$Q' = \int_{-\infty}^{\infty} \int_{0}^{\infty} U \cdot C \, dzdy$$

$$= Q - \int_{-\infty}^{\infty} \int_{0}^{x} W_d \cdot C \, dxdy$$

where Q' represents the amount of the material remaining in the air and is called the effective source strength, while the last term accounts for deposition.

Terminal Settling Velocity

When a solid particle falls freely in a viscous medium, such as air or water, there is resistance to this movement and its value increases with the velocity. As the equilibrium state is attained among the fluid resistance, gravitational and buoyant forces, the particle reaches its

terminal settling velocity and thereafter falls at a uniform rate. Diffusion and deposition of the particles will be affected if their terminal velocities are large enough to be significant fractions of the turbulent eddy velocity. Consider a spherical particle of diameter D_p and density ρ_p falling under gravity in air of density ρ in an equilibrium state. The particle is acted on by a downward gravitational force ($M_p \cdot g$), an upward buoyant force ($M \cdot g$), and an upward drag force (D). The equation of motion is expressed by

$$M_p \cdot g - M \cdot g - D = 0$$

where M_p is the mass of the particle, M is the displaced air mass, and g is the gravitational acceleration. Since the drag can be expressed by

$$D = \frac{1}{8}\pi\rho W_f^2 D_p^2 C_d$$

the terminal settling velocity is then written as

$$W_f = \{4gD_p(\rho_p-\rho)/(3\rho C_d)\}^{0.5} \qquad (3.4)$$

where C_d is the drag coefficient.

It is noted that the drag coefficient (C_d) is a function of the Reynolds number (Re) which is defined by

$$Re = \rho D_p W_f/\mu$$

where μ is the molecular viscosity of the air. The relation between C_d and Re for different ranges of Re can be found in Appendix A, which has been developed by Morsi and Alexander (1972). The drag coefficient (C_d) is observed to decrease

with increasing particle diameter. We may conclude that the terminal settling velocity increases with particle size.

In general, air density is negligible compared with particle density, Eq. (3.4) then becomes

$$W_f = \{(4gD_p\rho_p)/(3\rho C_d)\}^{0.5}$$

Wills (1981) states that Stokes' law, in which $C_d = 24/Re$, is valid for particle diameter below 50 μm and the terminal settling velocity is calculated by

$$W_f = \{gD_p^2(\rho_p-\rho)\}/18\mu$$

Deposition Velocity

The removal of particulate materials and gases at the air-surface interface is generally described by a so-called dry deposition velocity (W_d). The deposition velocity provides a relationship between the airborne particulate concentration at the surface and the net rate at which the material is deposited.

Only a few researchers (Owen (1960), Sehmel (1980) and Hosker et al. (1982)) have reported the description of physical processes involved, tabular and graphical empirical results, and theoretical relations to estimate the values for W_d. It is observed that the deposition velocity generally depends on the particle density and diameter, surface roughness, vegetation type, and meteorological

conditions (Ermak, 1977).

Based on the description of Sehmel and Hodgson (1976), the dry deposition velocity is given by

$$W_d = \frac{W_f \, \mathrm{Cos}\alpha_s}{1 - \exp\{W_f \, \mathrm{Cos}\alpha_s \, (\mathrm{Int1} + \mathrm{Int2})/U^*\}} \qquad (3.5)$$

where Int1 is a stability dependent empirical resistance integral for deposition heights greater than 1 cm and Int2 is an empirical resistance integral for heights below 1 cm. For more information about Int1 and Int2, one can also refer to Herwehe (1984).

According to Eq. (3.5), it is observed that the dry deposition velocity is a function of the terminal velocity (W_f), slope of the terrain (α_s), friction velocity (U*), deposition height, surface absolute temperature, and particle density and diameter (Herwehe, 1984). It is noted that Eq. (3.5) was originally developed based on a particle density of 1500 kg/m^3. Sehmel and Hodgson (1976) suggest that for particle densities different from 1500 kg/m^3, Int2 will be independent of ρ_p. Also, for deposition height less than the 1 cm reference height, Int1 should be set to zero as recommended in a private communication of Becker (1978) with Sehmel.

Classification of Deposition Phenomena

The deposition phenomenon is much dependent on the relation between terminal settling velocity and deposition velocity. A range of deposition phenomena can be separated into a number of general classes which are useful in relating the model results to actual physical situations (Ermak, 1977).

1. $W_f = W_d = 0$. This trivial case is applicable to very fine particles (generally $D_p < 0.1$ μm), for which gravitational settling and deposition effects are negligible.
2. $W_f = 0$ and $W_d > 0$. This class also applies to very small particles where the gravitational settling is neglected; however, deposition does occur primarily due to non-gravitational effects.
3. $W_d > W_f > 0$. This is for small to medium-sized particles (generally $D_p = 0.1 - 50$ μm). Deposition is enhanced beyond that due to gravitational settling, primarily because of increased turbulent transfer resulting from surface roughness (Rao, 1983).
4. $W_d = W_f > 0$. In this class, deposition is entirely due to gravitational settling. This behavior is typical of the larger particles (generally $D_p > 50$ μm).

5. $W_f > W_d > 0$. In this class, the re-entrainment of the deposited particles from the surface into the atmosphere occurs. It also applies to the larger particles, for example, in a dust storm.

Table 1 (from Becker and Takle, 1979) shows the relationships between the different values of W_f and W_d and the material remaining in the air and deposited at the surface when the time (t) approaches infinity.

TABLE 1. Percentage of material remaining in the air and deposited at the surface in the limit as t approaches infinity

Case	Amount of material remaining in the atmosphere (%)	Amount of material deposited at the surface (%)
$W_d=W_f$:		
$W_d=W_f=0$	100	0
$W_d=W_f\neq 0$	0	100
$W_d\neq W_f$:		
$W_d=0, W_f\neq 0$	100	0
$W_d\neq 0, W_f=0$	0	indeterminate
$W_d\neq 0, W_f\neq 0$	0	100

In order to simplify the analyses, we will assume that $W_f = W_d > 0$ in the numerical investigations of present study.

Analytical Solutions for Point Source

Even in the simplified form of Eq. (3.2), analytical solutions corresponding to the boundary conditions, Eq. (3.3), exist only for few standard functional forms of velocities and eddy diffusivities with the assumption that $W = W_d = W_f = 0$.

Gaussian plume distribution

Based on the idea of reflection of the plume from the ground surface, the Gaussian plume formula is given by

$$C = \frac{Q}{2\pi U\sigma_y\sigma_z}\exp\{\frac{-y^2}{2\sigma_y^2}\}\{\exp\{\frac{-(z-H)^2}{2\sigma_z^2}\} + \exp\{\frac{-(z+H)^2}{2\sigma_z^2}\}\}$$

where σ_y and σ_z are the standard deviations of the plume in y and z directions, respectively, and are functions of downwind distance and the Pasquill-Gifford atmosphere stability classes A-F. σ_y and σ_z here are of the forms

$$\sigma_y^2 = 2K_y x/U$$

$$\sigma_z^2 = 2K_z x/U$$

It is the Fickian diffusion (K_y and K_z are constant) with the horizontal velocity U independent of x and z.

Observations of passive plumes have confirmed that the Gausian form is a satisfactory description for the crosswind

distribution, while for the vertical distribution, it has been found not generally Gaussian.

Roberts' solution

With constant eddy diffusivities and uniform wind velocity, Roberts (1923) obtained a solution for the elevated point source:

$$C = \frac{Q}{4\pi K R_1}\{\exp(-U(R_1-x)/2K)+\exp(-U(R_2-x)/2K)\}$$

where

$$R_1 = \sqrt{\{x^2+y^2+(z-H)^2\}}$$

$$R_2 = \sqrt{\{x^2+y^2+(z+H)^2\}}$$

However, the above solution does not agree well with field and wind tunnel measurements.

Bosanquet and Pearson's solution

Bosanquet and Pearson (1936) assumed a linear variation of K_y and K_z with longitudinal distance and height, respectively, in a uniform wind field. The solution, for the ground point source, is written as

$$C = \frac{Q}{\sqrt{(2\pi)}\ pqUx^2}\exp\{-(z/px)-(y^2/2q^2x^2)\}$$

where p and q are constant with $K_y = q^2\ U\ x$ and $K_z = p\ U\ z$.

Davies' solution

Davies (1952) obtained a solution for the ground point source with power-law profiles for the wind velocity and mass eddy diffusivities

$$U = U_1(z/z_1)^m$$

$$K_z = A_z U_1^{1-n} z^{1-m}$$

$$K_y = A_y U_1^{1-n} z^m y^{1-2m}$$

where U_1 is the mean velocity at height Z_1, $m = n/(2-n)$, and A_y and A_z are constants defined by

$$A_y/A_z = \{\overline{v'^2}/\overline{w'^2}\}^{1-n}$$

The solution is of the form

$$C = B_o x^{-(2+m)/a} \exp\{-(1/Aa^2)(z^a/x)\} \cdot \exp\{-(1/Ba^2)(y^a/x)\}$$

where

$$a = 1+2m$$

$$A = A_z z_1^m/U_1^n$$

$$B = A_y z_1^m/U_1^n$$

$$B_o = \frac{Qz_1^m a(Aa)^{-(1+m)/a}}{2U_1 B^{-a}\Gamma\{1/a\}\Gamma\{(1+m)/a\}a^{(1-2m)/a}}$$

and Γ is the Gamma probability function. Davies' solution is in good agreement with the experiment of Calder (1949).

We are interested in the diffusion of particles emitted from a line source. Numerical investigations and some analytical solutions will be discussed in the following chapter.

CHAPTER 4. NUMERICAL SOLUTIONS OF DIFFUSION EQUATION

The steady-state diffusion equation for the continuous line source located at (x, z) = (0, H) can be written as

$$U\frac{\partial C}{\partial x} + (W-W_f)\frac{\partial C}{\partial z} = \frac{\partial}{\partial z}(K_z\frac{\partial C}{\partial z}) \qquad (4.1)$$

The associated initial and boundary conditions are

$$C(0,z) = Q/U\cdot\delta(z-H)$$

$$\{K_z\cdot\partial C/\partial z\}_{z=0} = \{(W_d-W_f)C\}_{z=0}$$

$$C(x,\infty) = 0$$

where the line source strength Q is defined by

$$Q' = \int_0^\infty U\cdot C\, dz$$

$$= Q - \int_0^x W_d\, C\, dx$$

Some analytical solutions have been obtained by assuming W = 0, and U and K_z as specified functions of height z.

Analytical Solutions for Line Source

Roberts' solution

Roberts, in an unpublished paper, derived the following solution for a ground line source with K_z and U varying as power functions of height and with $W_f = W_d = 0$:

$$C = \frac{Q\Lambda^{\Lambda-1}\exp\{(-\Lambda z^\gamma)/(\lambda\gamma^2 x)\}}{\gamma^{2\Lambda-1}\lambda^\Lambda\Gamma(\Lambda)x^\Lambda}$$

where

$$U = Az^m$$

$$K_z = \lambda z^n$$

$$\gamma = 2 + m - n > 0$$

and

$$A = (m+1) / \gamma \qquad (4.2)$$

Calder (1949) adopted this solution under the following definitions of K_z and U which apply to a layer of constant shearing stress,

$$U/U_1 = (z/z_1)^{\alpha}$$

$$K_z = MU_1^{2\beta-1} z_1^{\alpha(1-\beta)} z^{1-\alpha}$$

$$M = (\varepsilon'/\alpha)\delta^{2\alpha\beta}$$

where the parameters M, ε', and β are defined for smooth and rough flows. For smooth flow,

$$\beta = 1/(1+\alpha), \quad \delta = \nu, \quad \varepsilon' = (1/q)^{2/(1+\alpha)}$$

and q satisfies $U/U^* = q(zU^*/\nu)^{\alpha}$. For rough flow,

$$\beta = 1, \quad \delta = z_o, \quad \varepsilon' = 1/q'^2$$

and q' satisfies $U/U^* = q'(z/z_o)^{\alpha}$. Essentially, Calder fits the wind profile at two points to a power law and then determines K_z from the expression for U such that

$$\tau = \rho K_z \cdot dU/dz = \text{Constant}$$

Bosanquet and Pearson's solution

Bosanquet and Pearson (1936) assumed a linear variation of K_z with height and a uniform wind field to obtain a solution for the ground line source:

$$C = Q \exp(zU/x\lambda)/\{\lambda\, x^{(1+W_f/\lambda)}\}$$

where λ is a constant defined as $K_z = \lambda z$ and $W_f = W_d$.

It is noted that Bosanquet and Pearson also showed that the value of C at ground level due to a source at height H is the same as the value of C at height H due to a source at ground level.

Rounds' solution

By using Deacon's (1949) approximations of power-law profiles for the velocity and eddy diffusivity in Eq. (4.2), Rounds (1955) derived a solution for an elevated line source of the form,

$$C = \frac{QH^{1-n}(z/H)^{\gamma p/2}}{\gamma\lambda x}\exp\{\frac{-A(z^{\gamma/2}-H^{\gamma/2})^2}{\gamma^2\lambda x}\} \cdot \exp(-E)\cdot I_{-p}(E)$$

where

$$E = \frac{2A(zH)^{\gamma/2}}{\gamma^2\lambda x}$$

$$P = \begin{cases} (1-n)/\gamma & \text{if } W_f = 0 \\ -W_f/\gamma\lambda & \text{if } W_f \neq 0 \text{ and } n = 1 \end{cases}$$

and I is the Bessel function of purely imaginary argument. If $n \neq 1$ and $W_f \neq 0$, no rigorous solution can be obtained. The concentration C at the surface is given by

$$C = \frac{Q H^{1-n-p\gamma} \gamma^{2p-1}}{x^{1-p} \Lambda^{p} \lambda^{1-p} \Gamma(1-p)} \exp(-\Lambda H^{\gamma}/\lambda \gamma^{2} x)$$

Finite-Difference Scheme and Boundary Conditions

A number of finite-difference schemes have been developed to solve parabolic partial differential equations. In the present study, the Crank-Nicolson scheme is selected as our solver. The finite-difference representation of the diffusion equation developed and revised by Liu and Karaki (1972) is expressed in the following:

$$C_{i+1,k} = C_{i,k} + \frac{\Delta x_i}{2U_{i,k}} \{ \frac{(K_z)_{i,k+1/2}}{\Delta z_k \Delta z_{k-1/2}} \{ (C_{i+1,k+1} - C_{i+1,k}) + (C_{i,k+1} - C_{i,k}) \}$$

$$- \frac{(K_z)_{i,k-1/2}}{\Delta z_{k-1/2} \Delta z_{k-1}} \{ (C_{i+1,k} - C_{i+1,k-1}) + (C_{i,k} - C_{i,k-1}) \} - \frac{(W_{i,k} - W_f)}{(\Delta z_k + \Delta z_{k-1})} \{ (C_{i+1,k+1} - C_{i+1,k-1}) + (C_{i,k+1} - C_{i,k-1}) \} \}$$

where $\Delta x_i = x_{i+1} - x_i$ and $\Delta z_k = z_{k+1} - z_k$. The Crank-Nicolson scheme can be modified to be the Gauss-Seidel

scheme with Successive-Over-Relaxation (S.O.R.) which can accelerate the convergence rate. Thus, we can solve the finite-difference equation by an iterative procedure.

Initial condition

Mathematically, the continuous line source represents a singularity at the point of release as depicted in Eq. (4.2). In order to avoid this singularity, the initial condition can be approximated by the appropriate analytical solution discussed before at a short distance downstream from the point of release. This distance should be short enough that the applied analytical solution is a good approximation as the initial condition to the physical problem. However, the selected distance should be large enough to avoid regions of extremely large concentration gradient, which may cause appreciable error in the numerical calculation. A recommended criterion is to find the distance (X_o) at which the numerical source strength is close enough to the initially specified value.

Lower boundary condition

With the assumption that $W_d = W_f$, the boundary condition at the ground becomes

$$\{K_z \cdot \frac{\partial C}{\partial z}\}_{z=0} = 0$$

Many analytical solutions show that the concentration is an exponential function of z, so we can apply the polynomial of the form

$$\ln C(x,z) = A'(x,z) + B'(x,z)\, z + C'(x,z)\, z^2$$

to find the concentration on the ground. Here, A', B', and C' are calculated from the information of three points above the ground in the previous iteration solution. This manipulation works very well for the ground source problems. However, for the elevated source, it may yield bad vertical concentration distribution near the surface unless the maximum is at the ground. The following can be used as an alternative:

$$C(x,z_w) = \{3\, C(x,z_{w+1}) - C(x,z_{w+2})\}/4$$

Upper boundary condition

The numerical domain has been limited to regions where concentrations are negligibly small. The upper boundary of the domain for the numerical calculation thus forms a free boundary on which the concentration can not be solved directly in the marching x-direction. The boundary values again may be extrapolated by an exponential function from the calculated values adjacent to the free boundary by using the same form as that expressed for the lower boundary:

$$\ln C(x,z) = A''(x,z) + B''(x,z)\, z + C''(x,z)\, z^2$$

Test of the Finite-Difference Scheme

Three test problems with known analytical solutions are solved by using the present finite-difference scheme. The numerical solutions are compared with Roberts', Bosanquet's and Rounds' analytical solutions. From Figure 3 to Figure 9, it is observed that the numerical solutions and the analytical solutions are in very good agreement.

A Special Treatment in Separated Regions

Before solving the diffusion problem, we have to note that the steady advection-diffusion equation (Eq. 4.1) is parabolic. For $U > 0$, the solution is marched in the positive x direction. If $U < 0$, the equation remains parabolic but the correct marching direction is in the negative direction. So if separation occurs in the flow region, a solution procedure must be devised to overcome the problem associated with the 'correct' marching direction.

The FLARE approximation is employed in our calculation to overcome this problem. In the FLARE approximation, the convective term $U\,\partial C/\partial x$ for $U < 0$ in the diffusion equation is replaced by

$$|F|U\frac{\partial C}{\partial x}$$

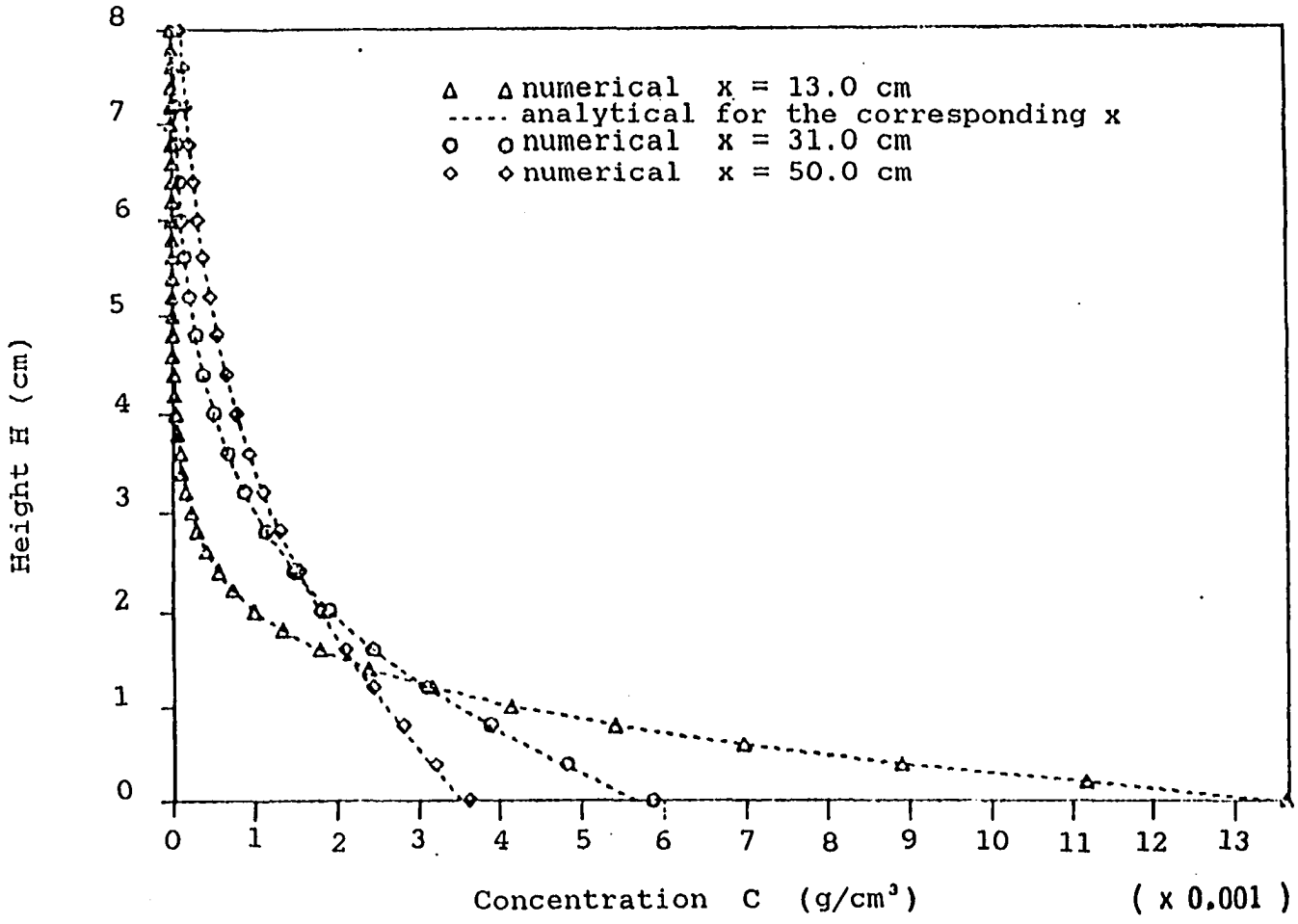

FIGURE 3. Concentration distribution with height for $U=100Z^{1/7}$, $K_z=5.0Z$, $W_f=0.$, and H=0.

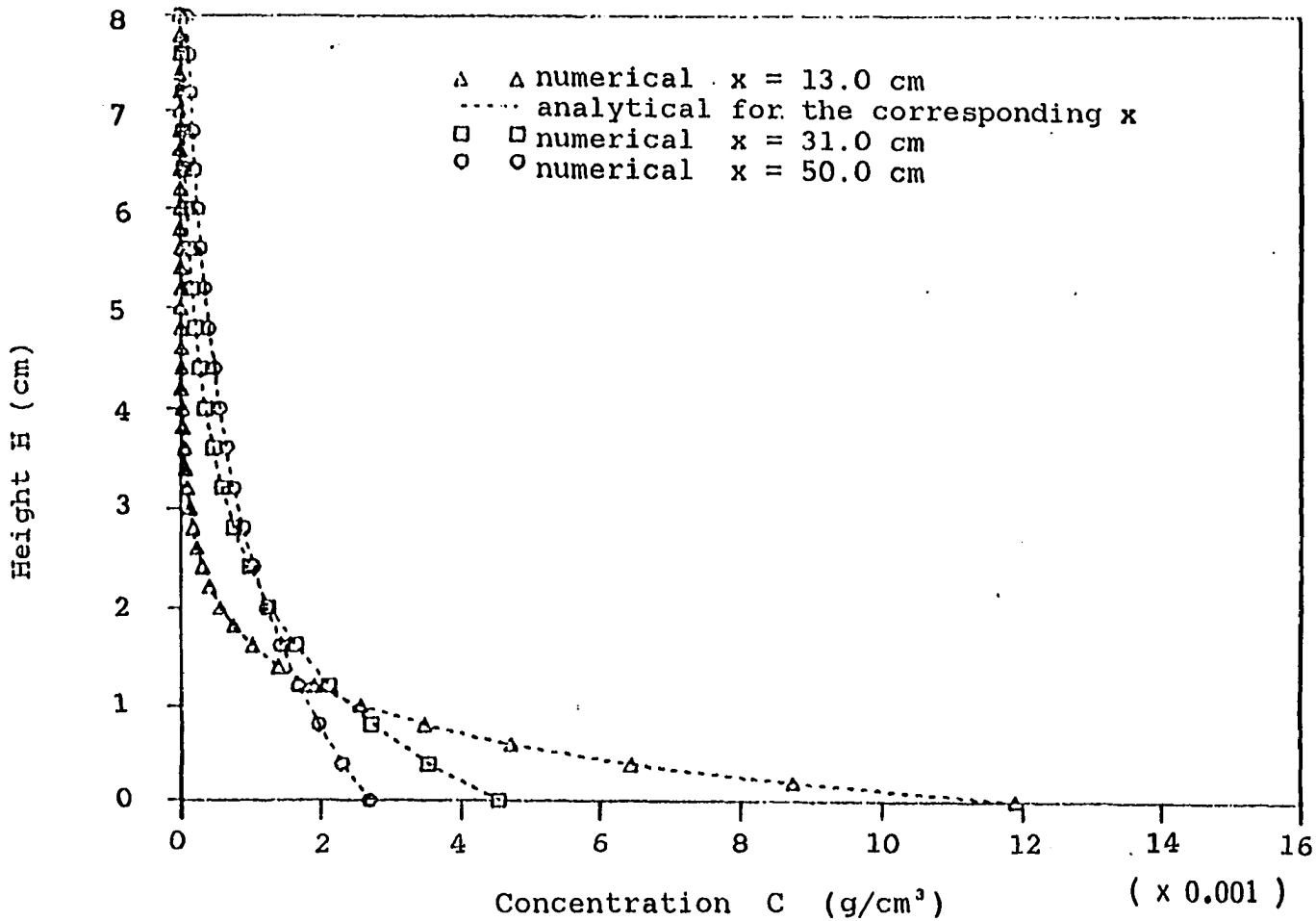

FIGURE 4. Concentration distribution with height for U=100, K_z=5.0Z, W_f=0.5, and H=0.

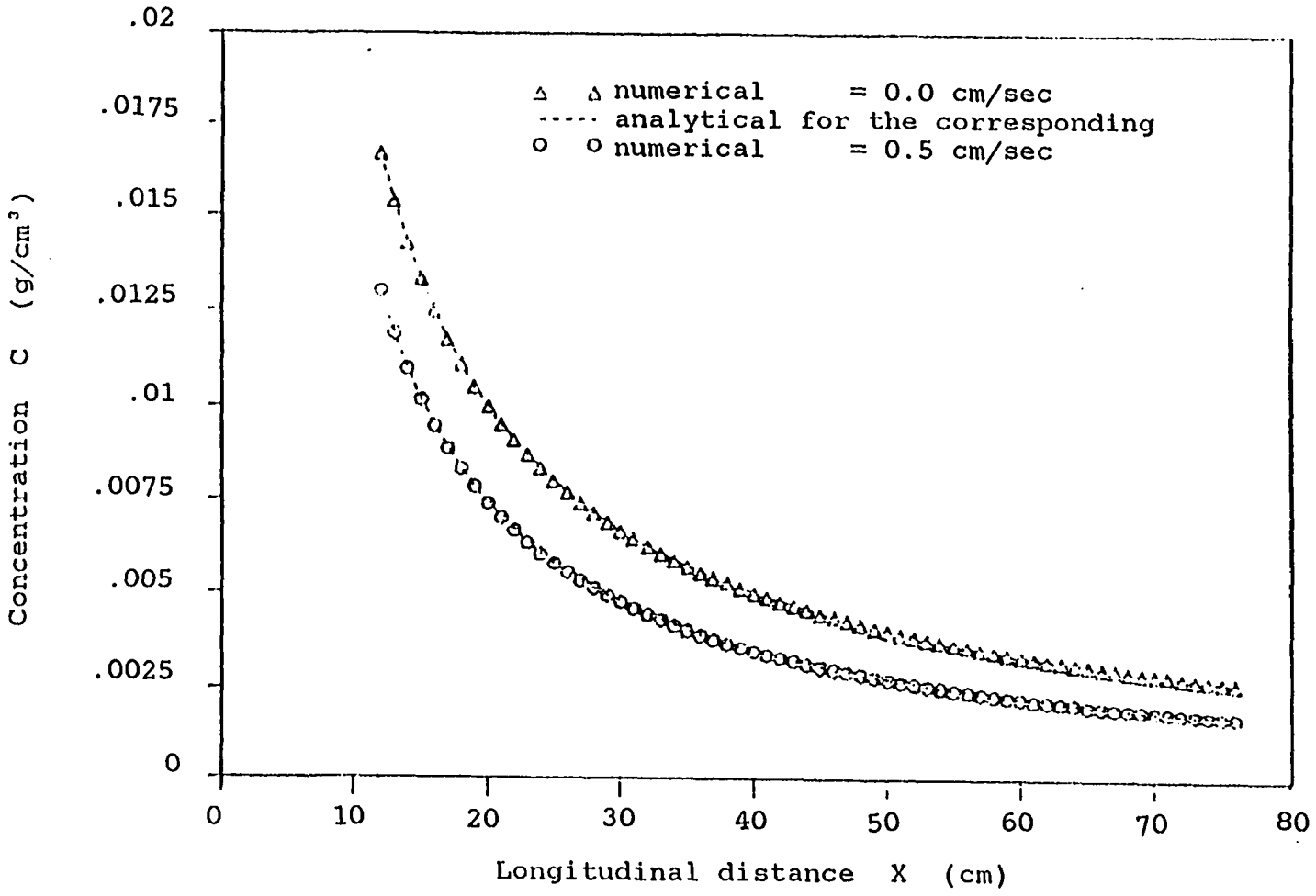

FIGURE 5. Concentration distribution with height for U=100, K_z=5.0Z, and H=0.

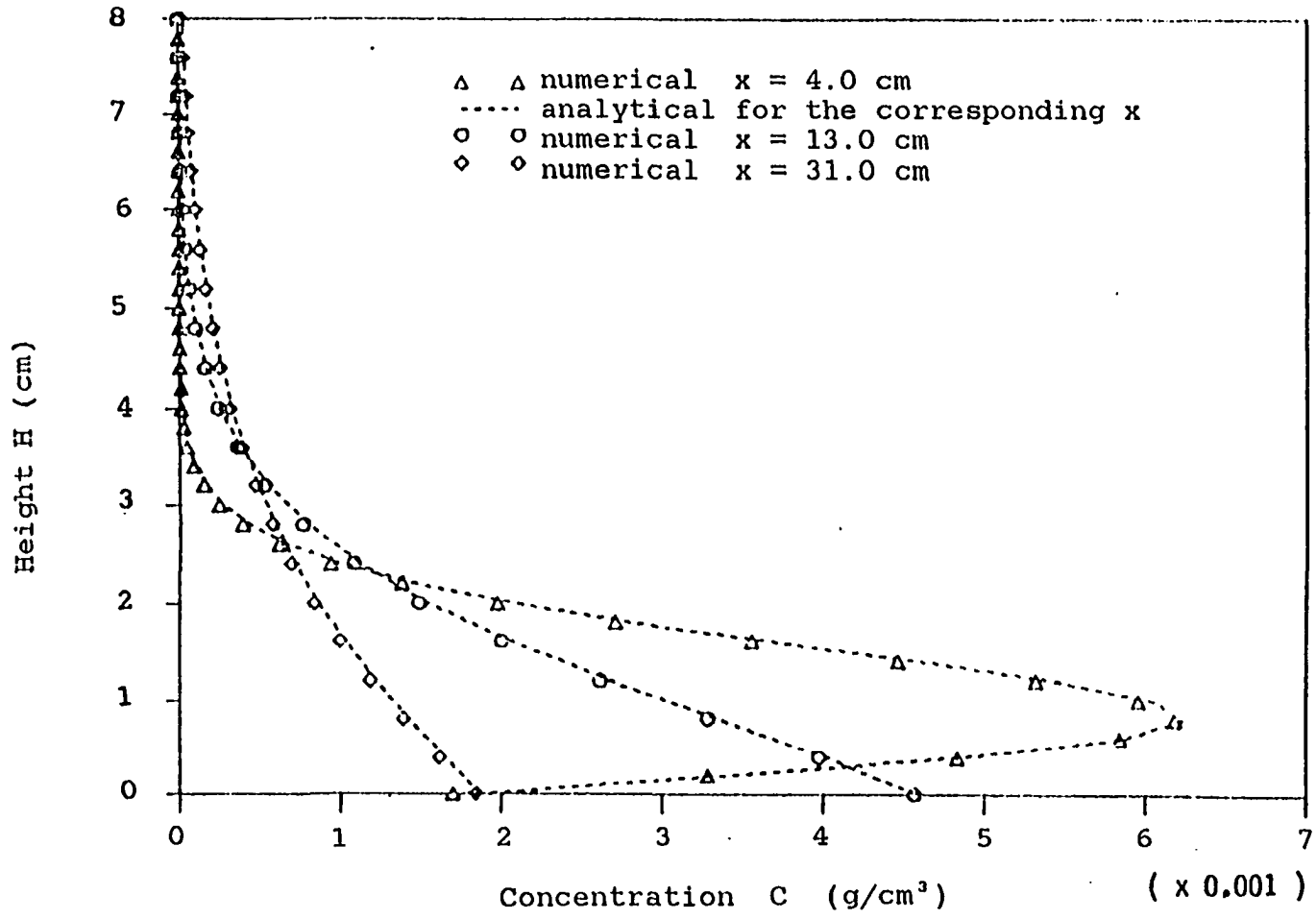

FIGURE 6. Concentration distribution with height for $U=100Z^{1/7}$, $K_z=5.0Z$, $W_f=40/7$, and H=1.2

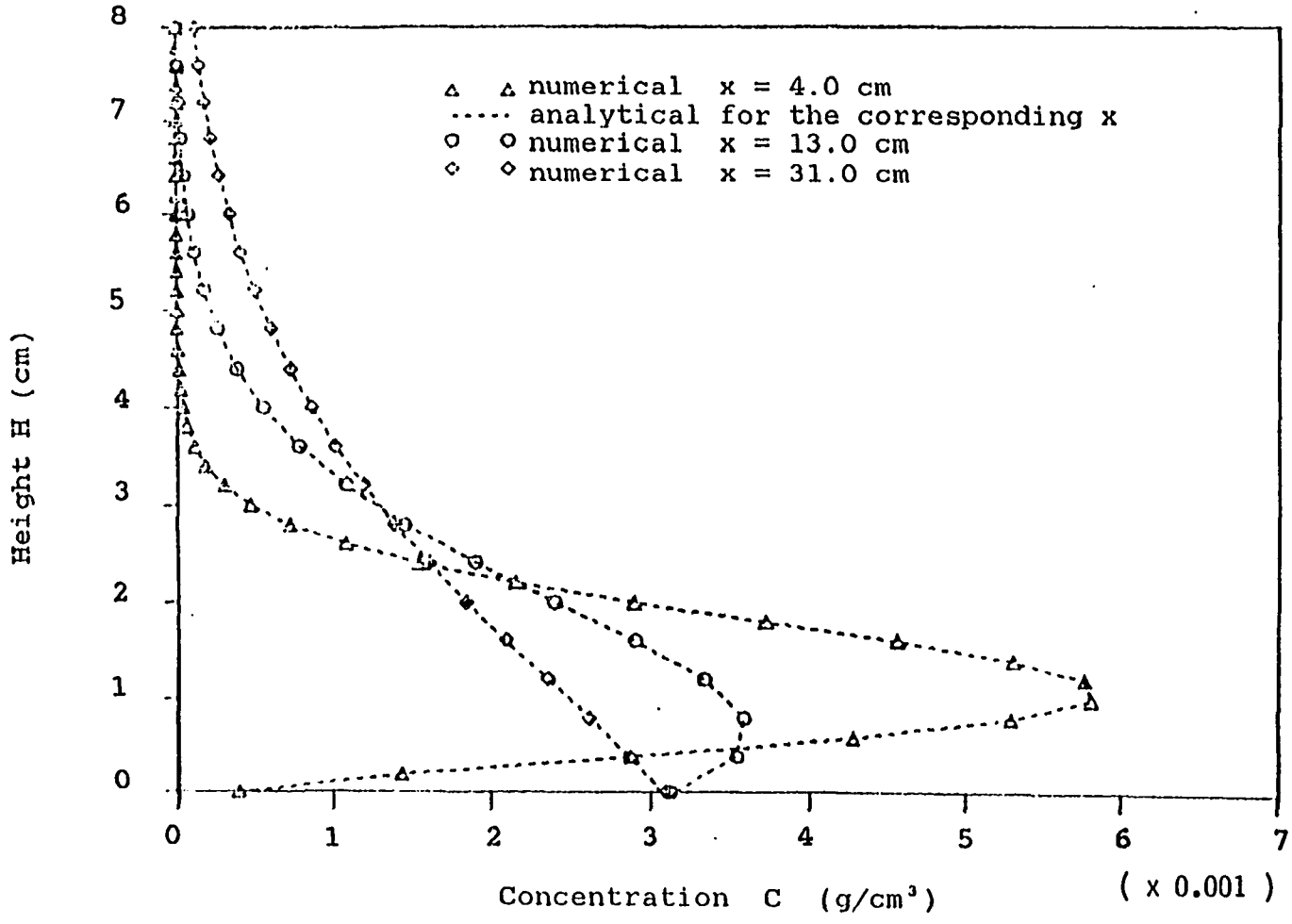

FIGURE 7. Concentration distribution with height for $U=100Z^{1/7}$, $K_z=5.0Z$, $W_f=0.$, and H=1.2

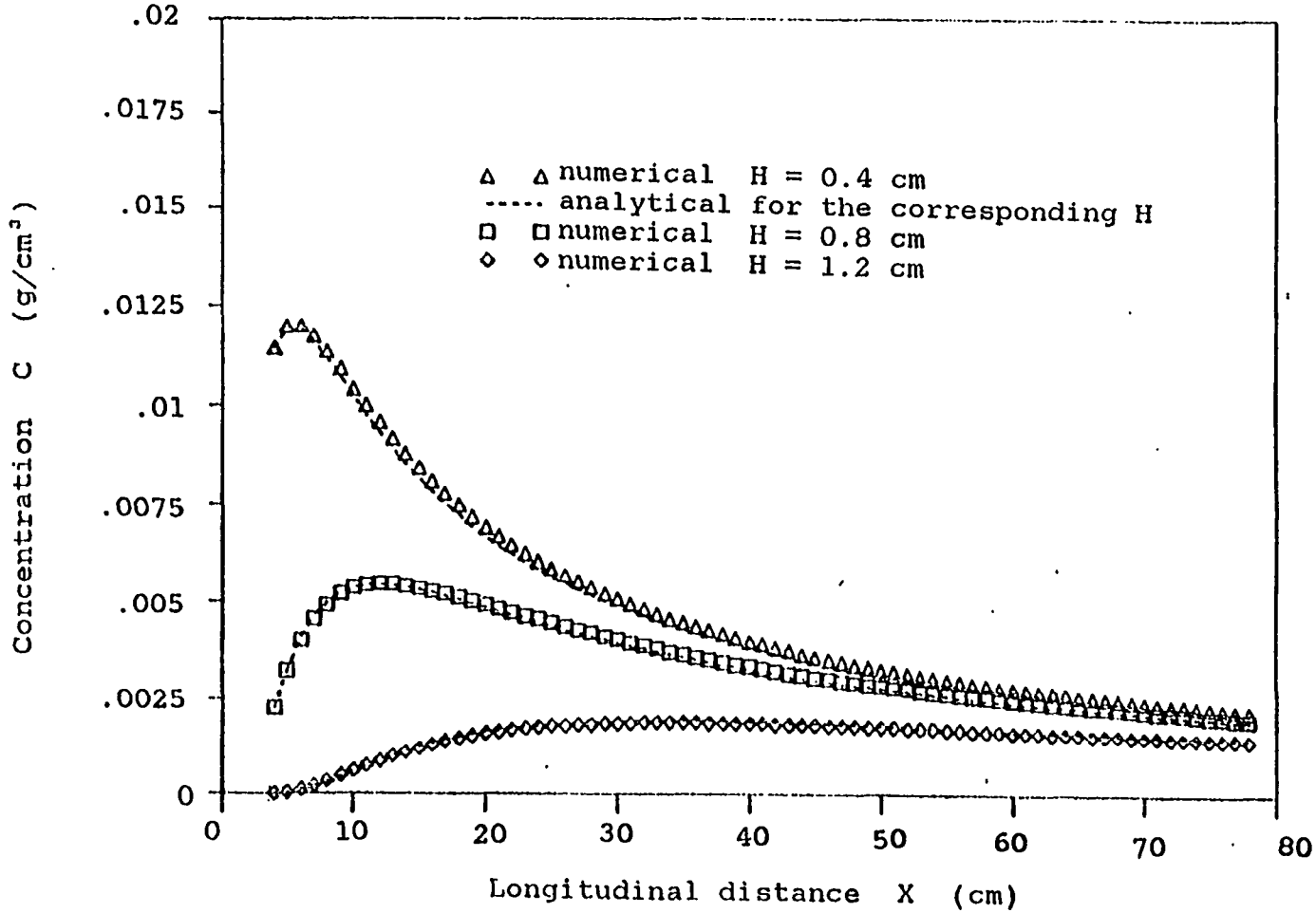

FIGURE 8. Concentration distribution on the ground for $U=100Z^{1/7}$, $K_z=5.0Z$, and $W_f=0$.

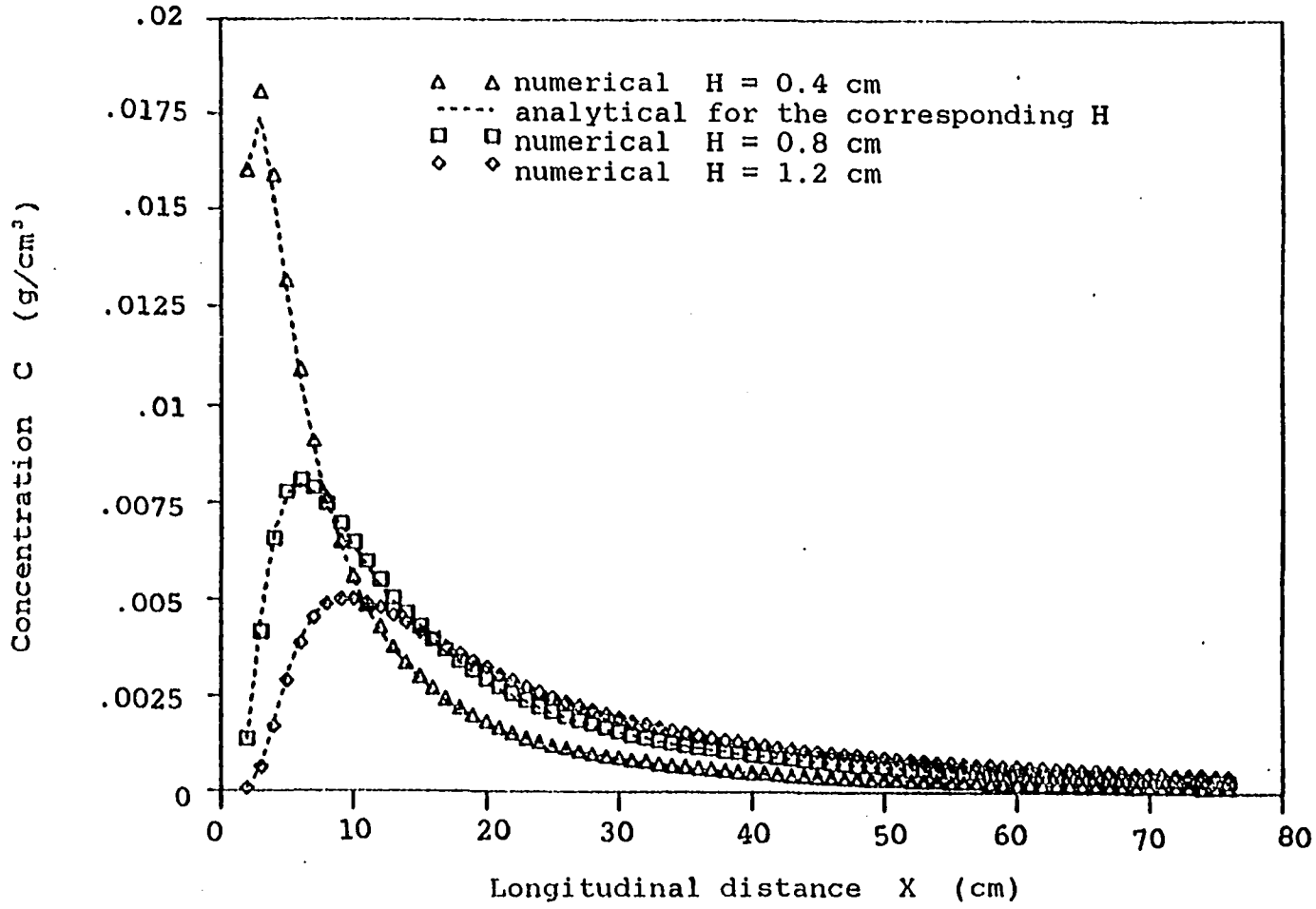

FIGURE 9. Concentration distribution on the ground for $U=100Z^{1/7}$, $K_z=5.0Z$, and $W_f=40/7$.

where F is a small positive constant. This representation permits the marching procedure to go through the separated regions. Obviously, the FLARE procedure introduces an assumption that the term $U\,\partial C/\partial x$ is small relative to other terms in the advection-diffusion equation. Details of the FLARE approximation employed on the parabolic boundary-layer equations can be found in the work of Cebeci (1976) and Carter (1978). The constant F is chosen to be 0.1 in our concentration calculations.

CHAPTER 5. NUMERICAL SOLUTION OF THE NAVIER-STOKES EQUATIONS

Before solving the advection-diffusion equation, we must obtain information about the velocity field. Steady-state two-dimensional Navier-Stokes equations with a k-ε two-equation turbulence model will be applied. We are limited to the lowest region of the atmospheric layer, which is neutrally stable, so the Coriolis effect in the momentum equations is assumed negligible due to the small scale of motion under consideration. The atmospheric flow is usually assumed to be a fully rough turbulent flow.

Governing Equations

The equations of motion for steady-state turbulent flow can be written in cartesian tensor notation as follows:

Continuity:

$$\frac{\partial u_i}{\partial x_i} = 0$$

Momentum:

$$\frac{\partial \rho u_j u_i}{\partial x_j} = -\frac{\partial p}{\partial x_i} + \frac{\partial}{\partial x_j}\{\mu_{eff}\,(\frac{\partial u_i}{\partial x_j} + \frac{\partial u_j}{\partial x_i})\}$$

Here, μ_{eff} is the effective viscosity defined by

$$\mu_{eff} = \mu + \mu_t$$

and μ and μ_t are molecular and eddy viscosities, respectively. The eddy viscosity is determined from the turbulent kinetic energy k and its dissipation rate ε according to

$$\mu_t = \rho C_\mu k^2/\varepsilon \tag{5.1}$$

The turbulence model can be written as (Spalding and Launder, 1972):

$$\frac{\partial \rho u_j k}{\partial x_j} = \frac{\partial}{\partial x_j}\left(\frac{\mu_{eff}}{\sigma_k}\frac{\partial k}{\partial x_j}\right) + G - \rho\varepsilon$$

$$\frac{\partial \rho u_j \varepsilon}{\partial x_j} = \frac{\partial}{\partial x_j}\left(\frac{\mu_{eff}}{\sigma_\varepsilon}\frac{\partial \varepsilon}{\partial x_j}\right) + C_1\frac{\varepsilon}{k}G - C_2\rho\frac{\varepsilon^2}{k}$$

where

$$G = \mu_t \frac{\partial u_i}{\partial x_j}\left(\frac{\partial u_i}{\partial x_j} + \frac{\partial u_j}{\partial x_i}\right)$$

Making use of the stream function and vorticity, the above governing equations for two-dimensional flow can be expressed in the common form of an elliptical partial differential equation suitable for simultaneous numerical integration:

$$a\left\{\frac{\partial}{\partial x}\left(\Phi\frac{\partial \psi}{\partial z}\right) - \frac{\partial}{\partial z}\left(\Phi\frac{\partial \psi}{\partial x}\right)\right\} - \left\{\frac{\partial}{\partial x}\left(b\frac{\partial}{\partial x}(c\Phi)\right) + \frac{\partial}{\partial z}\left(b\frac{\partial}{\partial z}(c\Phi)\right)\right\} + d = 0 \tag{5.2}$$

where the constants a, b, c, and d, and the dependent variable are given in Table 2 and Table 3.

It is noted that the pressure gradients have been eliminated and do not appear in the equations. This is the big advantage of the vorticity-stream function approach. If the wall pressure is to be calculated, we can simply apply the tangential momentum equation for the wall pressure distribution. For a wall located at z = 0, the steady tangential momentum (x momentum) equation reduces to

$$\frac{\partial p}{\partial x}\Big|_{wall} = \frac{\partial}{\partial z}\left(\mu_{eff}\frac{\partial u}{\partial z}\right)\Big|_{wall}$$

or

$$\frac{\partial p}{\partial x}\Big|_{wall} = -\frac{\partial}{\partial z}\left(\mu_{eff}\omega\right)\Big|_{wall}$$

For a constant grid size, it can be differenced as

$$\frac{p_{i+1,1} - p_{i-1,1}}{2\Delta x} = -\frac{-3(\mu_{eff}\omega)_{i,1} + 4(\mu_{eff}\omega)_{i,2} - (\mu_{eff}\omega)_{i,3}}{2\Delta z}$$

If Δx is non-uniform, we will use the following form for $\partial p/\partial x$:

$$\frac{\partial p}{\partial x}\Big|_i = \{(p_{i+1}-p_i)(\Delta x_-/\Delta x_+) + (p_i-p_{i-1})(\Delta x_+/\Delta x_-)\} /(\Delta x_+ + \Delta x_-)$$

TABLE 2. Coefficient functions of Equation (5.2)

Φ	a	b	c	d
ψ	0	$1/\rho$	1	$-\omega$
ω	1	1	μ_{eff}	$-S_\omega$
k	1	μ_{eff}/σ_k	1	$-S_k$
ε	1	$\mu_{eff}/\sigma_\varepsilon$	1	$-S_\varepsilon$

TABLE 3. Expressions for source term, -d

Φ	S_Φ
ψ	ω
ω	$2\{-\frac{\partial u}{\partial x}\frac{\partial^2 \mu_{eff}}{\partial x\,\partial z} - \frac{\partial w}{\partial x}\frac{\partial^2 \mu_{eff}}{\partial z^2} + \frac{\partial w}{\partial z}\frac{\partial^2 \mu_{eff}}{\partial z\,\partial x} - \frac{\partial u}{\partial z}\frac{\partial^2 \mu_{eff}}{\partial x^2}\}$
k	$\mu_t\{2(\frac{\partial u}{\partial x})^2 + 2(\frac{\partial w}{\partial z})^2 + (\frac{\partial u}{\partial z}+\frac{\partial w}{\partial x})^2\} - \rho\varepsilon$
ε	$C_1\frac{\varepsilon\mu_t}{k}\{2(\frac{\partial u}{\partial x})^2 + 2(\frac{\partial w}{\partial z})^2 + (\frac{\partial u}{\partial z}+\frac{\partial w}{\partial x})^2\} - \frac{\rho C_2 \varepsilon^2}{k}$

where $\Delta x_+ = x_{i+1} - x_i$ and $\Delta x_- = x_i - x_{i-1}$. It is noted that the above difference form (Eq. 5.6) for $\partial p/\partial x$ may yield oscillating solutions behind the sharp corner. In that case, the simple forward difference is recommended. Similarly, for a wall located at x = 0, we will have

$$\frac{\partial p}{\partial z}\Big|_{wall} = \frac{\partial}{\partial x}(\mu_{eff}\omega)\Big|_{wall}$$

Finite-Difference Scheme

Gosman et al. (1969) used an integral method to develop an upwind finite-difference scheme for Eq. (5.2). The finite-difference representation is given in Appendix B. For convenience, we may write the finite-difference equation in the following form:

$$\Phi_p = \frac{ANUM - d_p}{ADNM} \tag{5.3}$$

We will basically apply Gosman's scheme with a relaxation technique to solve the four transport equations. However, due to the non-linearity of these governing equations, a very small under-relaxation parameter must be used in the ω equation to prevent divergence. This will greatly slow down the iteration process and thus increase the computing time. A time marching procedure is normally used to simultaneously solve the ω, k, and ε equations. Thus, we modify the

finite-difference representation, i.e., Eq. (5.3), by adding the unsteady term:

$$\Phi_p^{n+1} = \frac{\{(ANUM - d_p)^n + (\Phi_p^{n+1} - \Phi_p^n)/\Delta t\}}{ADNM}$$

where n is the time step level. The final finite-difference representation is then expressed as:

$$\Phi_p^{n+1} = \frac{\{\Phi_p^n + \Delta t\ (ANUM - d_p)^n\}}{(1 + \Delta t\ ANUM)}$$

In order to uncouple k and ε equations in the time marching approach, we use Eq. (5.1) to eliminate the variable ε in the source term S_k. Similarly, we can eliminate the variable k in the source term S_ε. Then, the source terms S_k and S_ε will contain $(k^2)^n$ and $(\varepsilon^{3/2})^n$, respectively. Unfortunately, these terms could vary so widely as to provoke divergence. A remedy has been specially devised by replacing $(k^2)^n$ and $(\varepsilon^{3/2})^n$ by $(k)^{n+1}(k)^n$ and $(\varepsilon)^{n+1}(\sqrt{\varepsilon})^n$, respectively. Here, n is the time step level in the marching procedure. Thus, the finite-difference equations for k and ε will be modified a little bit according to this remedy. The point about this new substituting formula is that the variations in the modified source terms can be expected to be much less than those of the original ones (Gosman et al., 1969).

Discussion of Boundary Conditions

Three different obstructions, the forward-facing step, the backward-facing step and the rectangular block, are considered in the present study. The flow regime considered extends about ten step heights in the upstream and twenty step heights in the downstream directions and about ten step heights in the vertical direction. The numerical coordinate systems are chosen such that the origin is located at the lower left corner with positive x-axis pointing in the downstream direction parallel to the wall and with the z-axis directed normally to it.

The distributions of the grid points for all three geometries are shown in Figure 10, Figure 11, and Figure 12.

Inflow

At the inflow, a logarithmic velocity profile of the form

$$u = \frac{u^*}{\kappa} \ln\left(\frac{z+z_o}{z_o}\right)$$

is assumed. With the definition of ψ

$$\rho u = \frac{\partial \psi}{\partial z}$$

$$\rho w = - \frac{\partial \psi}{\partial x}$$

the corresponding ψ condition is given by

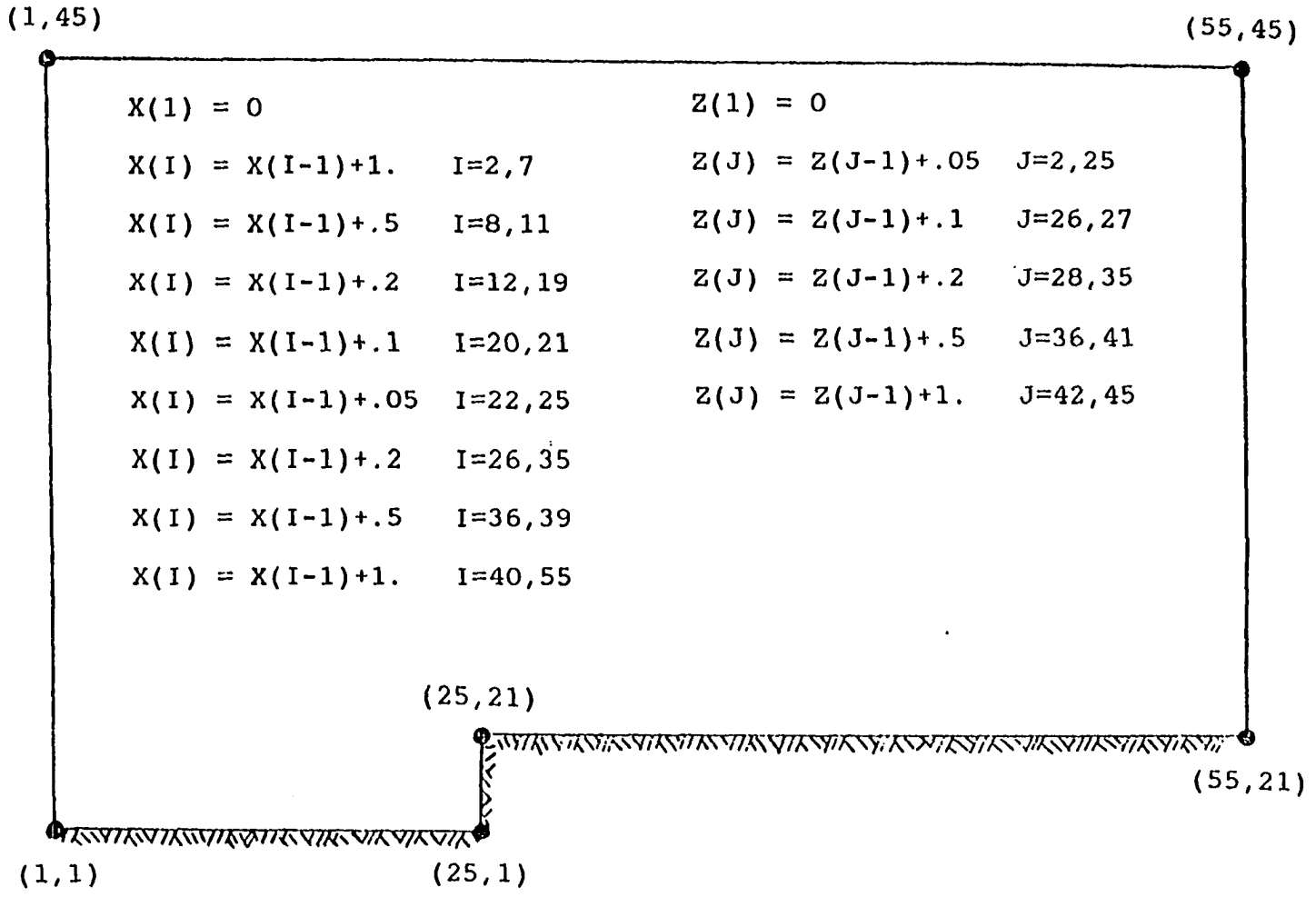

FIGURE 10. Grid distribution for the forward-facing step flow problem

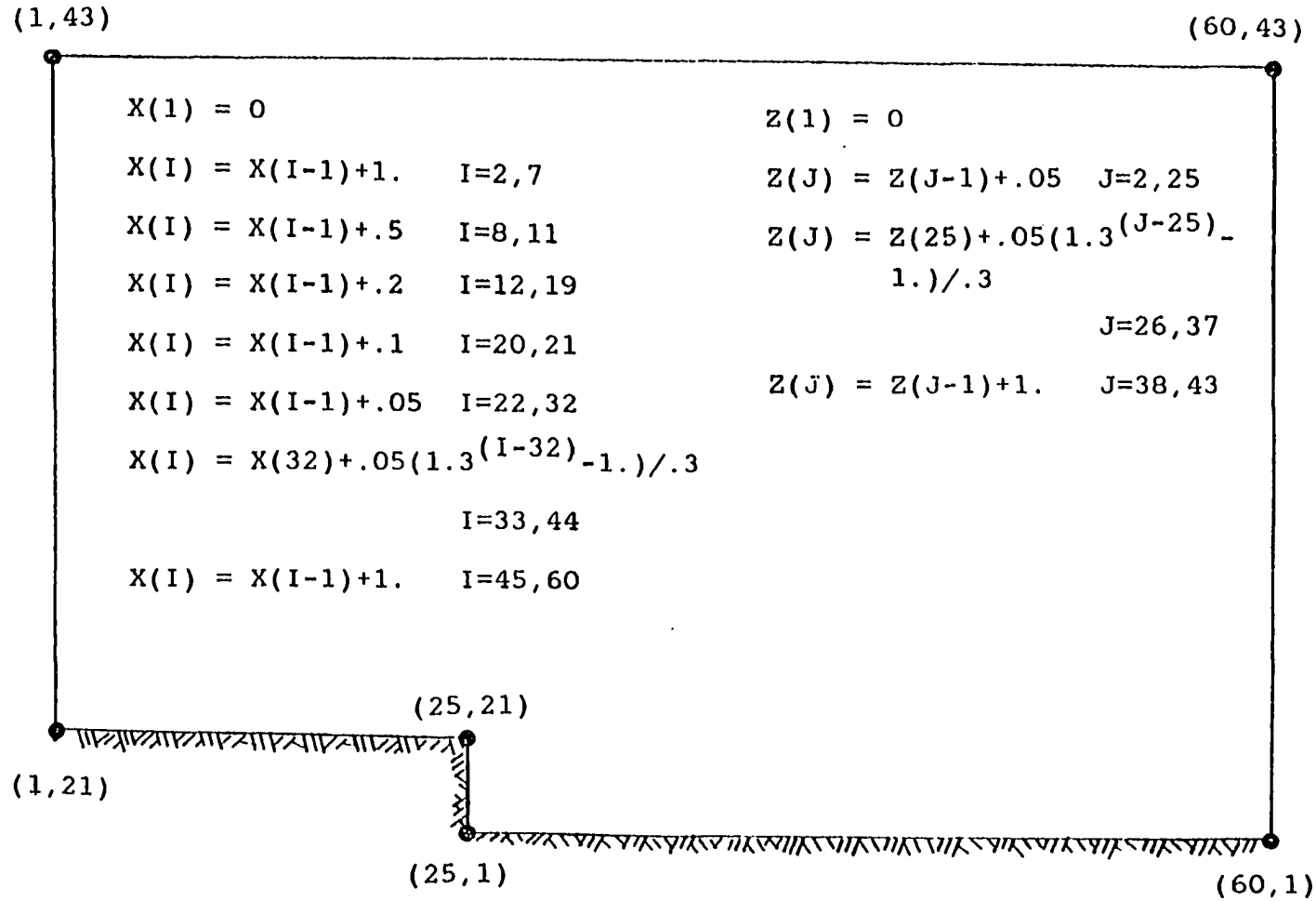

FIGURE 11. Grid distribution for the backward-facing step flow problem

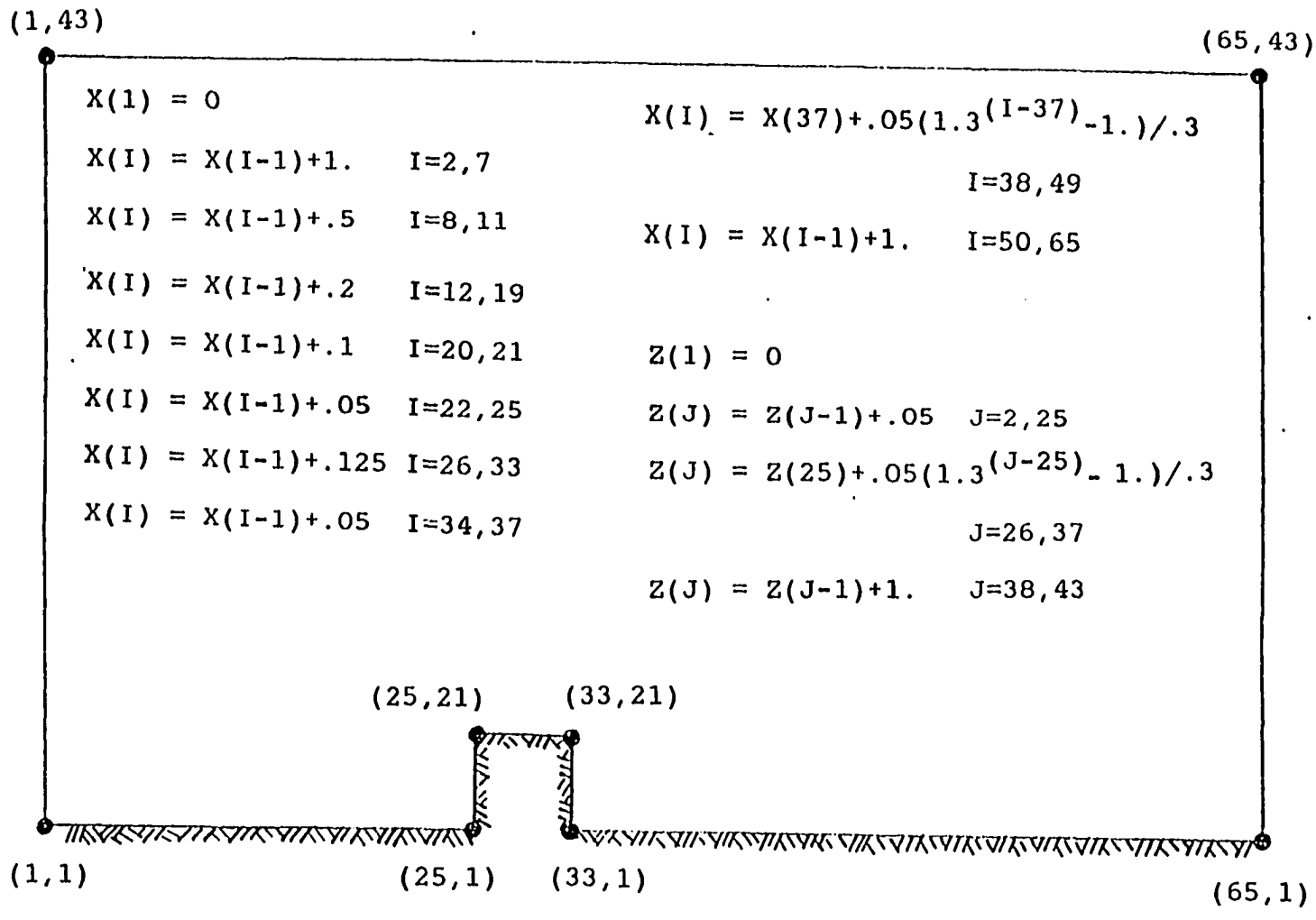

FIGURE 12. Grid distribution for the rectangular block flow problem

$$\psi = \rho \frac{u^*}{\kappa}\{(z+z_o)(\ln \frac{z+z_o}{z_o} - 1) + z_o\}$$

with $\psi = 0$ at the wall. The condition for ω is

$$\omega = \frac{\partial w}{\partial x} - \frac{\partial u}{\partial z}$$

$$= \frac{\partial w}{\partial x} - \frac{u^* \, 1}{\kappa \, z+z_o}$$

where $\partial w/\partial x$ can be considered as part of the solution by approximating

$$\frac{\partial^2 w}{\partial x^2} = 0$$

and setting

$$\frac{\partial w}{\partial x}|_{1,j} = \frac{\partial w}{\partial x}|_{2,j} = -\frac{1}{\rho} \frac{\partial^2 \psi}{\partial x^2}|_{2,j}$$

In the surface layer of constant shear stress, we have

$$\tau_t = -\rho \, \overline{u'w'} = \rho \, u^{*2}$$

Applying the Prandtl (1945) and Kolmogorov's (1942) suggestion

$$\tau_t = \mu_t \frac{\partial u}{\partial z} = \rho \, k^{1/2} \, \ell \, C_k \frac{\partial u}{\partial z}$$

we will have

$$k = (\frac{u^*}{C_k})^2 \qquad (5.4)$$

with the mixing length ℓ calculated by

$$\ell = (z + z_o)$$

The inflow condition for ε is thus determined by

$$\varepsilon = (k^{3/2} C_\mu) / (\ell C_k)$$

Outflow

In the outflow, we assume that

$$\frac{\partial \omega}{\partial x} = 0$$

$$\frac{\partial k}{\partial x} = 0$$

$$\frac{\partial \varepsilon}{\partial x} = 0$$

for ω, k, and ε, respectively, at the exit boundary. For the ψ condition, the assumptions

$$\frac{\partial w}{\partial x} = 0 \text{ and } \frac{\partial \omega}{\partial x} = 0$$

yields that

$$\frac{\partial^2 \psi}{\partial x^2}\Big|_{IN,J} = \frac{\partial^2 \psi}{\partial x^2}\Big|_{IN-1,J} = 0$$

Upper boundary

We assume that the upper boundary is far enough away from the obstruction that the velocity deflections caused by the obstruction are negligibly small. Consequently, we have

$$\psi = \text{constant}$$

We may make the following assumption for ω

$$\frac{\partial \omega}{\partial z} = 0$$

For k and ε we use

$$\frac{\partial k}{\partial x} = 0$$

$$\frac{\partial \varepsilon}{\partial x} = 0$$

as the upper boundary conditions.

Wall boundary

$\psi = 0$ along the entire wall boundary. The condition for ω can be derived from a Taylor-series expansion of the stream function ψ around a near wall point (np) in terms of the wall point (p) condition. By applying the non-slip conditions, we have

$$\omega_p = - \frac{3\psi_{np}}{\rho(\Delta n)^2} - \frac{\omega_{np}}{2} \qquad (5.5)$$

A special treatment for evaluation of the vorticity at corners must be carried out. Seven different methods were discussed by Roache (1972). One of them is to apply the Eq. (5.5) to the upstream side (face) of the step. (See Figure 13.) We will use this method in our calculations because it forces the separation to occur tangentially to the upstream wall.

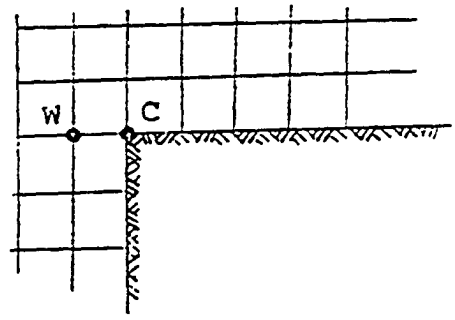

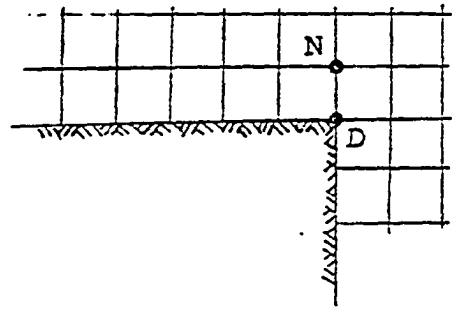

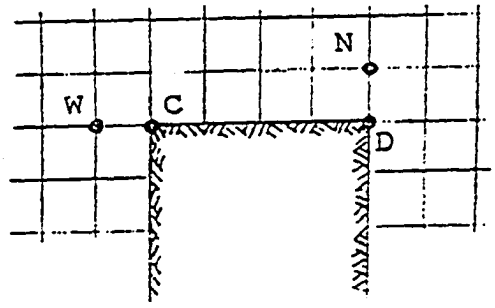

$$\omega_C = - \frac{3\psi_W}{\rho(\Delta x)^2} - \frac{1}{2}\omega_W$$

$$\omega_D = - \frac{3\psi_N}{\rho(\Delta z)^2} - \frac{1}{2}\omega_N$$

FIGURE 13. Boundary conditions for vorticities at upper corners of the step

Applying Prandtl's mixing length hypothesis

$$\mu_t = \rho \ \ell^2 \frac{\partial u}{\partial z}$$

we can obtain

$$(u^*)_w = \kappa \ z_o \ |\omega|$$

where we have used the relation $(\ell)_w = \kappa \ z_o$ at the wall. With the above relation we can obtain, similar to inflow conditions, that

$$k_w = (\kappa z_o \omega / C_k)^2$$

$$\varepsilon_w = (k^{3/2} C_\mu)/(\kappa z_o C_k)$$

Turbulence-Model Constants

Fichtl (1973) reported that for the atmospheric boundary layer it has been experimentally determined that

$$\overline{u'^2} = (2.5 \ u^*)^2$$

$$\overline{v'^2} = (1.9 \ u^*)^2$$

$$\overline{w'^2} = (1.3 \ u^*)^2$$

for a neutral atmosphere. These relationships give

$$k = 5.78 \ u^{*2}$$

Assuming that this is true for the surface layer where τ is constant and using the Eq. (5.4), one can obtain

$$C_k = 0.416$$

Experimental observations show that very near the wall convection and diffusion of the turbulent kinetic energy (k)

are usually negligible. Thus, generation and dissipation of the turbulent kinetic energy are in balance. With this empirical fact, we will obtain

$$C_\mu = 0.03$$

The values of C_1, C_2, σ_k and σ_ε will be selected to be 1.44, 1.92, 1.0 and 1.3, respectively, which were proposed by Launder and Spalding (1974). It is noted that a different value for C_2, i.e., $C_2 = 2.08$, is chosen for the rectangular block case based on numerical experience in the present study and available experiments.

Algorithm of the Finite-Difference Method

In the iteration procedure, the field is swept in the direction left to right from the upper boundary to the lower boundary. The time-marching procedure is described by the following steps:

1. Specify initial values for all the variables ψ, ω, k, and ε at time $t = 0$.
2. Solve ω, k, and ε equations at time $t+\Delta t$.
3. Iterate for new ψ values by solving the Poisson equation using the new ω distribution.
4. Update the boundary conditions for ω, k, and ε.
5. Return to step 2 if the solution is not converged.

6. Find the velocity components from the ψ distribution and find the eddy vicosity from the k and ε distributions.

One iteration cycle is completed when all four equations have been solved. The iteration process is continued until the following convergence criterion has been satisfied:

$$\left\{\frac{\Phi^{n}-\Phi^{n-1}}{\Phi^{n}}\right\}_{max} \leq 0.03 - 0.05$$

A second convergence criterion may also be used:

$$\left\{\frac{\Phi^{n} - \Phi^{n-1}}{\Phi^{n-1}_{max}}\right\}_{max} \leq 0.00001 - 0.00005$$

This is sometimes necessary because of the fact that when the magnitude of the Φ-value at a particular node becomes very small, the variation, $\Phi^{n}-\Phi^{n-1}$, at that node can still be large since it depends on the values at the surrounding nodes; and thus the first criterion is sometimes difficult to satisfy even though the rest of the field has converged (Gosman et al., 1969).

It is noted that this modified Gosman's scheme has been tested to solve the driven cavity problem and has yielded good results compared with experiments and other numerical solutions.

CHAPTER 6. RESULTS AND DISCUSSIONS

Based on experimental evidence, the perturbation in the original boundary layer primarily depends upon the ratio of step height to boundary layer thickness, h/δ_r. Generally, the disturbance is classified as follows:

1. Overwhelming perturbation: $h/\delta_r >> 1$.
2. Strong perturbation: $h/\delta_r = O(1)$.
3. Weak perturbation: $h/\delta_r << 1$.

Obviously, the overwhelming perturbation will yield the largest pressure variation and separation region. Most of the wind tunnel tests have been done for the measurement of strong and overwhelming perturbations. Since the atmospheric boundary layer is relatively much larger than any step height, we are actually considering the weak perturbance in the present study.

The friction speed u* is specified to be 0.75 m/sec throughout the study. Different surface roughness heights (z_o) will be examined for comparisons:

1. $z_o = 0.01$ m
2. $z_o = 0.03$ m
3. $z_o = 0.045$ m
4. $z_o = 0.075$ m
5. $z_o = 0.2$ m

It is noted that the ratio z_o/h is also a characteristic parameter similar to h/δ_r. The smaller z_o/h is, the larger

the disturbance will be, due to the larger amount of mass displaced.

The Successive-Over-Relaxation technique is utilized to solve the Poisson ψ equation with relaxation parameter equal to 1.25. The time step Δt is set to be 0.01 (based on numerical experience) while using the time-marching approach to solve ω, k, and ε equations simultaneously. It turns out that about 1500 time steps are required to obtain the convergent solutions with convergence criterion in the range 0.03 - 0.05. Experience shows that k and ε solutions always converge much faster than ψ and ω.

Flow Pattern Estimations

For a viscous flow, the phenomenon of separation occurs due either to the influence of both viscosity and adverse pressure gradient or to an abrupt change of geometry. Both effects can be observed in the flow patterns from our numerical solutions. Based on these numerical solutions, the flow properties are examined and interpreted physically.

Forward-facing step

Results for the forward-facing step (Figure 14.a) show a small separated region at the base corner and another at the top. The shape of these separation regions vary with the surface roughness parameter z_o. The top reattachment length changes substantially, while the front eddy size

varies only slightly. Figures 15 and 16 show the geometry of the separation and reattachment regions as characteristics by the distances Xs, Zr, and Xr.

It is found that a decrease in z_o will produce small front separation regions which tend to approach some asymptotic value for a smooth surface. This is expected since roughness reduces the velocity near the surface, decreasing the momentum available to overcome the adverse pressure gradient forces.

The reattachment length Xr is increasing with decreasing z_o, implying a smoother surface or larger step height would have a larger top separation. For smaller z_o, the mass flow rate is larger and the flow carries more mass near the wall. The protrusion of the step will create a locally accelerated flow region. In accordance with this flow acceleration, the turbulent intensities are smaller near the vicinity of the upper step corner and then yield lower effective viscosities and shear on the top of the step, causing Xr to increase. If z_o is large enough, the separation region is too thin and small to be found or separation even does not occur.

The typical distribution of surface pressure (p) along the streamwise direction and step face is shown in Figure 17 and 18, respectively. Qualitatively compared with the measurements by Taulbee and Robertson (1972) in Figures 19

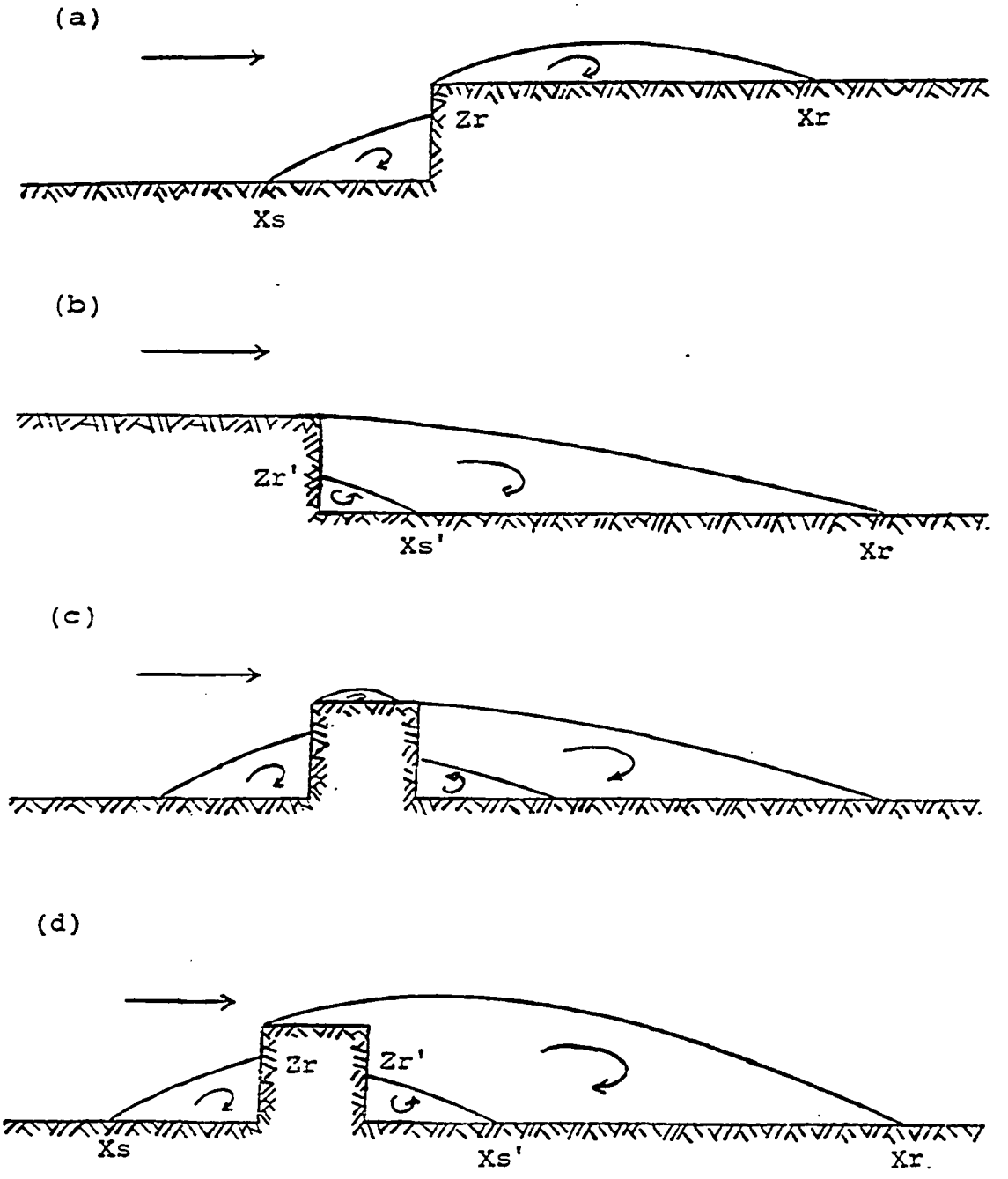

FIGURE 14. Flow zones near (a) a forward-facing step, (b) a backward-facing step, and (c), (d) a rectangular block

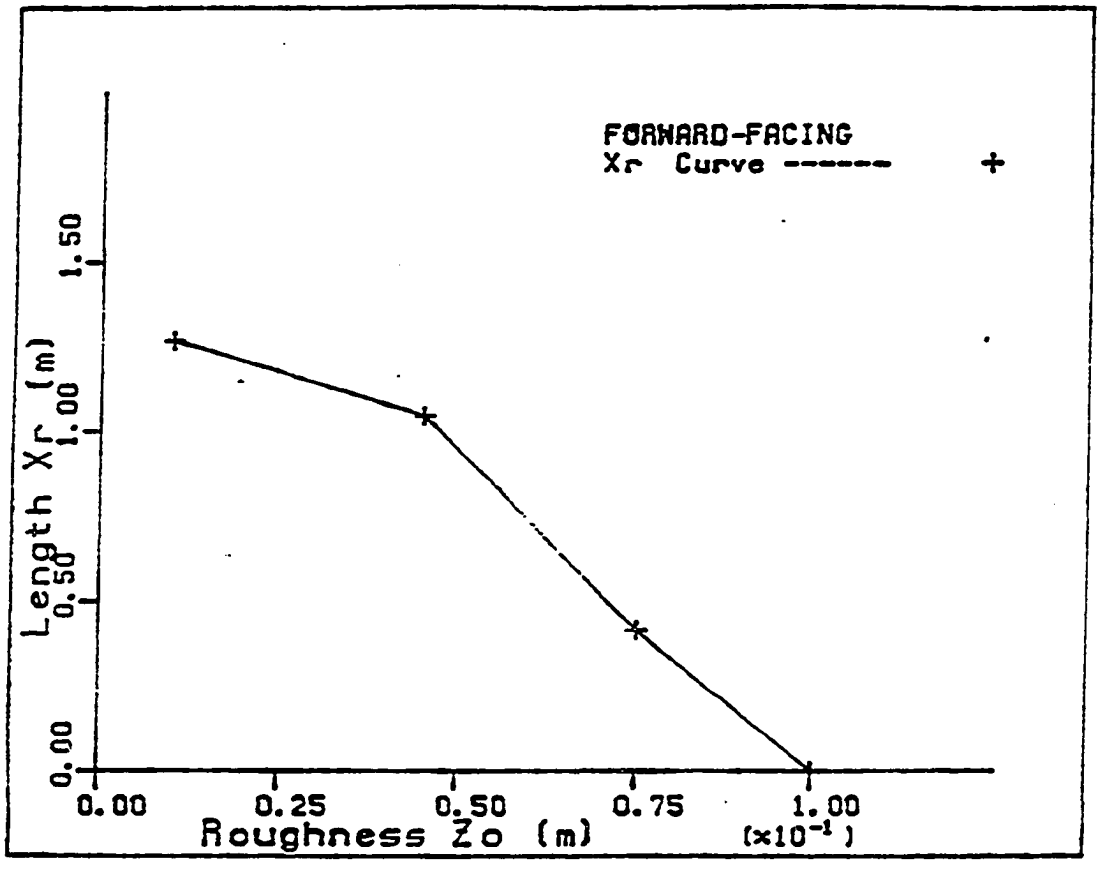

FIGURE 15. Reattachment length of top separation region for forward-facing step flow

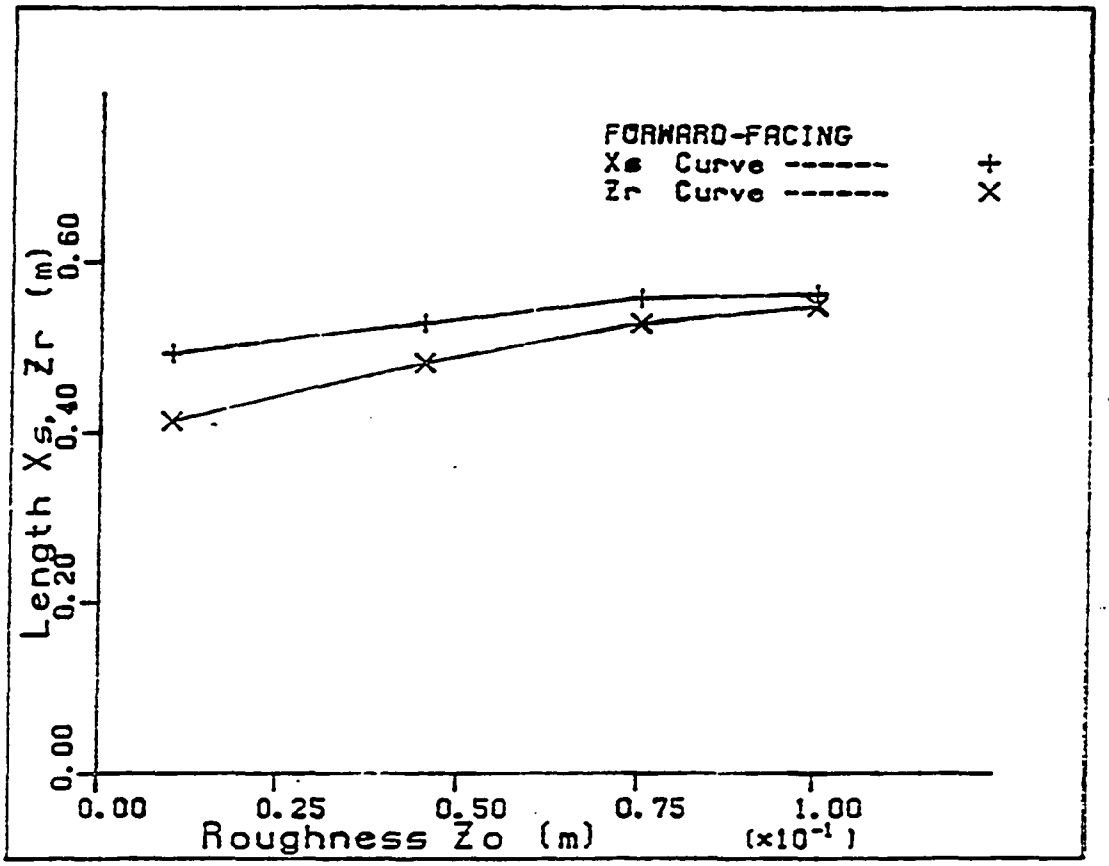

FIGURE 16. Forward separation region for forward-facing step flow

and 20, the wall pressure distribution is well-predicted. Upstream of the step, a smaller z_o produces a stronger adverse pressure gradient. The wall pressure on the step face is increasing upwards to reach a maximum and then decreasing. The position of this maximum can be interpreted as the location of the stagnation point.

In spite of the larger pressure loss at the top corner for smaller z_o, the pressure is, however, increasing along the top surface with a higher rate again.

Backward-facing step

For the backward-facing step (Figure 14.b), there are two contra-rotating eddies resulting in the solutions, the corner eddy being the smaller one and rotating in the counter-clockwise direction, and the recirculation eddy being the larger one and rotating in the clockwise direction. The size of the corner eddy varies slightly with z_o. However, the larger recirculation region is sensitive to z_o. Figures 21 and 22 show the relations of the distances Xs', Zr' and Xr, and the surface roughness height z_o. When the flow separates from the corner, a shear layer with high initial vorticity level and low static pressure spreads out with downstream distance. Similar to that for the forward-facing step, the fuller approach velocity profile yields both higher momentum and lower turbulence intensity level near the wall, so the reattachment length Xr

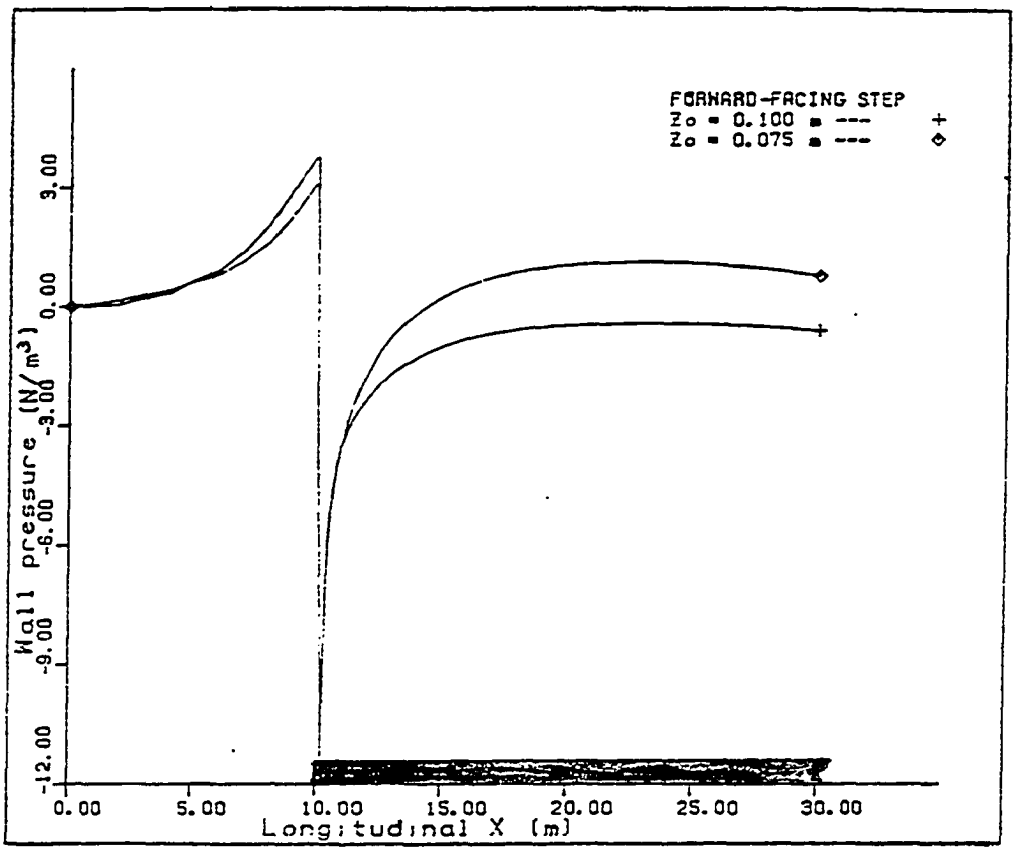

FIGURE 17. Wall pressure distribution in the longitudinal direction for forward-facing step flow

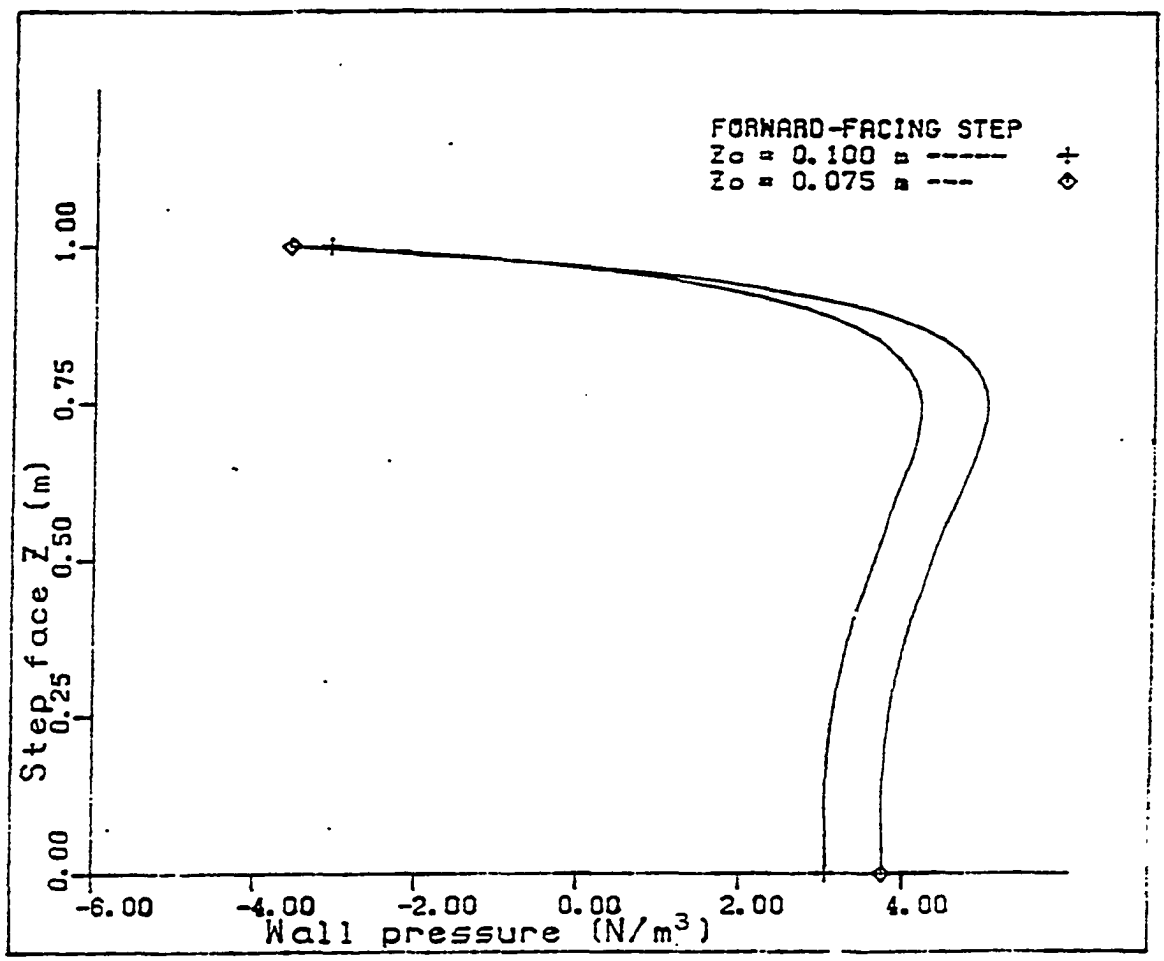

FIGURE 18. Wall pressure distribution on the step face for forward-facing step flow

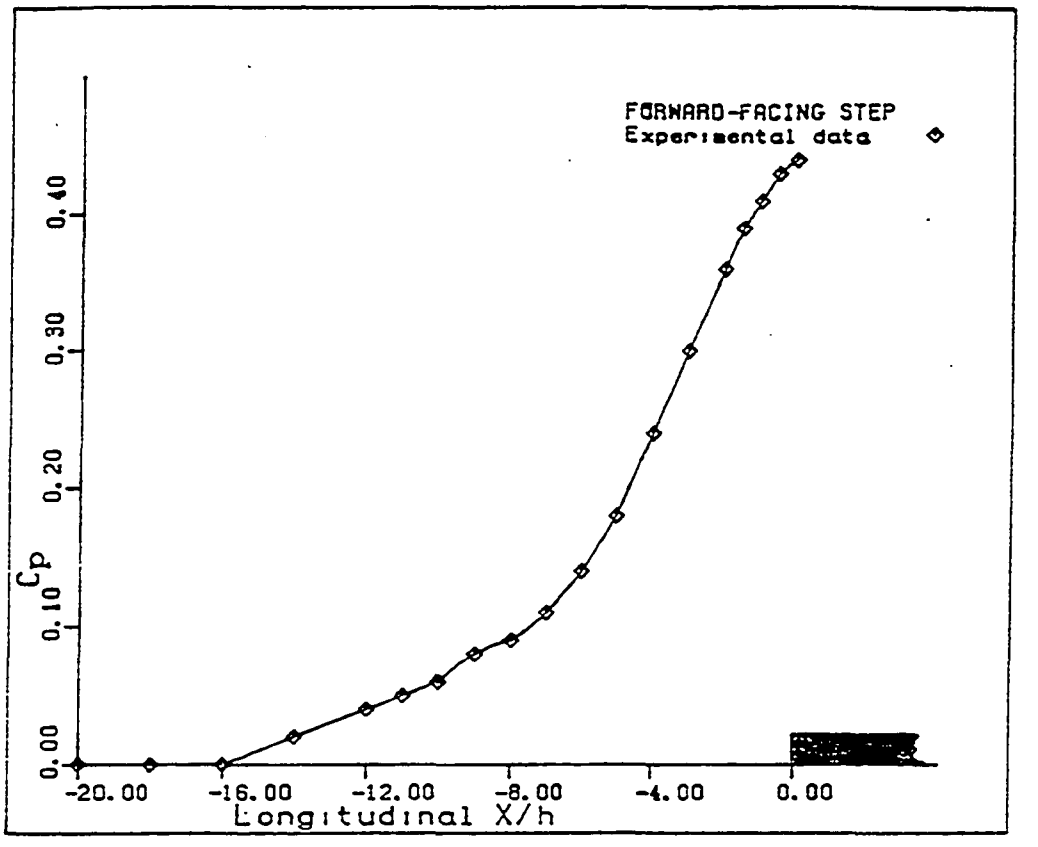

FIGURE 19. Wall pressure distribution in the longitudinal direction for forward-facing step flow (Taulbee and Robertson, 1972)

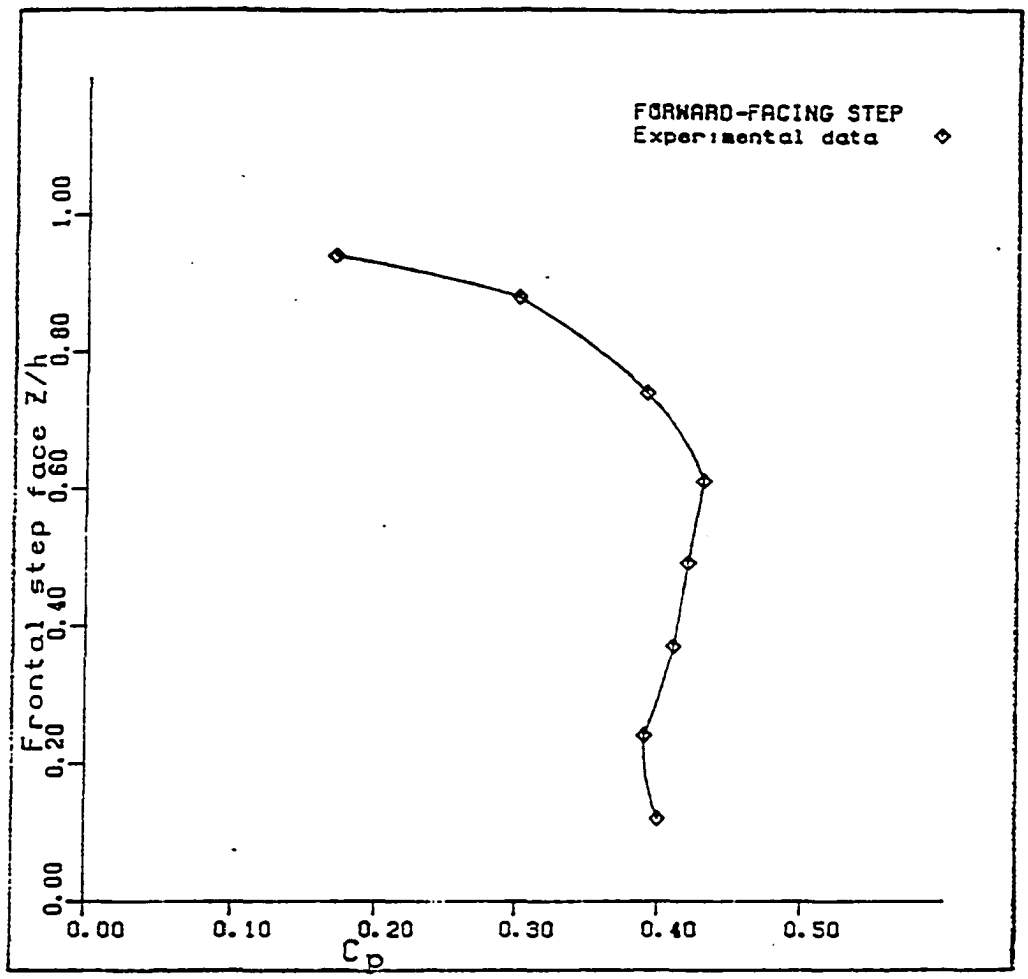

FIGURE 20. Wall pressure distribution on the step face for forward-facing step flow (Taulbee and Robertson, 1972)

is larger for a smaller z_o.

The size of the corner eddy, exemplified by the values Xs' and Zr', is found to be increasing with z_o and then decreasing. This small eddy is formed as a result of a shear-layer separation which is induced by the reverse flow now approaching the step as a forward-facing step.

Figures 23 and 24 give the numerical solutions for surface pressure distributions. These calculations are compared with to Tani et al.'s (1961) measurements and Atkin et al.'s (1980) measurements shown in Figures 25.a and 25.b, respectively. Again, we see the surface pressure distributions of numerical predictions are of the correct shape over most of the region. The surface pressure, for smaller z_o, increases first as x increases and then decreases with a higher and faster rate close to the corner, and yields less pressure loss in the backward region. In the downstream the pressure is increasing and reaching a maximum then decreasing very slowly. This maximum pressure is higher for smaller z_o.

For backward-facing step flow, Tani et al. (1961), Bradshaw et al. (1972), and Denham et al. (1975) all found in their experiments that the reattachment length is about six to seven step heights downstream of the step. Taulbee and Robertson (1972) and Bowen and Lindley (1974) observed that the frontal eddy for the forward-facing step occurs at

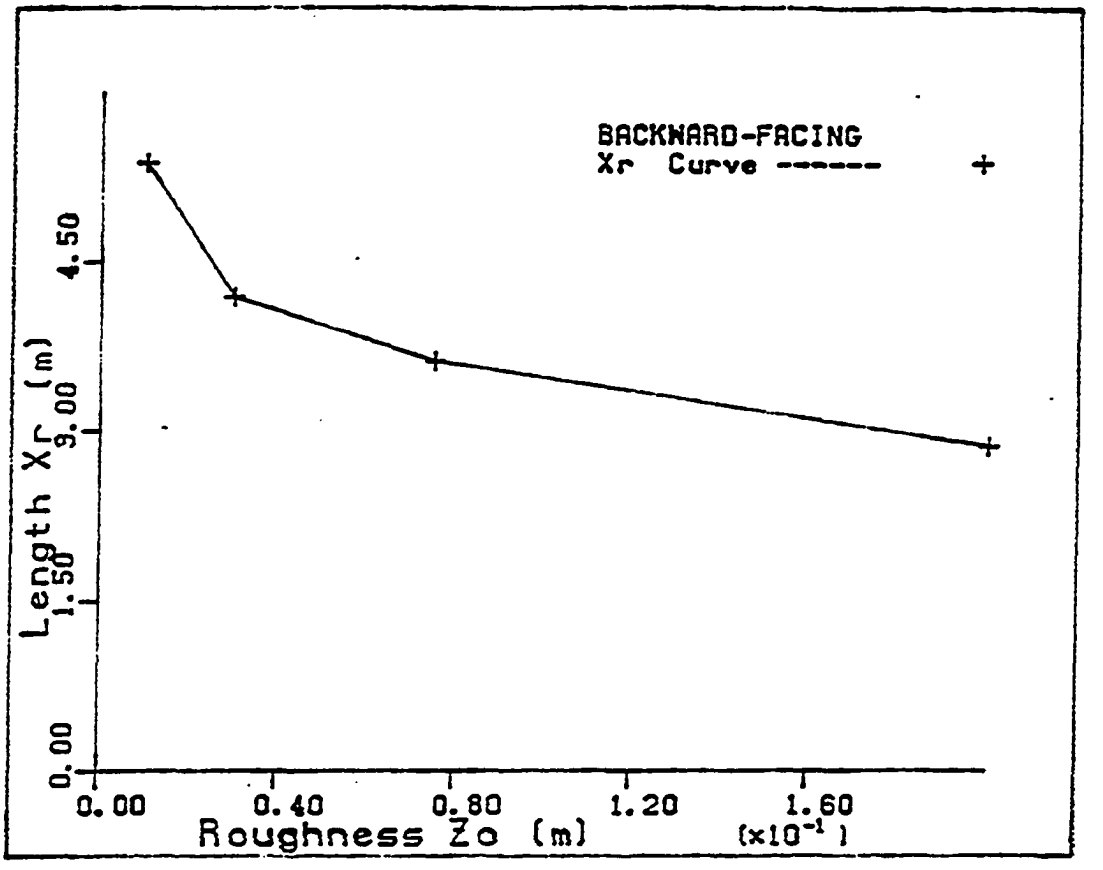

FIGURE 21. Reattachment length of separation region for backward-facing step flow

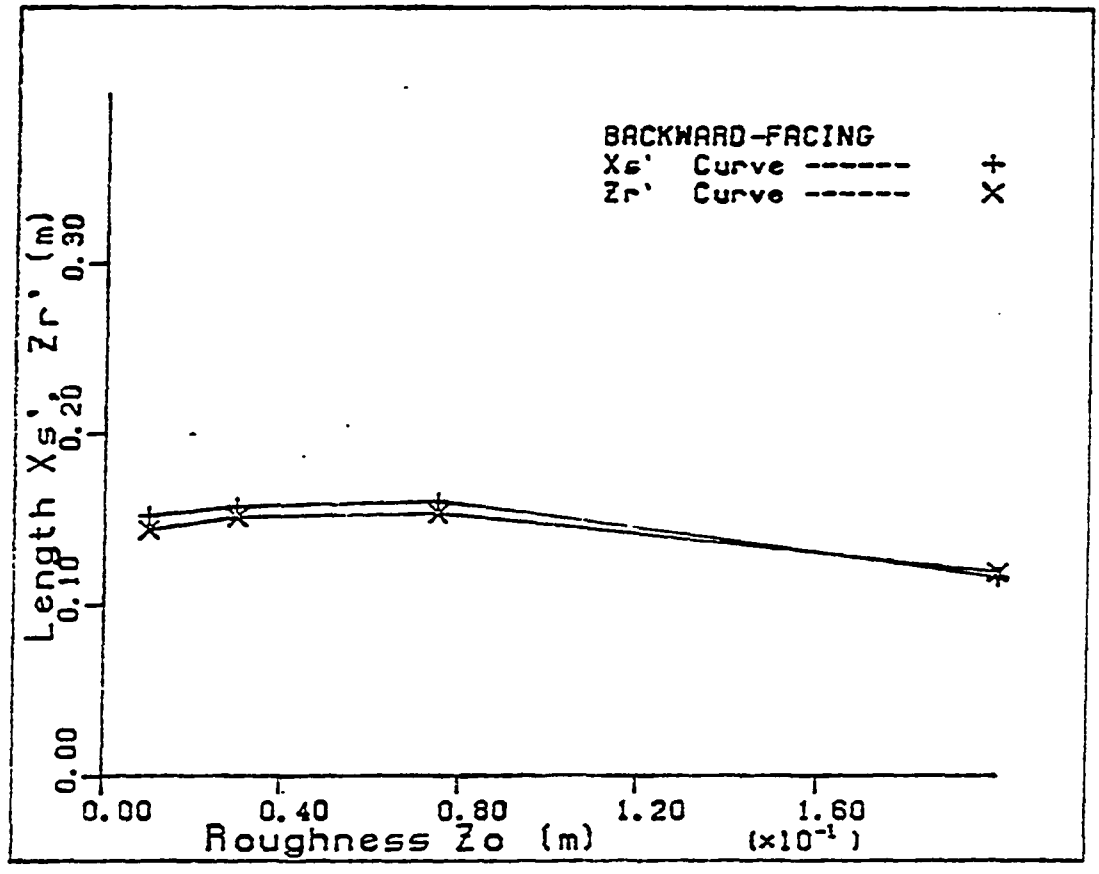

FIGURE 22. Corner eddy region for backward-facing step flow

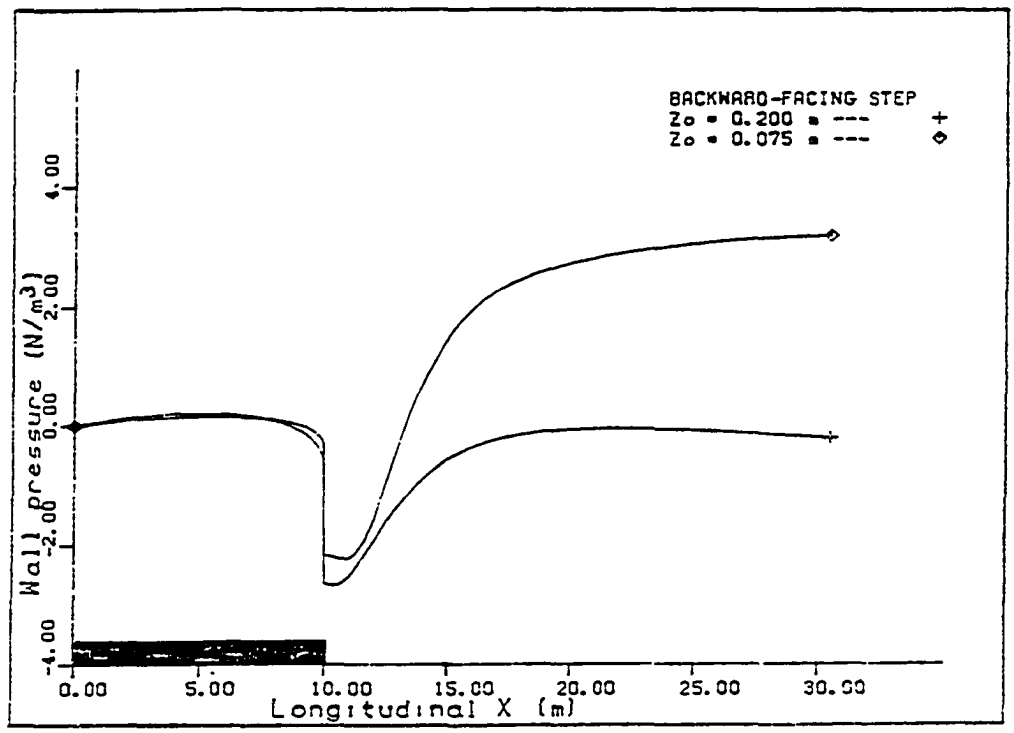

FIGURE 23. Wall pressure distribution in the longitudinal direction for backward-facing step flow

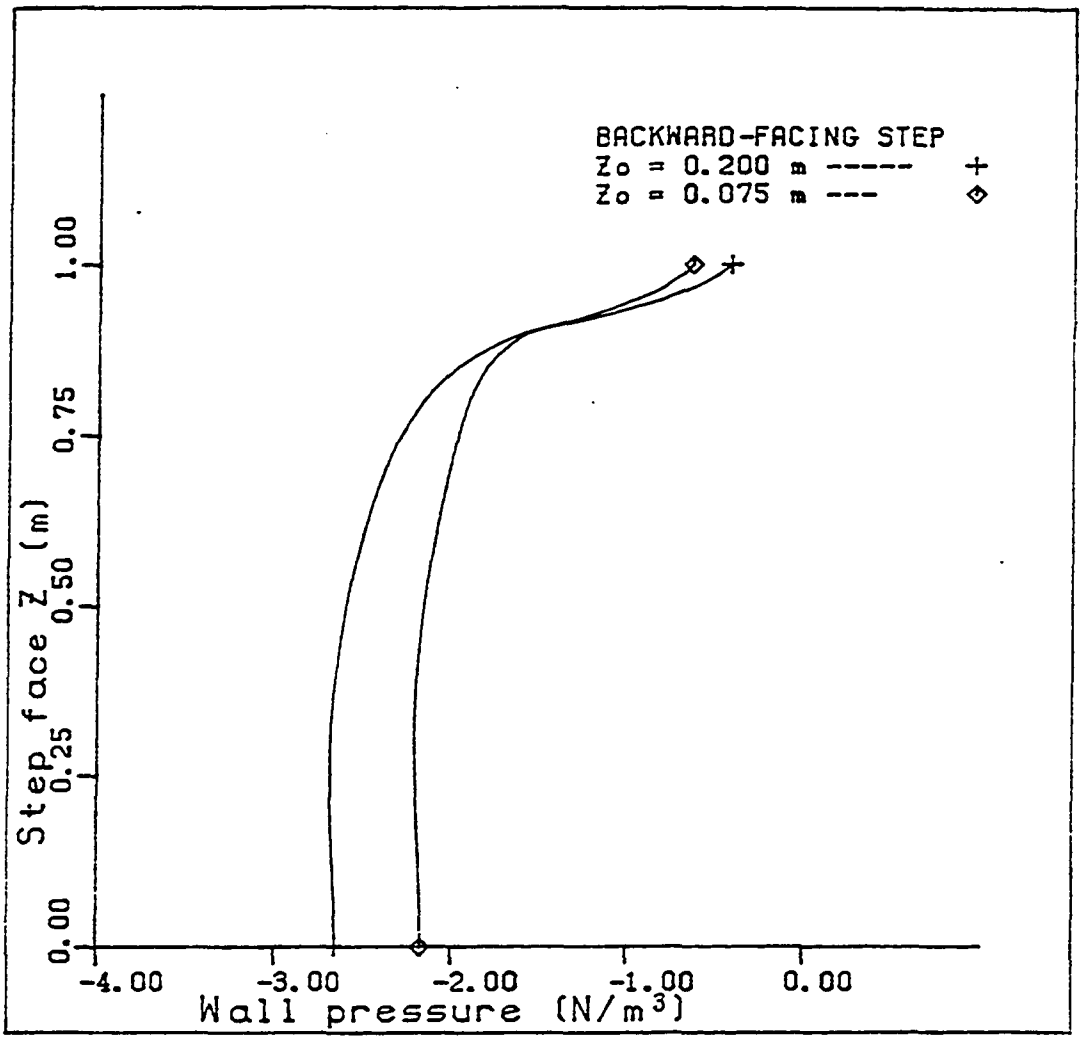

FIGURE 24. Wall pressure distribution on the step face for backward-facing step flow

(a)

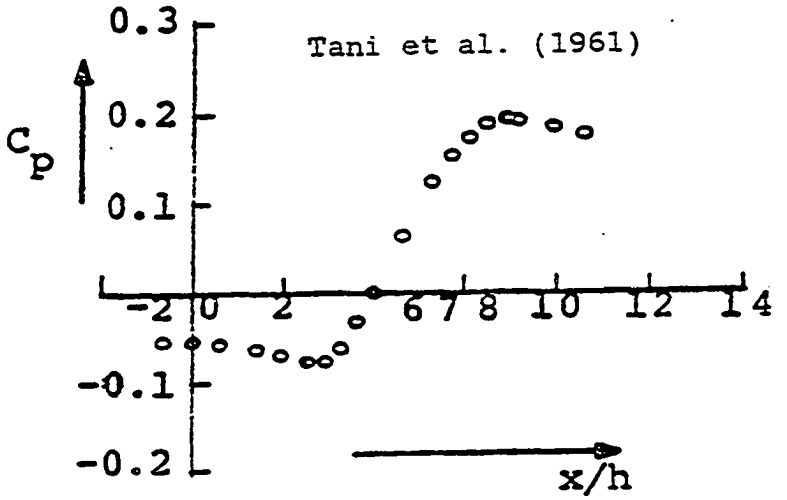

(b)

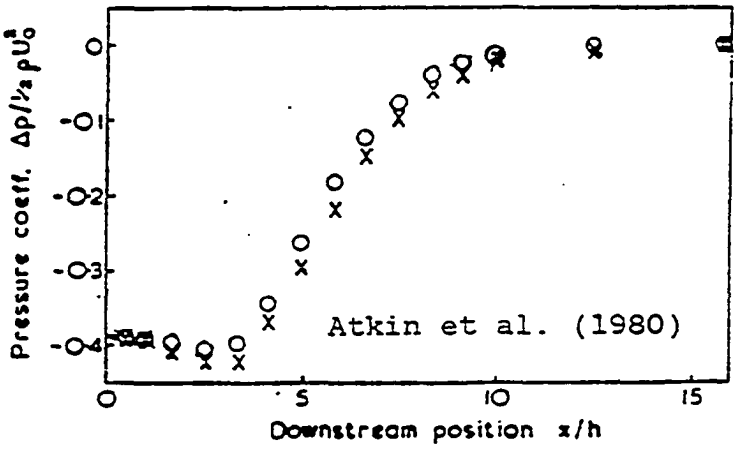

FIGURE 25. Wall pressure distribution in the longitudinal direction for backward-facing step flow (Tani et al. (1961) and Atkin et al. (1980))

about one step height upstream. No information about the surface roughness parameter z_o was given in all of the above works, it is believed that the surfaces were rather smooth. Compared with their experimental data, our numerical prediction of separation region seems somewhat underestimated. This is expected because the present calculations are for weak perturbation flow ($h/\delta_r << 1$) while their wind tunnel tests are for strong perturbation flow ($h/\delta_r = O(1)$).

Rectangular block

The flow over a rectangular block consists of the flow patterns for both the forward-facing step and the backward-facing step (Figure 14.c). If the surface roughness parameter z_o is sufficiently small or the block is not long enough, the roof reattachment will not occur (Figure 14.d). The relationships of the characteristic lengths (Xs, Zr, Xs', Zr', and Xr) and z_o are similar to those for forward- and backward-facing steps discussed above and are shown in Figures 26, 27, and 28.

It is interesting that the stream function (ψ) solution for z_o = 0.075 m reveals no roof separation. However, from the vorticity (ω) distribution, it is found that there does exist a roof separation region with the reattachment length equal to 0.3 H from the leading edge. This implies that the roof separation region may be too small and thin to be

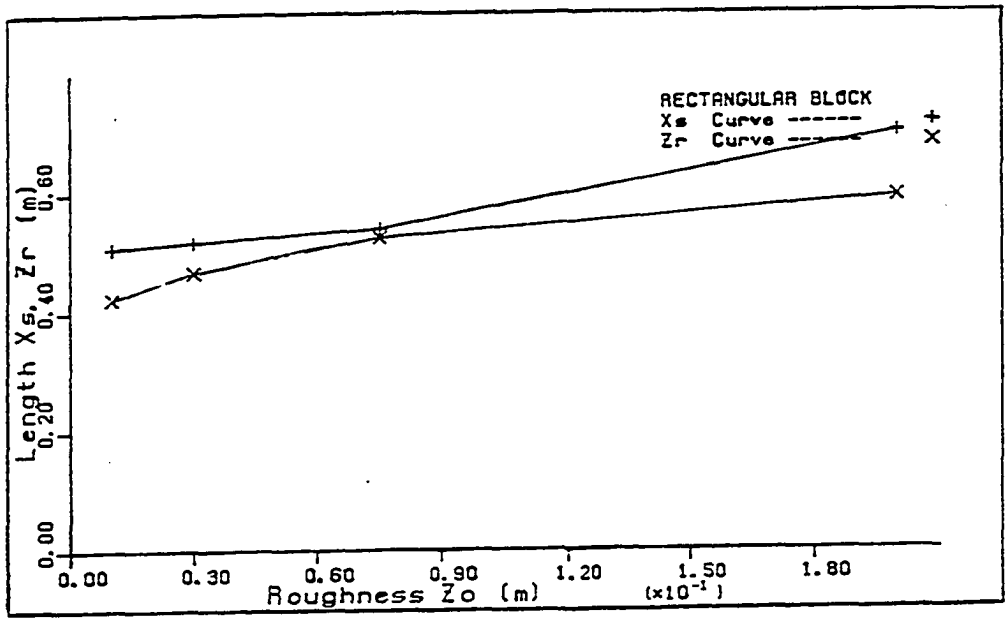

FIGURE 26. Forward separation region for rectangular block flow

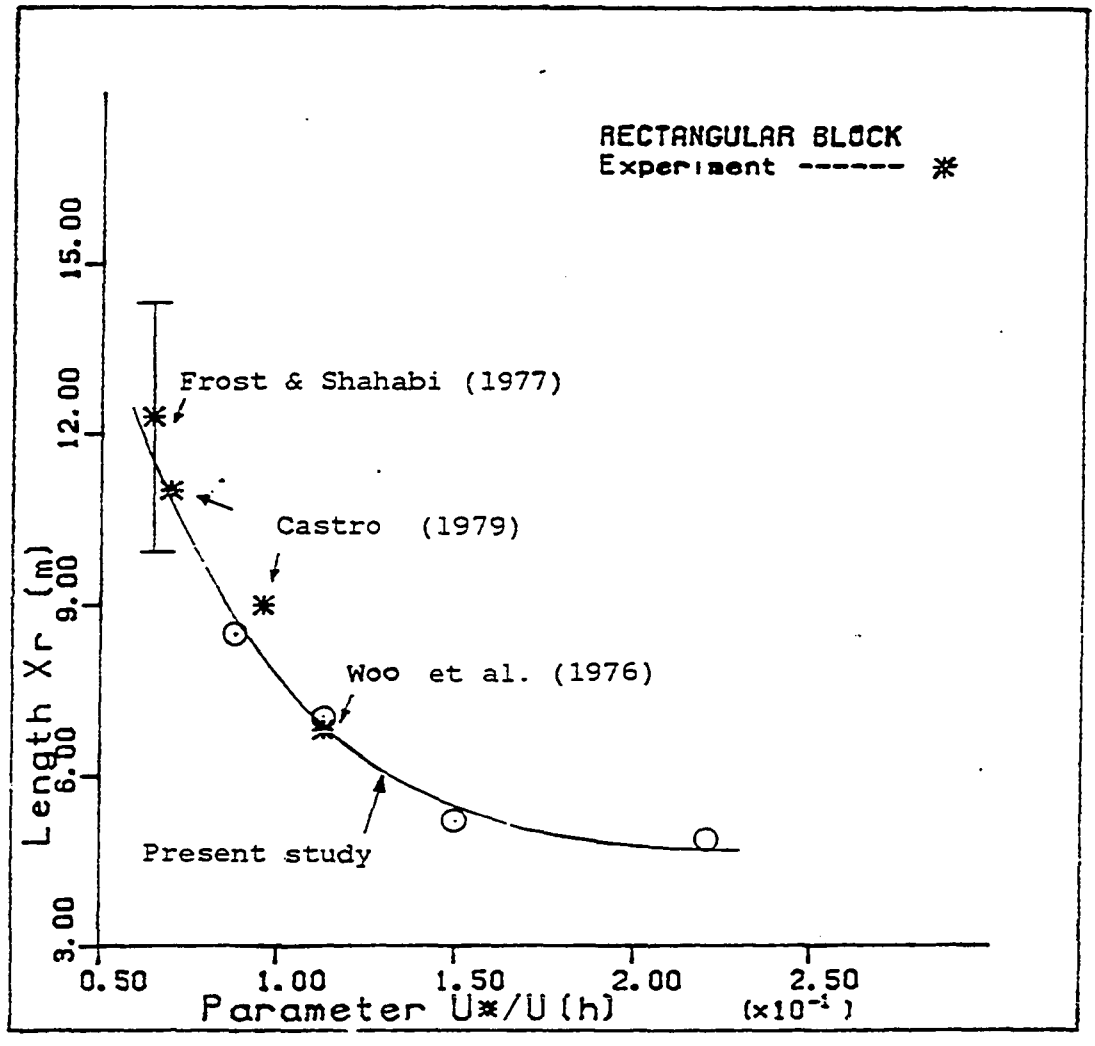

FIGURE 27. Reattachment length of separation region for rectangular block flow

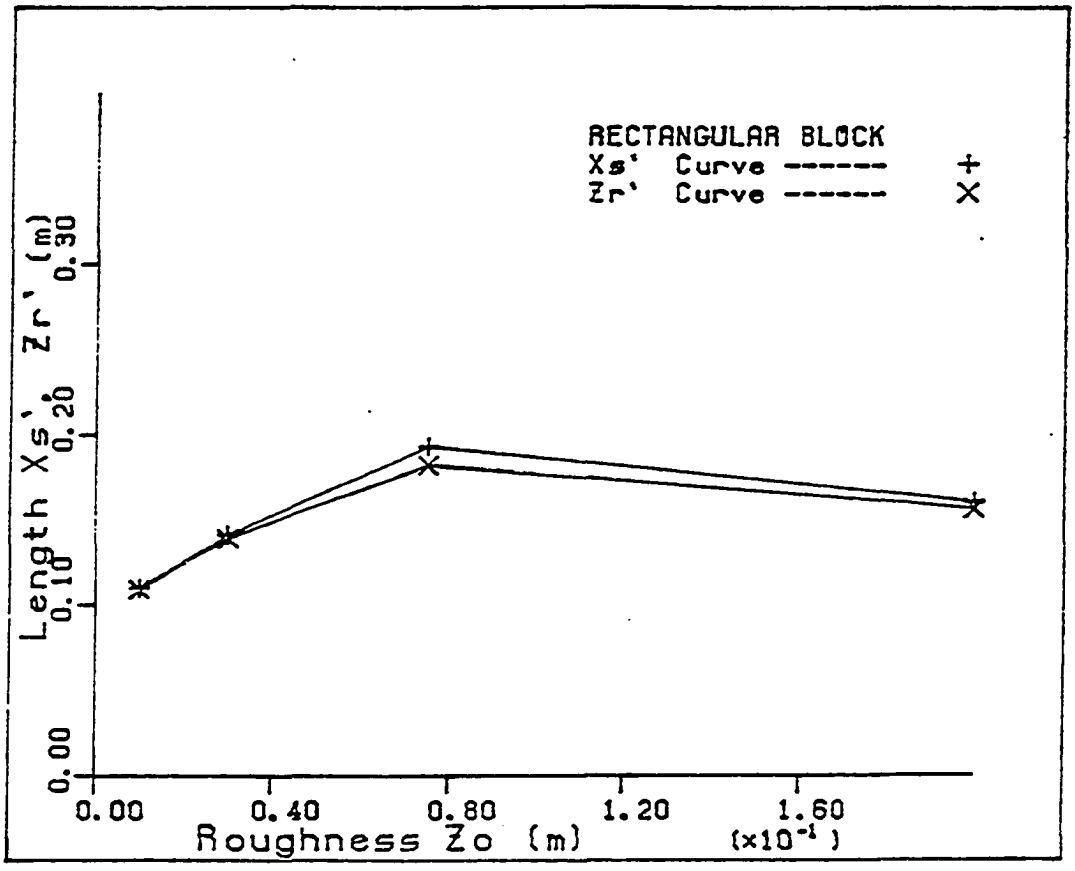

FIGURE 28. Corner eddy region for rectangular block flow

observed from the ψ distribution if z_o is sufficiently large. The assertion that the flow may remain attached on the roof when z_o is large (or the turbulence intensity level is high) is also supported by the experimental works of Ogawa et al. (1983a,b).

It is noted that in Figure 27 we have the plot Xr vs. u^*/U_h instead of Xr vs. z_o due to the availability of experimental data. The numerical data have been smoothed to a continuous curve and are, although somewhat underestimated, in reasonable agreement with measurements.

The calculated wall pressure distributions in Figure 29 to 31 are in good qualitative agreement with the measurements of Crabb et al. (1977) in Figure 32. The effects are similar to the combined effects of forward- and backward-facing steps. As h/z_o decreases (i.e., for larger z_o), the adverse pressure gradient upstream of the block is less strong so that the drag and overturning moment decrease, as expected. It is also observed that there is a significant pressure recovery on the top surface. This rate of pressure recovery is higher for larger h/z_o. The pressure distribution is rather uniform on both step faces except for the regions near the upper corners.

The longitudinal friction speed (u*) distributions for all three cases are shown in Figures 33 to 35. Corresponding to the larger adverse pressure gradient

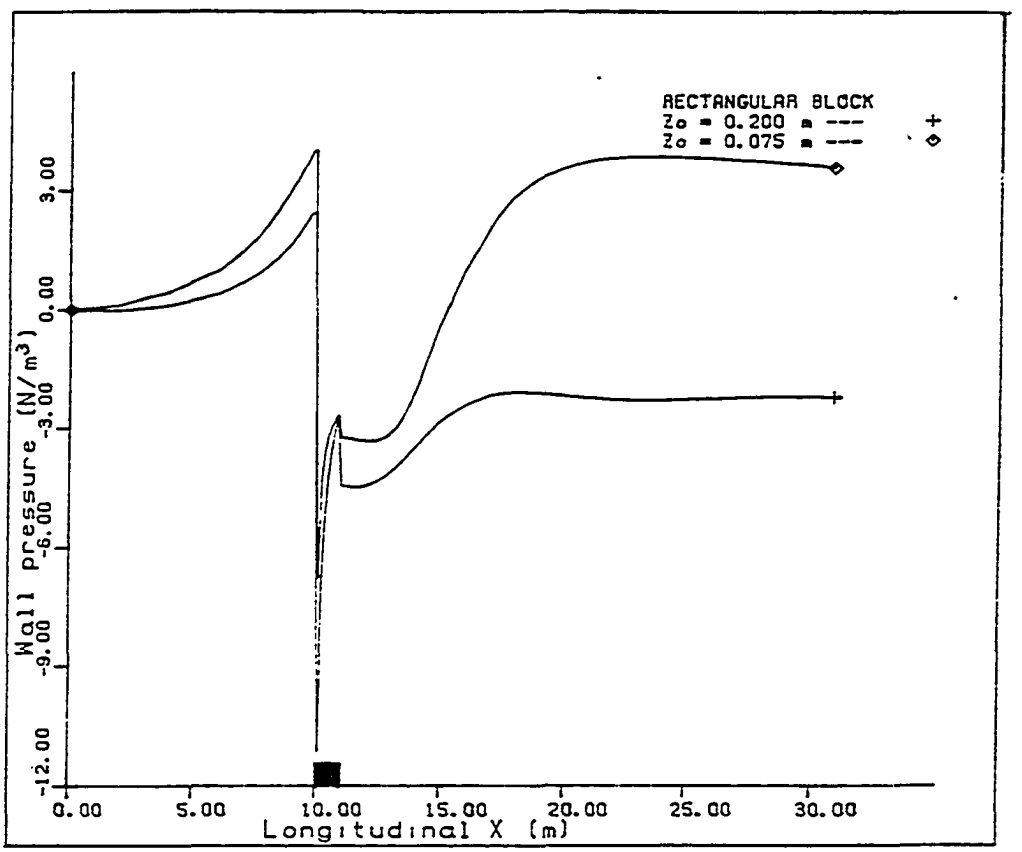

FIGURE 29. Wall pressure distribution in the longitudinal direction for rectangular block flow

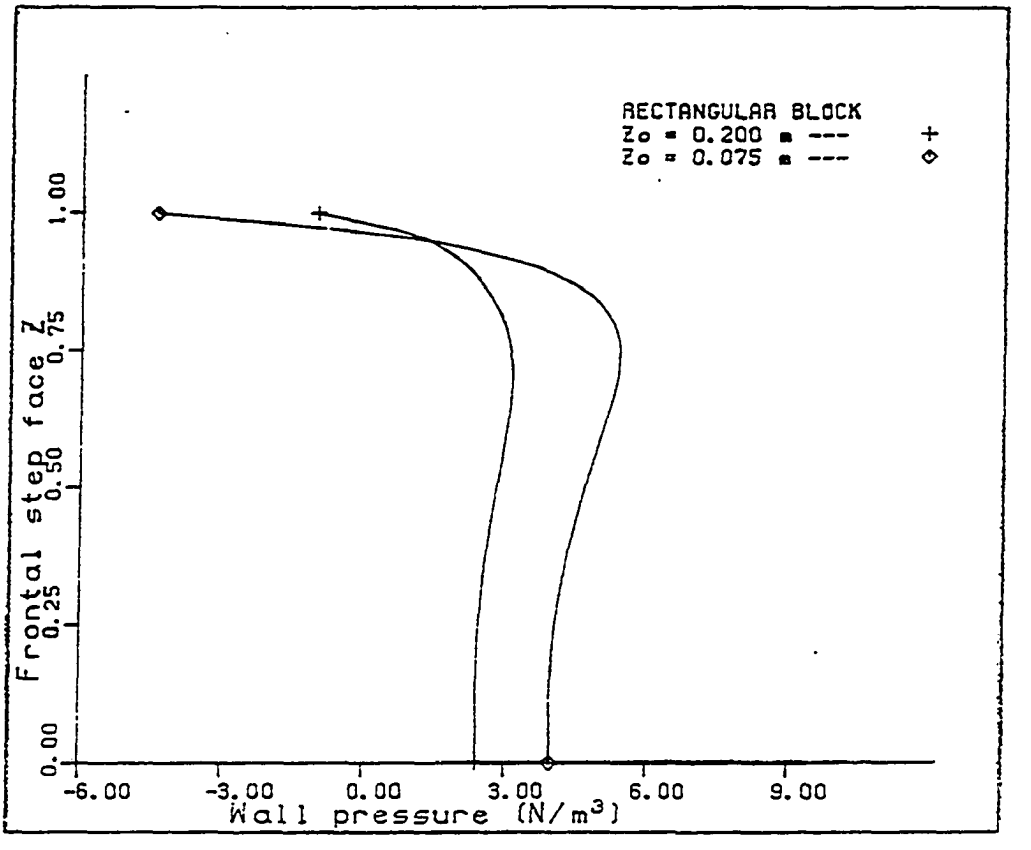

FIGURE 30. Wall pressure distribution on the frontal step face for rectangular block flow

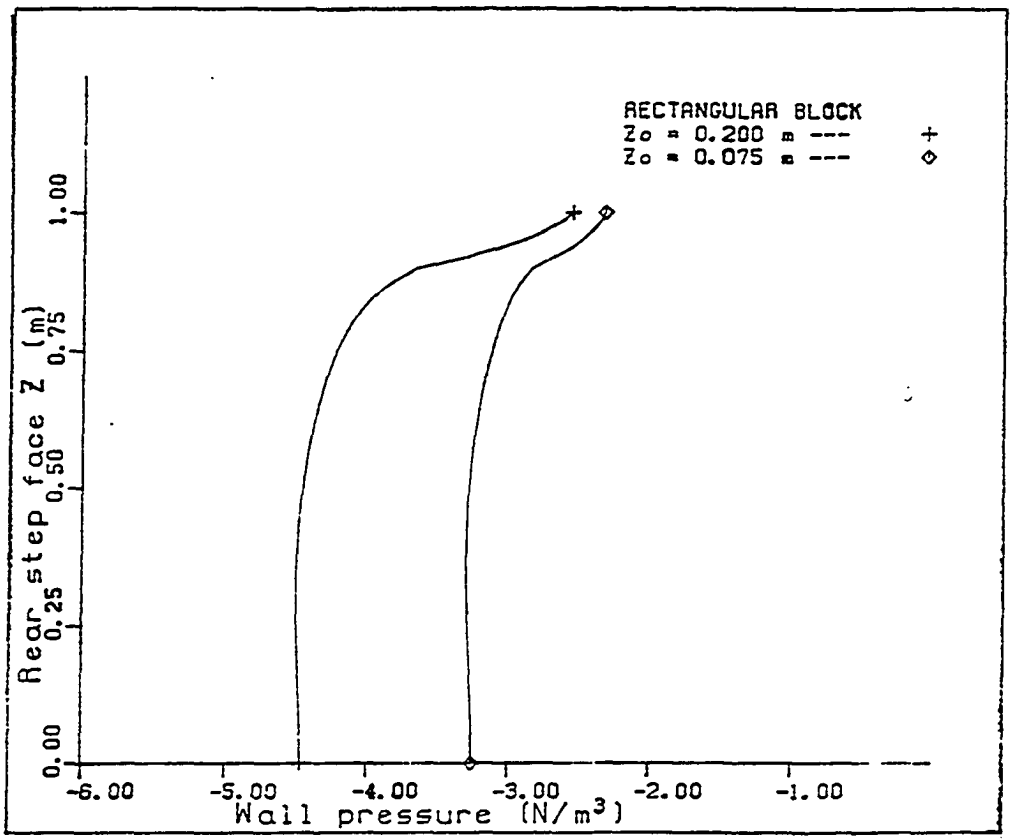

FIGURE 31. Wall pressure distribution on the rear step face for rectangular block flow

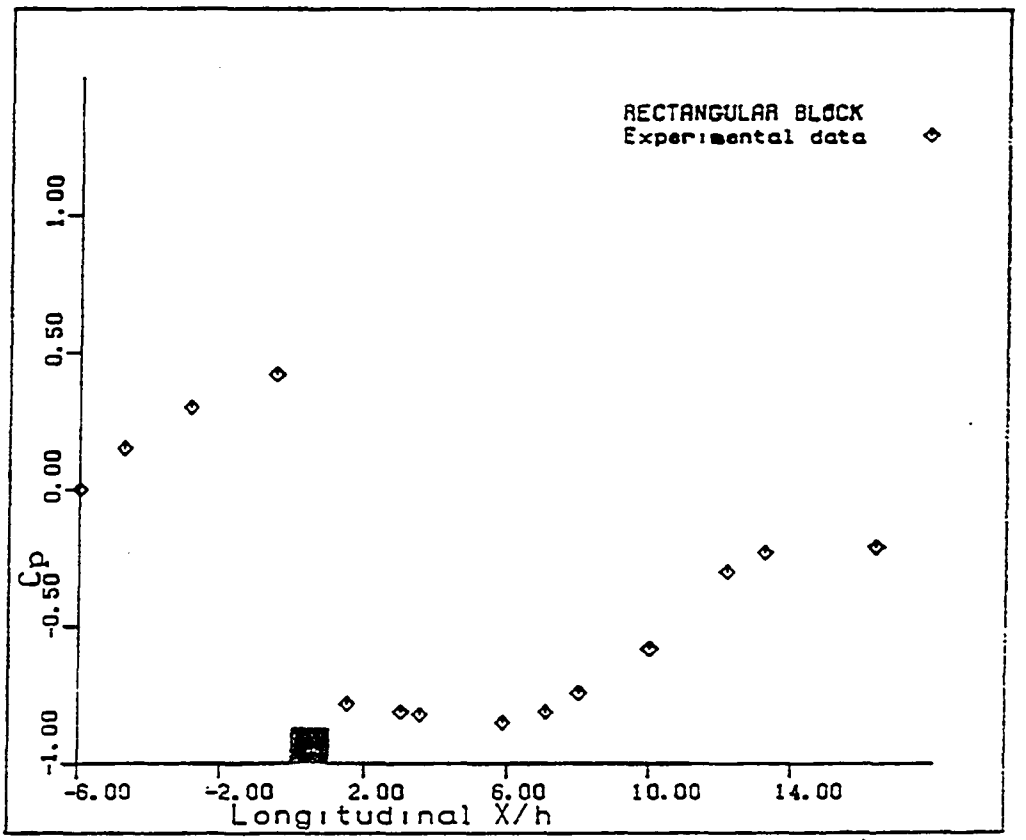

FIGURE 32. Wall pressure distribution in the longitudinal direction for rectangular block flow (Crabb et al., 1977)

upstream of the step, the friction speed gradient is more negative for smaller z_o. The negative values of u* correspond to the reverse flow region. The friction speed results from the effective viscosity and the wall vorticity (or velocity gradient). In the vicinity of frontal corners, smaller z_o yields larger friction speed due to larger wall vorticity. However, in the vicinity of rear corners, the larger z_o results in larger friction speed due to larger effective viscosity, although the wall vorticity is smaller.

Although the numerical predictions are qualitatively in good agreement with the observations, the experimental measurements are definitely necessary to investigate the validity of the numerical model in a quantitative sense. We may adjust the turbulence-model constants to improve the numerical solutions or to fit the experimental measurements.

According to numerical experience, a larger separation region can be obtained by making any one of the following adjustments:

1. decreasing C_μ
2. increasing C_1
3. decreasing C_2
4. decreasing C_k

It is noted that, based on the numerical experience, the separation region is found to be fairly sensitive to the values of C_1 and C_2.

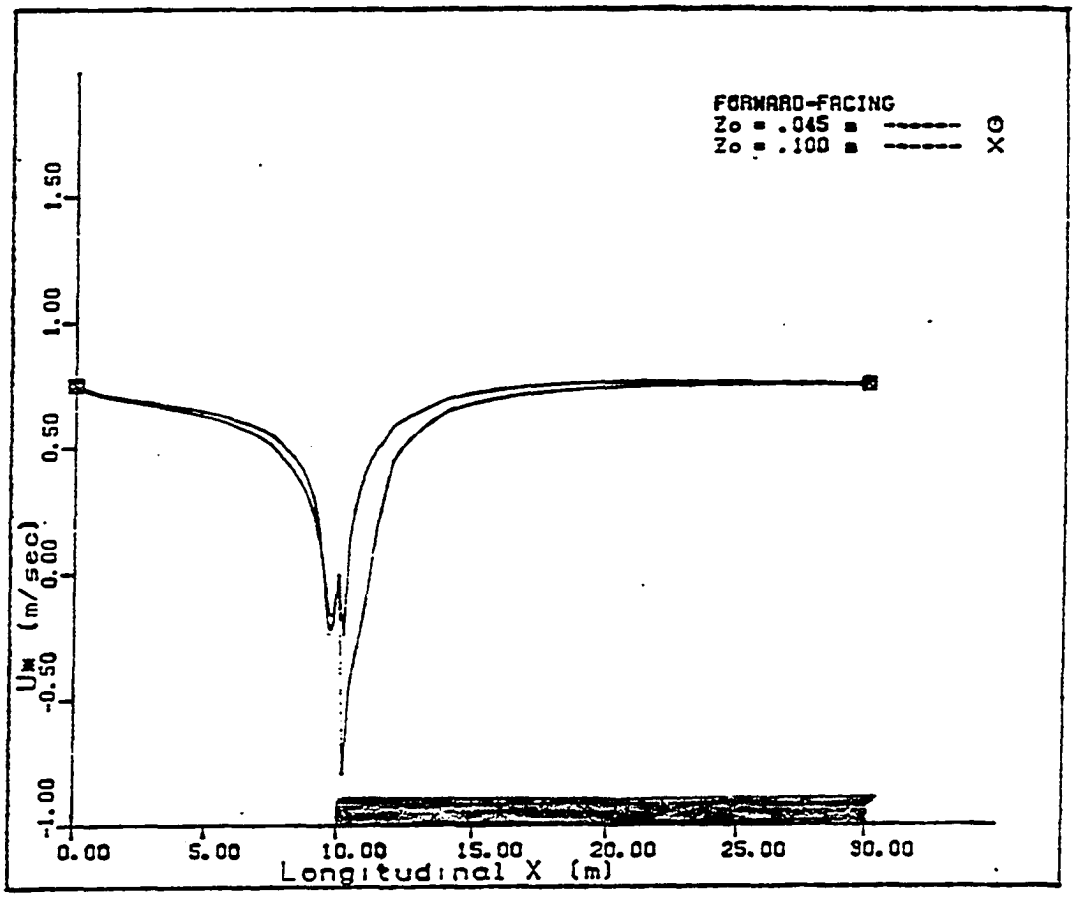

FIGURE 33. Friction speed distribution in the longitudinal direction for forward-facing step flow

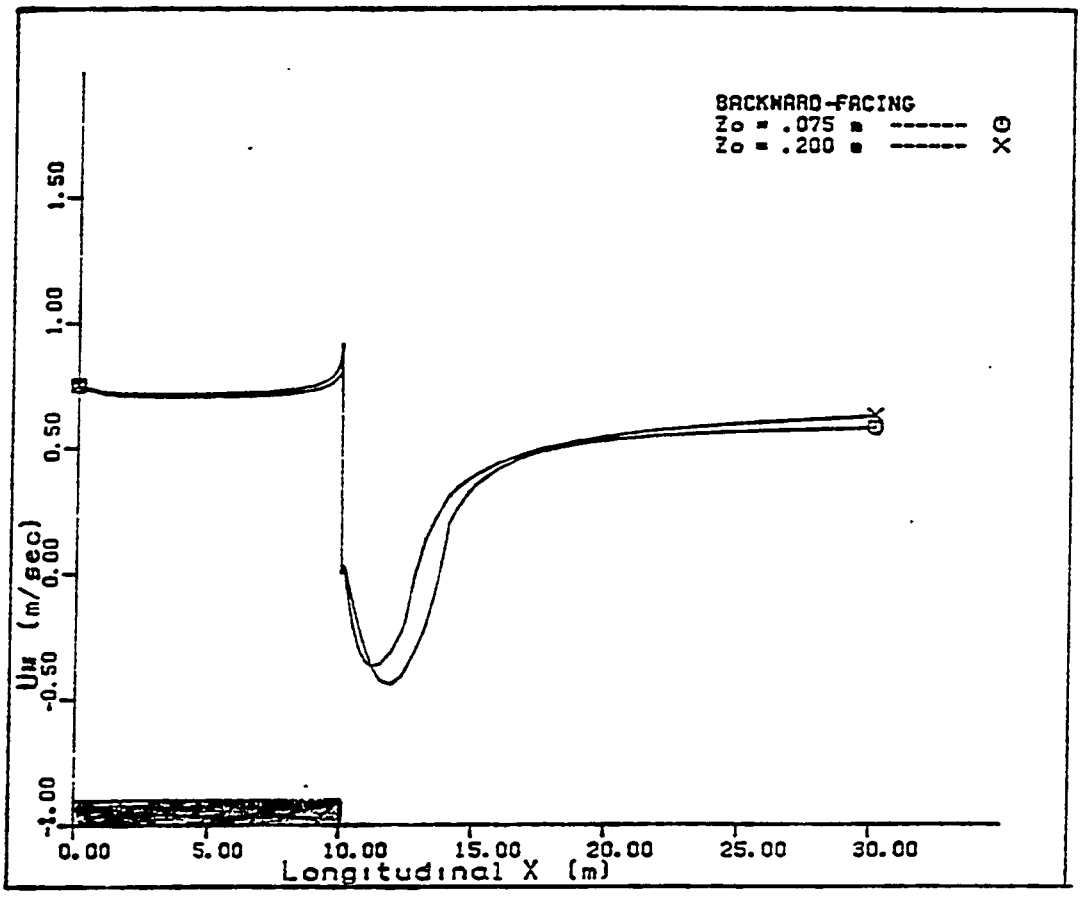

FIGURE 34. Friction speed distribution in the longitudinal direction for backward-facing step flow

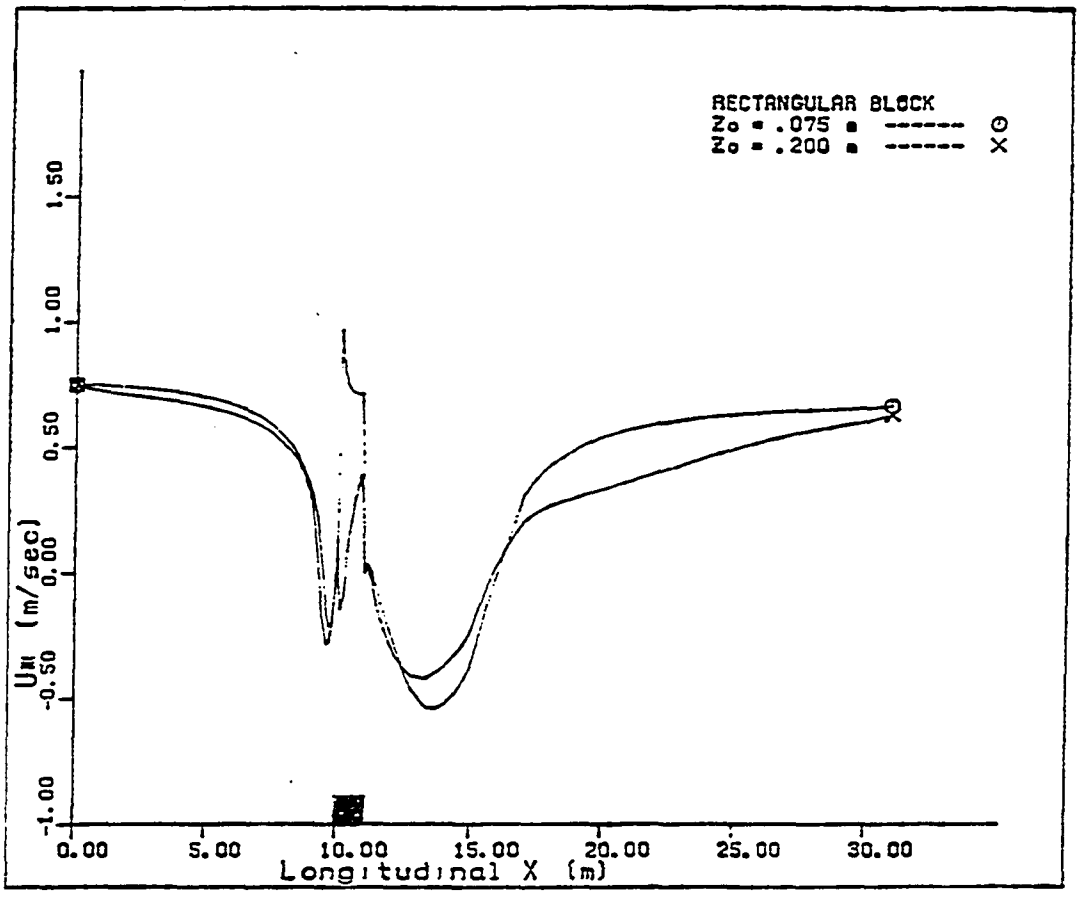

FIGURE 35. Friction speed distribution in the longitudinal direction for rectangular block flow

Some factors may also cause the discrepancy between the numerical solutions and experimental measurements:

1. The weakness of the turbulence model. No turbulence model can totally describe the flow turbulence. Also, it may not be satisfactory to use one set of turbulence-model constants for the entire complex flow region. Those constants are all empirically determined.
2. The artificial viscosity error associated with the finite-difference scheme. Gosman's scheme is an upwind finite-difference scheme. In general, an upwind scheme will underpredict the gross features of the recirculation zone due to the false numerical diffusion associated with the upwind dependence of the convective term.
3. The coordinate system. Due to the large gradients near the wall and the coupling of the dependent variables (ψ, ω, k, ε) at the surface, the grid distribution should be carefully selected and the grid size must be very small in the large gradient regions.

Concentration and Deposition Estimation

Observations show that a two-dimensional obstruction creates an abrupt change in the concentration distribution. Near the upstream side of the obstruction, ground-level concentrations will be higher than would be observed in its absence. But, at downwind, the concentration is much reduced. The degree of the effects of the obstruction on concentration distribution is normally decreased with the distance of the source upstream from it and with the source height.

If a ground source is rather close upwind to the obstruction, most of the plume depth is inside the frontal eddy. The particles striking the obstruction's upwind face will be largely entrained into this frontal eddy. Then only a small portion of the effluent will be transported downstream of the body, where the resulting concentration is therefore rather low.

For the elevated source or for the ground source farther upwind of the obstruction, the plume may be relatively deeper than the frontal eddy of the obstruction. Relatively more particles can be diverted upward to pass around the obstruction and enter the downstream region. In this case, the downstream concentration compared to the upstream will not be as low as that in the previous case. If the flow that has separated from the upwind roof edge

reattaches on the roof of the obstruction, it will bring the effluent closer to the roof level and possibly induce relatively high concentration there. Otherwise, the incident plume will be deflected above the roof level and the concentration will be similar to that found on the rear face and will be even less in the cavity region.

Calculations of concentration

The flow pattern for z_o = 0.075 m and u* = 0.75 m/sec is selected for the concentration calculations. Lycopodium spores with diameter equal to 40 μm are considered as diffusing particles. The line source is located at fifteen step heights upwind of the obstruction with strength Q = 1 kg/sec m. The source height H and the associated power-law velocity profile $u = \alpha z^m$ are listed in Table 4.

TABLE 4. The source heights (H) and the corresponding numerical initial power-law velocities ($u = \alpha z^m$)

Source height H	α	m
0.00 m	5.80	0.58
0.50 m	5.00	0.49
1.00 m	4.80	0.36

With these power-law velocity distributions the initially numerical concentrations are approximated by appropriate Roberts' and Rounds' solutions calculated at 5 meters downstream of the source, which is determined by the method discussed in Chapter IV.

The numerical solutions of the ground concentration and source strength distributions for all the geometries are shown in Figures 36 to 43. For a ground source, the location of maximum concentration of vertical distribution is always at the ground level at any streamwise location. The ground concentration is decreasing monotonically along the downstream surface. For an elevated source, the location of maximum concentration of vertical distribution is located initially at the source height and moves toward the ground with distance downstream. At some point downstream, this vertical maximum will reach the ground and remain on the ground further downstream. The ground concentration is increasing from its minimum (actually, it is zero at source location) to a maximum downstream where the vertical maximum just reaches the ground, and then is decreasing monotonically. This concentration maximum occurs farther from the source for a higher elevated source. The magnitude of this concentration maximum is larger for the ground source because fewer particles are diffused into the air.

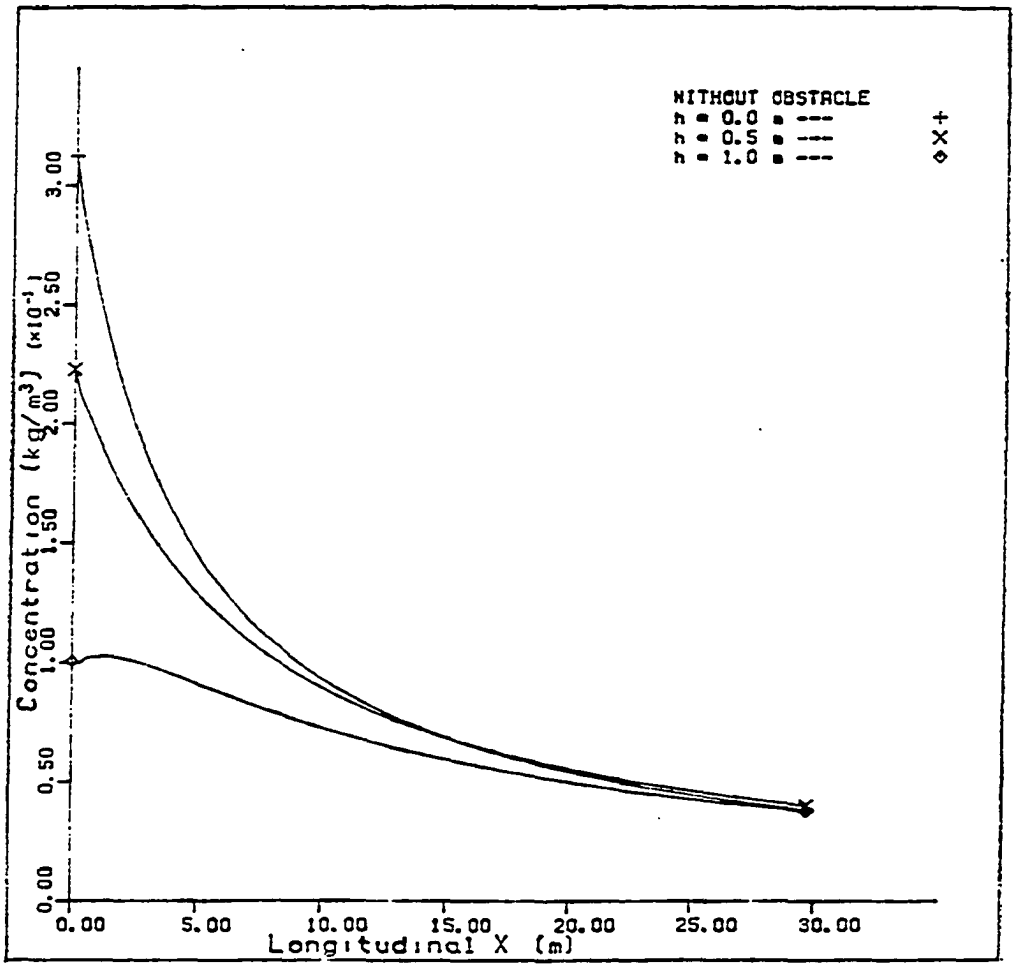

FIGURE 36. Longitudinal concentration distribution on the ground for flow without any obstruction

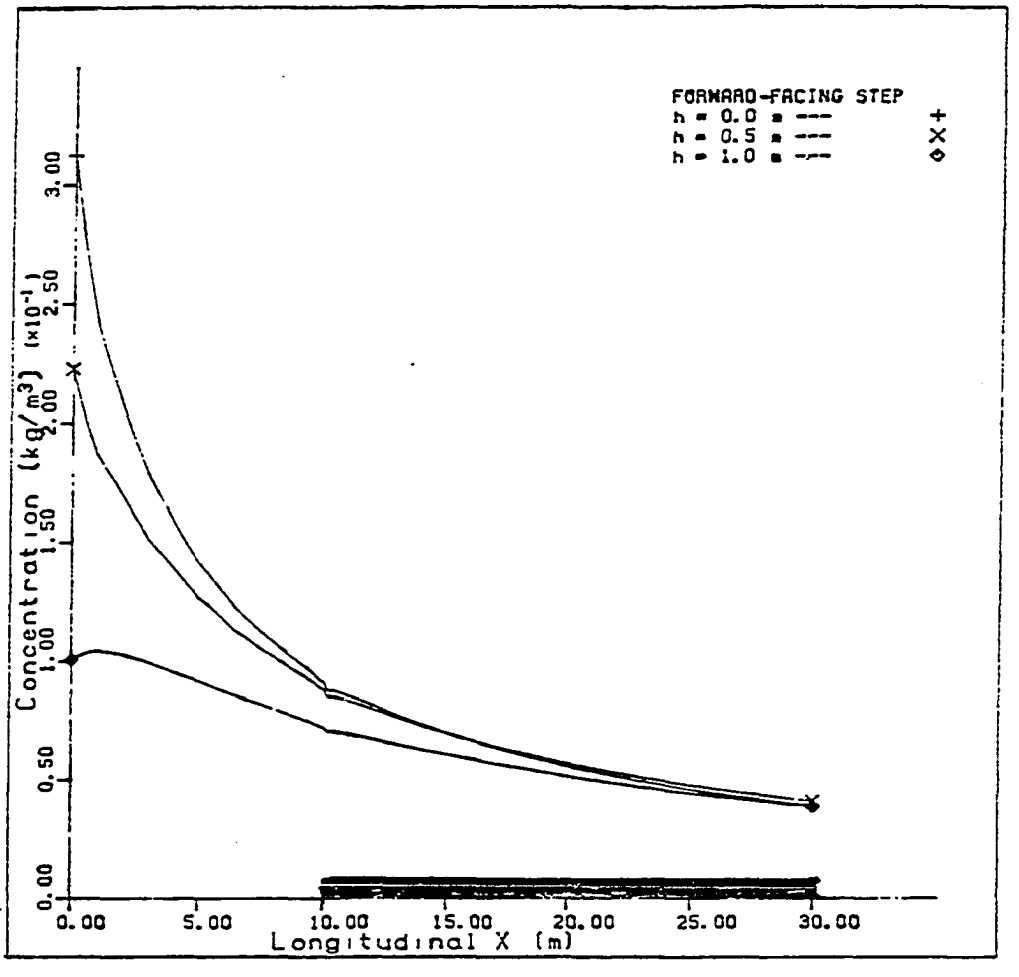

FIGURE 37. Longitudinal concentration distribution on the ground for forward-facing step flow

The concentration decay rate is found to be higher for the particles with a non-zero deposition velocity. It is also found that for the same deposition velocity, the concentration decay rate is higher for a ground source than an elevated source. This is expected because at any streamwise location far downstream, more particles have been deposited for the ground source. Conversely, there are more particles remaining in the air for the elevated source. There must, therefore, exist a streamwise location far downstream after which the elevated source will yield higher ground concentration than the ground source.

From the numerical solutions for forward-facing step flow, we can see a small concentration discontinuity at the corner. The concentration downstream of the step face is reduced. However, this concentration reduction is not as significant as expected. This is because the step is not relatively high and is rather far downstream from the source so that the particles have already been diffused widely.

For the backward-facing step flow, there is a big concentration discontinuity at the corner. A region of very small concentration is confined in the cavity zone right behind the step. The diffusion process behaves somewhat like particles emitted from an 'imperfect' elevated line source, with an elevation of the order of the step height. There is a very fast concentration recovery in this small

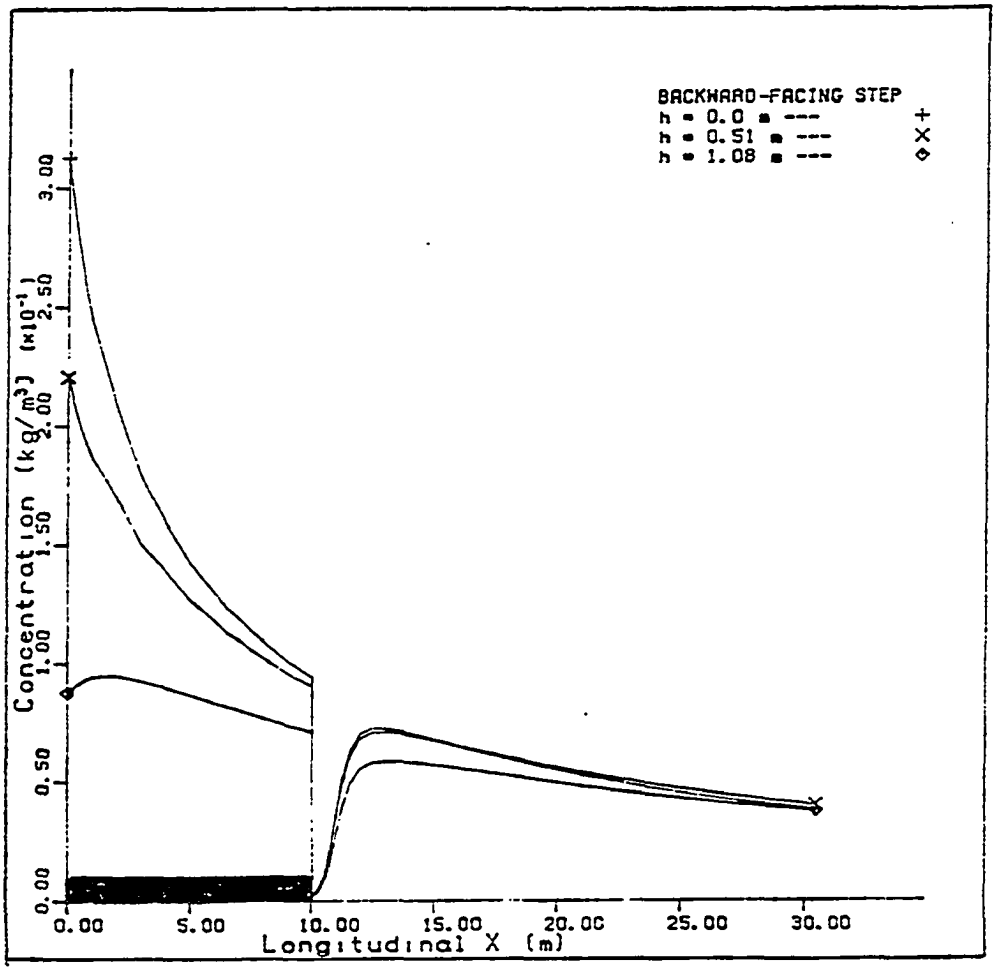

FIGURE 38. Longitudinal concentration distribution on the ground for backward-facing step flow

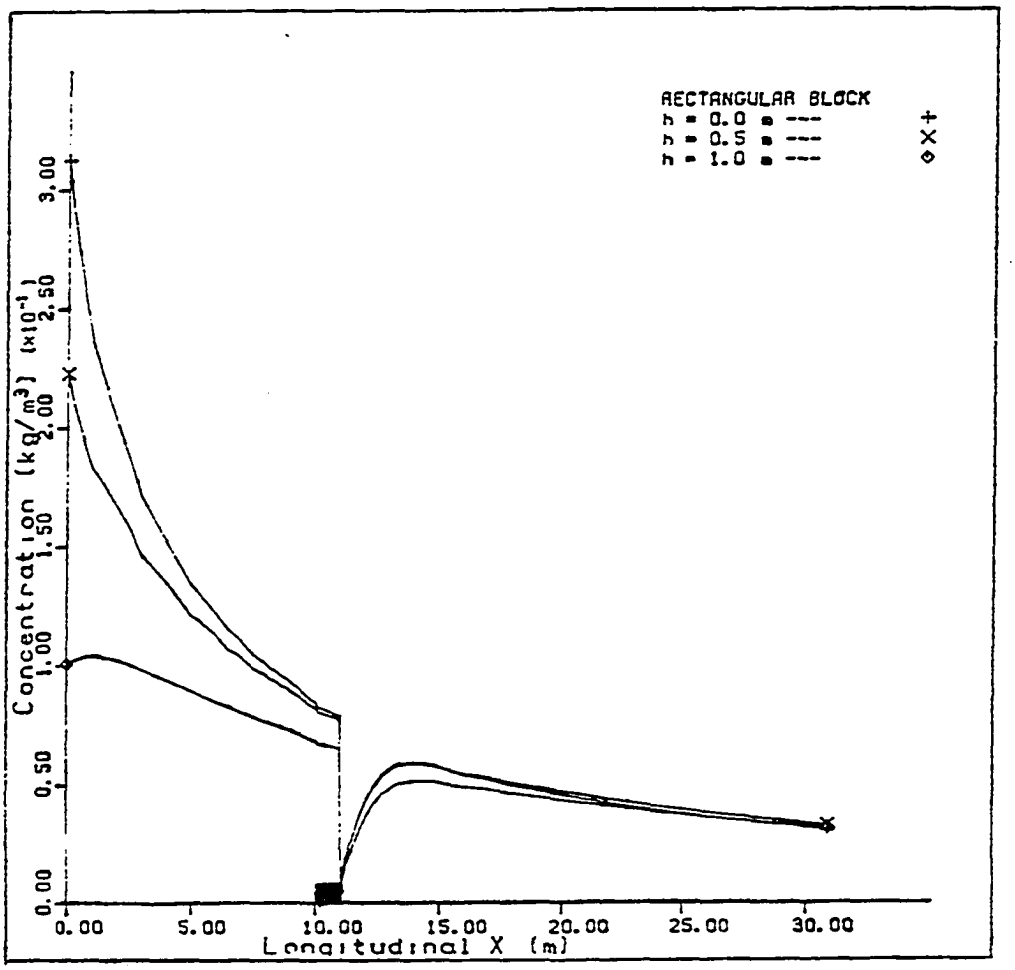

FIGURE 39. Longitudinal concentration distribution on the ground for rectangular block flow

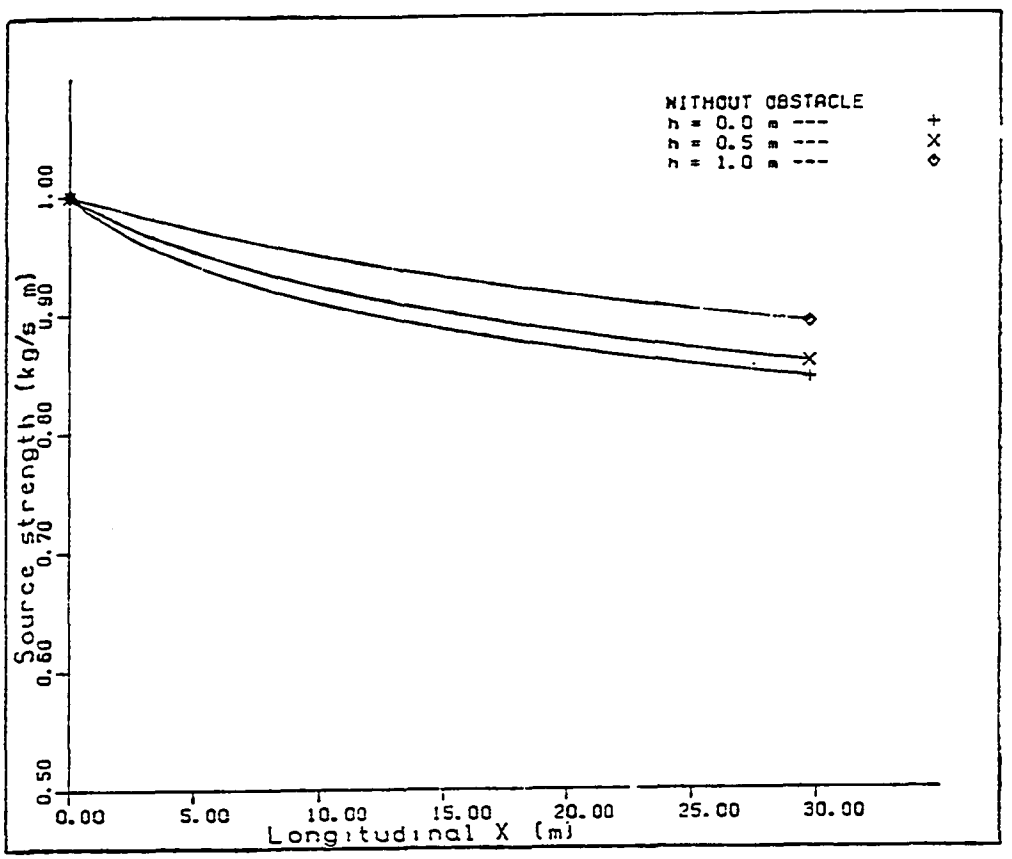

FIGURE 40. Longitudinal distribution of the effective source strength for flow without any obstruction

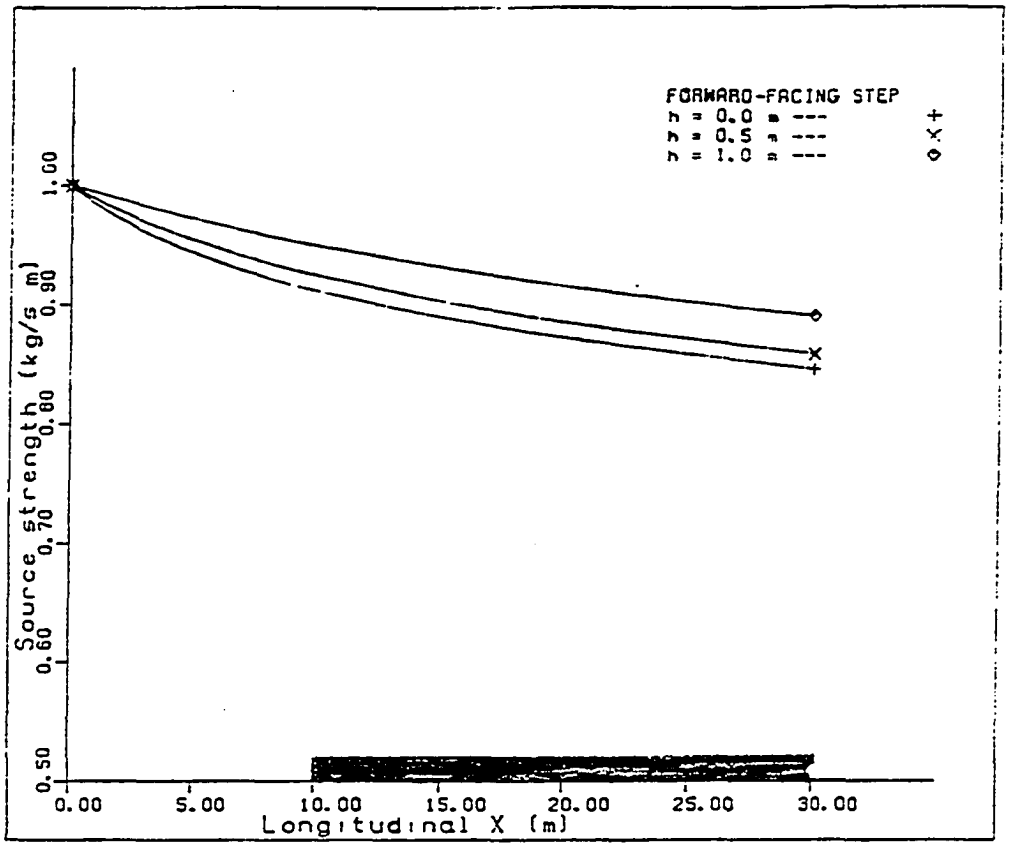

FIGURE 41. Longitudinal distribution of the effective source strength for forward-facing step flow

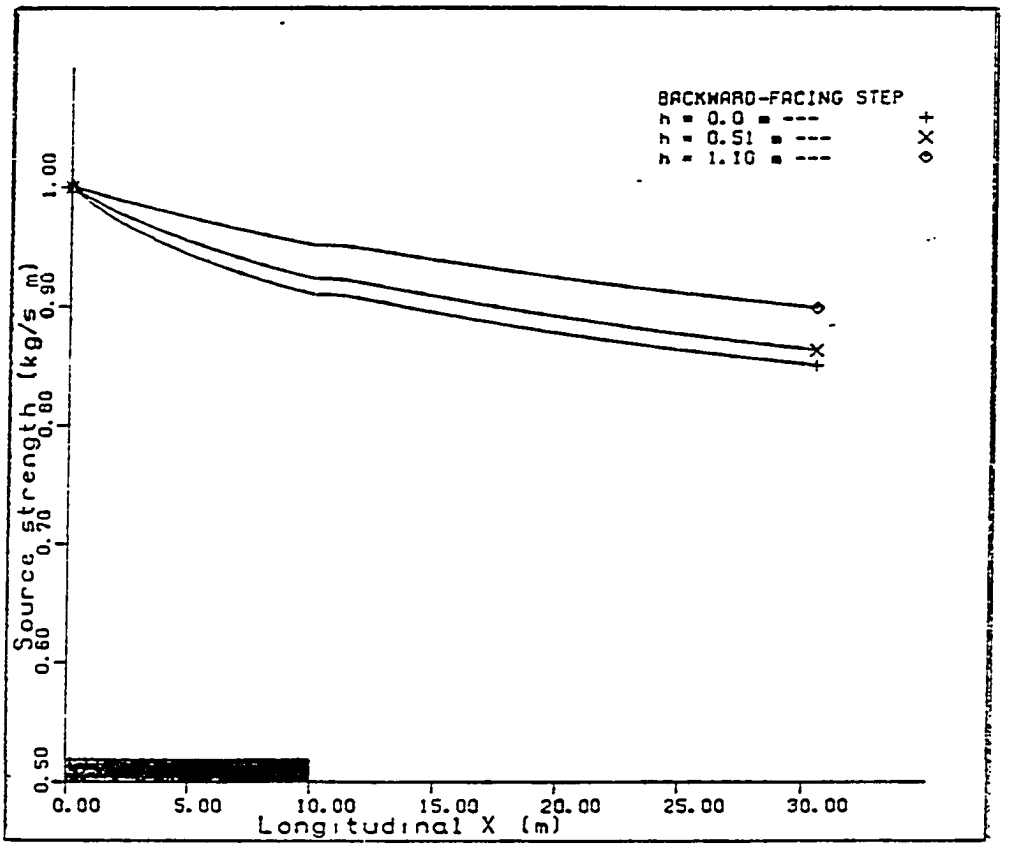

FIGURE 42. Longitudinal distribution of the effective source strength for backward-facing step flow

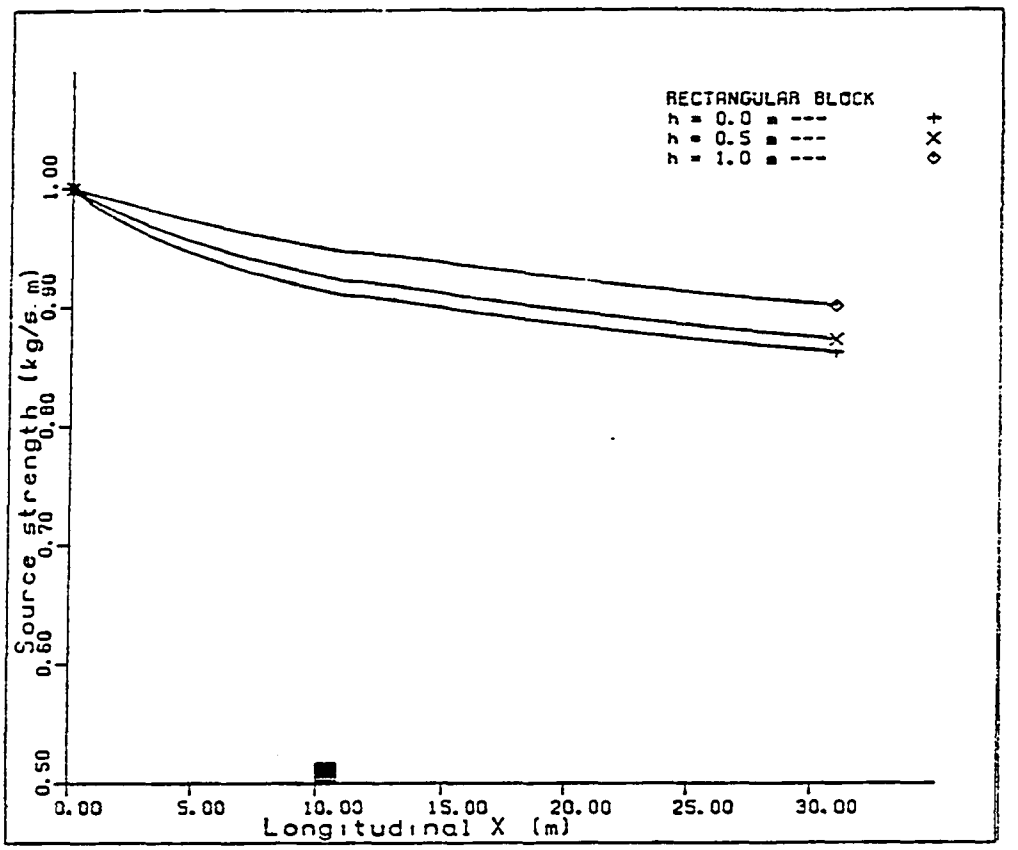

FIGURE 43. Longitudinal distribution of the effective source strength for rectangular block flow

concentration region behind the step. The ground concentration increases to reach a maximum at about 2.5 step heights downstream after which it decreases monotonically. This concentration recovery zone is rather short due to the high turbulence intensity level and high eddy diffusivity. If the flow pattern were chosen for a smaller z_o, the concentration recovery zone would likely be larger.

It is obvious that the effect of a forward-facing step is to cause an effective source strength loss in terms of downstream collection by preferentially collecting particles upstream of the step. Conversely, the backward-facing step causes an effective source strength increase in terms of downstream collection due to the small concentration region behind it. Again, for a rectangular block flow, the upstream concentration distribution is similar to that for a forward-facing step flow and the downstream concentration distribution is the same as that for a backward-facing step flow.

Comments on gradient-advection model

Due to the assumption that the longitudinal diffusion term $\partial/\partial X(K_x \partial C/\partial X)$ is negligible compared to the convective term, we could solve the parabolic advection-diffusion equation (Eq. 4.1) by a marching procedure in the X-direction. This simplification works well for the flow problem without any obstruction. However, in the disturbed

flow problem, the longitudinal diffusion term should not be neglected in the regions near the obstruction. That is why the present numerical solutions show no bulge in the ground concentration distribution in front of the step. The vertical wall boundary conditions could not be fully applied. For the backward-facing step, the situation is a little bit better. Because the concentration on the rear step face is believed to be very small, the assumption of zero concentration is acceptable.

Fortunately, the source is far from the obstruction in the present solutions and the particles have been widely spread before they reach the effective region of the obstruction. Thus, the error in concentration prediction which is caused due to the weakness of our mathematical model can be neglected in present study.

It is noted that the advection-diffusion equation becomes elliptic if we include the longitudinal diffusion term. In general, we have two difficulties in solving this equation. First, the calculation of the eddy diffusivity K_x is more uncertain than that of K_z. Secondly, we need to know all the boundary conditions. This will normally be provided by experimental measurements. However, if all the required information is available, this more complete mathematical model is strongly encouraged.

CHAPTER 7. SUMMARY AND RECOMMENDATION

Flow problems for particles emitted from a continuous line source into the disturbed neutrally atmospheric boundary layer have been numerically solved. Two subproblems were organized under this subject. The Navier-Stokes equations with k-ε two-equation turbulent model were solved for the description of the flow pattern. For the diffusion process, the gradient-transfer model was applied and then the advection-diffusion equation was solved.

Employing the Navier-Stokes equations in terms of the vorticity-stream function variables, the four modeled equations governing the flow field can be expressed in a general form of elliptical partial differential equation. Gosman's upwind finite-difference scheme is modified, so we can solve these equations by time-marching procedure. Numerical predictions agree qualitatively well with experimental measurements. Accuracy can be improved by adjusting the constants in the turbulence model.

For diffusion predictions, Liu's Crank-Nicolson finite-difference method was applied. This technique has been shown to work very well for some test problems with analytical solutions. No suitable field measurements are available for comparison with our numerical predictions. From our calculations, however, we can have better physical understanding of concentration and deposition distributions.

Some researches are recommended here for further study:

1. Three dimensional effects. This will make the modeling problem more practical due to the fact that most boundary layer obstructions in the real world are three dimensional.
2. The effect of obstruction aspect ratio and the geometry. It would be very interesting to understand how the flow patterns and deposition distributions are influenced by obstruction aspect ratio and geometry.
3. The effect of the source positions. Moving the source close to the obstruction, on the obstruction roof, or downstream of the obstruction will cause much different diffusion and deposition processes. This would further understanding of particle diffusion phenomena in the environment.

Finally, I would like to mention that the present study is purely computational fluid dynamics work. The investigation of the experimental measurements are required for the application and validity of numerical modeling.

ACKNOWLEDGMENTS

The auther wishes to express most sincere gratitude to Dr. J. D. Iversen for his continued guidance and support throughout this study. Also, I would like to acknowledge Dr. C. T. Hsu, Dr. J. C. Tannehill, Dr. D. N. Yarger, Dr. D. K. Holger, and Dr. J. A. Wilson for their helpful suggestions and serving on my committee and Dr. L. N. Wilson for the allocation of computer time.

A very special and loving thanks is extended to my wife, Li-Yueh, for her patience, understanding and encouragement during my years of graduate work. Without her support, it would have been a much more difficult task.

BIBLIOGRAPHY

Anderson, D. A., J. C. Tannehill, and R. H. Pletcher. Computational Fluid Mechanics and Heat Transfer. McGraw-Hill Book Company, New York, 1984.

Atkin, D. J., S. J. Maskell, and M. A. Patrick. "Numerical Prediction of Separated Flows." Int. J. Numer. Methods Eng., 15 (1980), 129-144.

Bagnold, R. A. The Physics of Blown Sand and Desert Dune. Methuen, London, 1941.

Becker, D. L. "Quantifying the Environmental Impact of Particulate Deposition from Dry Unpaved Roadways." M.S. Thesis. Iowa State University, Ames, Iowa, 1978.

Becker, D. L. and E. S. Takle. "Particulate Deposition from Dry Unpaved Roadways." Atmos. Environ., 13 (1979), 661-668.

Benodekar, R. W., A. J. H. Goddard, A. D. Gosman, and R. I. Issa. "Numerical Prediction of Turbulent Flow over Surface-Mounted Ribs." AIAA Journal, 23, No. 3 (March 1985), 359-366

Bitte, J. and W. Frost. "Atmospheric Flow over Two-Dimensional Bluff Surface Obstructions." NASA Contract Report, NASA CR-2750, October 1976.

Bosanquet, C. H., and J. L. Pearson. "The Spread of Smoke and Gases from Chimney." Transactions, Faraday Society, 32 (1936), 1249-1264.

Bowen, A. J., and D. Lindley. "Measurements of the Mean Wind Flow over Various Escarpment Shapes." 5th Aust. Conf. Hydr. & Fluid Mech., Christ Church, New Zealand, 1974, p. 21.

Bradshaw, P., and P. V. Galea. "Step-Induced Separation of a Turbulent Boundary Layer in Compressible Flow." J. Fluid Mech., 27 (1967), 111-130.

Bradshaw, P., and F. Y. F. Wong. "The Reattachment and Relaxation of a Turbulent Shear Layer." J. Fluid Mech., 52 (1972), 113-135.

Businger, J. A. "Turbulent Transfer in the Atmospheric Surface Layer." In D. A. Haugen (Ed.) Workshop on Micrometeorology. Am. Meteorol. Soc., Boston, Mass., 1973.

Businger, J. A., J. C. Wyngaard, Y. Izumi, and E. F. Bradley. "Flux-Profile relationships in the atmospheric surface layer." J. Atmos. Sci., 28 (1971), 181-189.

Calder, K. L. "Eddy Diffusion and Evaporation in Flow over Aerodynamically Smooth and Rough Surfaces." Q. J. Mech. Appl. Math., 2 (1949), 153-176.

Carter, J. E. "A New Boundary-Layer Interaction Technique for Separated Flows." NASA TM-78690, 1978.

Castro, I. P. "Relaxing Wakes behind Surface-Mounted Obstacles in Rough Wall Boundary Layers." J. Fluid Mech., 93 (1979), 631-659.

Cebeci, T. 'Separated Flows and Their Representation by Boundary Layer Equations." Report ONR-CR215-234-2. Office of Naval Research, Arlington, Virginia, 1976.

Chang, L. P. "A Finite-Element Sea-Breeze Model." Ph.D. Thesis. Iowa State University, Ames, Iowa, 1981.

Counihan, J., J. C. R. Hunt, and P. S. Jackson. "Wakes behind Two-Dimensional Surface Obstacles in Turbulent Boundary Layers." J. Fluid Mech., 64 (1974), 529-563.

Crabb, D., D. F. G. Durao, and J. H. Whitelaw. "Velocity Characteristics in the Vicinity of a Two Dimensional Rib." Proceedings of the 4th Brazilian Congress on Mechanical Engineering, Florianopolis, Brazil, 1977. pp. 415-429.

Davenport, A. G. "The Relationships of Wind Structure to Wind Loading." National Physical Laboratory, Symposium No. 16. Wind Effects on Buildings and Structures. Her Majesty's Stationery Office, London, 1965, pp. 54-102.

Davies, D. R. "On Diffusion from a Continuous Point Source at Ground Level into a Turbulent Atmosphere." Q. J. Mech. & Appl. Math., 5 (1952), 168-178.

Deacon, E. L. "Vertical Diffusion in the Lowest Layers of the Atmosphere." Q. J. Royal Meteorol. Soc., 75 (1949), 89-103.

Denham, M. K., P. Briard, and M. A. Patrick. "A Directionally Sensitive Laser Anemometer for Velocity Measurements in Highly Turbulent Flow." J. Phys. E.: Scientific Instruments, 8 (1975), 681-683.

Ermak, D. L. "An Analytical Model for Air Pollutant Transport and Deposition from a Point Source." Atmos. Environ., 11 (1977), 231-237.

Fichtl, G. H. "Problems in the Simulation of Atmospheric Boundary Layer Flows." AGARD, CP-140, 1973.

Frost, W. and A. M. Shahabi. "A Field Study of Wind over a simulated Block Building." NASA Contract Report, NASA CR-2804, March 1977.

Frost, W., J. R. Maus, and G. H. Fichtl. "A Boundary-Layer Analysis of Atmospheric Motion over a Semi-elliptical Surface Obstruction." Boundary-Layer Meteorology, 7 (1974), 165-184.

Godson, W. L. "The Diffusion of Particulate Matter from an Elevated Source." Archiv fur Meteorol. Geophys. Bioklim., Series A, 10 (1958), 305-327.

Gosman, A. D., W. M. Pun, A. K. Runchal, D. B. Spalding, and M. Wolfshtein. Heat and Mass Transfer in Recirculating Flows. Academic Press, New York, 1969.

Hanna, S. R., G. A. Briggs, and R. P. Hosker, Jr. Handbook on Atmospheric Diffusion. Technical Information Center, U.S. D.O.E., Oak Ridge, Tennessee, 1982.

Hassid, S. "Turbulent Schmidt Number for Diffusion Models in the Neutral Boundary Layer." Atmos. Environ., 17 (1983), 523-527.

Herwehe, J. A. "Numerical Modeling of Turbulent Diffusion of Fugitive Dust from an Idealized Open-Pit Mine." M.S. Thesis. Iowa State University, Ames, Iowa, 1984.

Hino, M. "Computer Experiment on Smoke Diffusion over Complicated Topography." Atmos. Environ., 2 (1968), 541-558.

Hinze, J. Turbulence. McGraw-Hill Book Company, New York, 1959.

Horst, T. W. "Lagrangian Similarity Modeling of Vertical Diffusion from a Ground Level Source." J. Appl. Meteorol., 18 (1979), 733-740.

Hosker, R. P., Jr. "Methods for Estimating Wake Flow and Effluent Dispersion near Simple Block-Like Building." NOAA Technical Memorandum, ERL ARL-108, October, 1981.

Hosker, R. P., Jr., and S. E. Lindberg. "Review: Atmospheric Deposition and Plant Assimilation of Gasses and Particles." Atmos. Environ., 16 (1982), 889-910.

Iversen, J. D. "Wind Transportation of Dust from Coal Piles." Danish Ship Research Lab., SL Report 81054, Oct. 1981.

Jones, W. P. and B. E. Launder. "The Prediction of Laminarisation with a Two-Equation Model of Turbulence." Int. J. Heat & Mass Transfer, 15 (1972), 301-314.

Jones, W. P. and B. E. Launder. "The Calculation of Low-Reynolds-Number Phenomena with a Two-Equation Model of Turbulence." Int. J. Heat & Mass Transfer, 16 (1973), 1119-1130.

Kaul, U. K. and W. Frost. "Turbulent Atmospheric Flow over a Backward-Facing Step." NASA Contract Report, NASA CR-2749, October 1976.

Kemper, J. E., P. E. Long, and W. A. Schaffer. "Forecast Guidance Products from the Techniques Development Laboratory's Boundary Layer Model." In Fourth Conference on Numerical Weather Prediction. Am. Meteorol. Soc., Boston, Mass., 1979.

Kim, J., S. J. Kline, and J. P. Johnston. "Investigation of Reattaching Turbulent Shear Layer: Flow over a Backward-Facing Step." ASME J. Fluids Eng., 102 (1980), 302-308.

Kolmogorov, A. M. "Equations of Turbulent Motion of an Incompressible Turbulent Fluid." Izv. Akad. Nauk SSSR Ser. Phys. VI., 1-2 (1942), 56-58. Translated into English at Imperial College, Mechanical Engineering Department Report ON/6, 1968.

Launder, B. E. and D. B. Spalding. Lectures on the Mathematical Models of Turbulence. Academic Press, London, 1972.

Launder, B. E. and D. B. Spalding. "The Numerical Computation of Turbulent Flows." Comput. Methods Appl. Mech. Eng., 3 (1974), 269-289.

Launder, B. E., C. H. Priddin, and B. I. Sharma. "The Calculation of Turbulent Boundary Layers on Spinning and Curved Surfaces." J. of Fluid Engineering, 99, No. 1 (March 1977), 231-239.

Liu, H. T. and S. Karaki. "Mass Diffusion over Water Waves." Tech. Rept. CER71-72HTL-SK46. Fluid Dynamics and Diffusion Labrotory, Colorado State University, Fort Collins, Colorado, 1972.

Morsi, S. A. and A. J. Alexander. "An Investigation of Particle Trajectories in Two-Phase Flow Systems." J. Fluid Mech., 55, Pt. 2 (1972), 193-208.

Ng, K. H. and D. B. Spalding. "Turbulence Model for Boundary Layers near Walls." Phys. Fluids, 15 (1972), 20-30.

O'Brien, J. J. "A Note on the Vertical Structure of the Eddy Exchange Coefficient in the Planetary Boundary Layer." J. Atmos. Sci., 27 (1970), 1213-1215.

Ogawa, Y., S. Oikawa, and K. Uehara. "Field and Wind Tunnel Study of the Flow and Diffusion around a Model Cube. I. Flow Measurements." Atmos. Environ., 17 (1983a), 1145-1159.

Ogawa, Y., S. Oikawa, and K. Uehara. "Field and Wind Tunnel Study of the Flow and Diffusion around a Model Cube. II. Nearfield and Cube Surface Flow and Concentration Patterns." Atmos. Environ., 17 (1983b), 1161-1171.

Overcamp, T. J. "A General Gaussian Diffusion-Deposition Model for Elevated Point Sources." J. Appl. Meteorol., 15 (November 1976), 1167-1171.

Owen, P. R. "Dust Deposition from a Turbulent Airstream." Int. J. Air Water Pollut., 3 (1960), 8-25.

Panofsky, H. A. and J. A. Dutton. Atmospheric Turbulence. John Wiley & Sons, New York, 1984.

Pasquill, F. and F. B. Smith. Atmospheric Diffusion. Halsted Press, New York, 1983.

Paulson, C. A. "The Mathematical Representation of Wind Speed and Temperature Profiles in the Unstable Atmospheric Surface Layer." J. Appl. Meteorol., 9 (1970), 857-861.

Plate, E. J. Aerodynamic Characteristics of Atmospheric Boundary Layers, USAEC. Available as TID-25465. NTIS, Springfield, VA, 1971.

Prandtl, L. "Ueber ein neues Formelsystem fuer die Ausgebildete Turbulenz." Nachrichten von der Akademie der Wissenschaften in Gottingen, Math. Phys. Kl., 6-19. Van den Loeck und Ruprecht, Gottingen, 1945.

Rao, K. Shankar. "Plume Concentration Algorithms with Deposition, Sedimentation, and Chemical Transportation." NOAA Technical Memorandum, ERL ARL-124, November 1983.

Roache, P. J. Computational Fluid Dynamics. Hermosa Publisher, Albuquerque, New Mexico, 1972.

Roberts, O. F. T. "The Theoretical Scattering of Smoke in a Turbulent Atmosphere." Proceedings Royal Society, Series A, 104 (1923), 640-654.

Robertson, J. M., and D. B. Taulbee. "Turbulent Boundary Layer and Separation Flow Ahead of a Step." In Developments in Mechanics. Vol. 5. H. J. Weiss, D. F. Young, W. F. Riley, and T. R. Rogge, editors. Iowa State University Press, Ames, Iowa, 1969, pp. 171-183.

Robin, A. G. "Plume Dispersion from Ground Level Sources in Simulated Atmospheric Boundary Layers." Atmos. Environ., 12 (1977), 1033-1044.

Rounds, W., Jr. "Solutions of the Two-Dimensional Diffusion Equations." Transactions, American Geophysical Union, 36, No. 2 (1955), 395-405.

Runchal, A. K., D. B. Spalding, and M. Wolfshtein. "Numerical Solution of the Elliptic Equations for Transport of Vorticity, Heat, and Matter in Two-Dimensional Flow." Phys. Fluids, 12 (1969), II-21-II-28:

Sehmel, G. A. "Particle Diffusivities and Deposition over a Horizontal Smooth Surface." J. Colloid. Interface Sci., 37 (1971), 891-906.

Sehmel, G. A. "Particle Eddy Diffusivities and Deposition Velocities for Isothermal Flow and Smooth Surfaces." Aerosol Sci., 4 (1973), 125-138.

Sehmel, G. A. "Particle and Gas Dry Deposition: A Review." Atmos. Environ., 14 (1980), 983-1011.

Sehmel, G. A. and W. H. Hodgoson. "Predicted Dry Deposition Velocities." Atmosphere-Surface Exchange of Particulate and Gaseous pollutants. Available as CONF-740921 from NTIS, Springfield, VA, 399-423 (1976).

Shieh, C. F., W. Frost, and J. Bittle. "Neutrally Stable Atmospheric Flow over a Two-Dimensional Rectangular Block." NASA Contract Report, NASA CR-2926, November 1977.

Shir, C. C. and R. D. Bornstein. "Eddy Exchange Coefficients in Numerical Models of Planetary Boundary Layer." Boundary-Layer Meteorol., 11 (1977), 171-185.

Slade, D. H. (Ed.). Meteorology and Atomic Energy, USAEC. Available as TID-24190. NTIS, Springfield, VA, 1968.

Smith, F. B. "The Diffusion of Smoke from a Continuous Elevated Point Source into a Turbulent Atmosphere." J. Fluid Mech., 2 (1957), 49-76.

Sutton, O. G. "The Theoretical Distribution of Airborne Pollution from Factory Chimneys." Q. J. Royal Meteorol. Soc., 73 (1947), 426-436.

Tani, I., M. Iuchi, and H. Komoda. "Experimental Investigation of Flow Separation Associated with a Step or a Groove." Aeronautical Research Institute Report No. 364. University of Tokyo, April, 1961.

Taulbee, D. B., and J. M. Robertson. "Turbulent Separation Analysis Ahead of a Step." J. Basic Engineering, Transactions of the ASME, 94 (1972), 544-550.

Taylor, G. I. "Diffusion by Continuous Movements." Proceedings London Mathematical Society, Series 2, 20 (1921), 196-202.

Tennekes, H. "Similarity Relations, Scaling Laws and Spectral Dynamics." In F. T. M. Nieuwstadt and H. Van Dop (eds.). Atmospheric Turbulence and Air Pollution Modelling. D. Reidel Publishing Company, Dordrecht, Holland, 1982.

Turner, D. B. Workbook of Atmospheric Dispersion Estimates. Public Health Service Publication No. 999-AP-26. U.S. Environmental Protection Agency, Research Triangle Park, NC, 1970.

Wills, B. A. Mineral Processing Technology. Pergamon Press Inc., Elmsford, New York, 1981.

Woo, H. G. C., J. A. Peterka, and J. E. Cermak. "Wind-Tunnel Measurements in the Wakes of Structures." Colorado State University, Report prepared for NASA under Contract NAS-8-29583, 1976.

Yeung, P. K., and S. C. Kot. "Computation of Turbulent Flows past Arbitrary Two-Dimensional Surface-Mounted Obstructions." J. of Wind Engineering and Industrial Aerodynamics, 18 (1985), 177-190.

APPENDIX A: THE RELATIONS BETWEEN C_d AND Re

Listed here are the formulas used to calculated the drag coefficient numerically in the computer programs that numerically solved the system of ordinary differential equations of the motion of the particle's trajectory.

$C_d = 24.0/Re$ for $Re \leq 0.1$

$C_d = 22.73/Re + 0.0903/Re^2 + 3.69$ for $0.1 < Re \leq 1.0$

$C_d = 29.1667/Re - 3.8889/Re^2 + 1.222$ for $1.0 < Re \leq 10.0$

$C_d = 46.5/Re - 116.67/Re^2 + 0.6167$ for $10.0 < Re \leq 100.0$

$C_d = 98.33/Re - 2778.0/Re^2 + 0.3644$ for $100.0 < Re \leq 1000.0$

$C_d = 148.62/Re - 4.75 \times 10^4/Re^2 + 0.357$
for $1000.0 < Re \leq 5000.0$

$C_d = -490.546/Re + 57.87 \times 10^4/Re^2 + 0.46$
for $5000.0 < Re \leq 10000.0$

$C_d = -1662.5/Re + 5.4167 \times 10^6/Re^2 + 0.5191$
for $10000.0 < Re \leq 5000C.0$

$C_d = 0.4$ for $Re > 50000.0$

APPENDIX B: GOSMAN'S UPWIND FINITE DIFFERENCE SCHEME

The finite-difference equation for the elliptic partial differential equation of the general form

$$a\left\{\frac{\partial}{\partial x}\left(\Phi\frac{\partial \psi}{\partial z}\right) - \frac{\partial}{\partial z}\left(\Phi\frac{\partial \psi}{\partial x}\right)\right\}$$

$$- \left\{\frac{\partial}{\partial x}\left(b\frac{\partial}{\partial x}(c\Phi)\right) + \frac{\partial}{\partial z}\left(b\frac{\partial}{\partial z}(c\Phi)\right\} + d = 0\right.$$

has been developed by Gosman et al. (1969). The differential equation is integrated over elements of area, and each surface integral is reduced by Green's theorem to a line integral round the boundary. By using mean value theorems, these line integrals are evaluated and approached in terms of known values at the grid nodes.

The following illustration shows a portion of the finite-difference grid. The dotted lines enclose the area of integration.

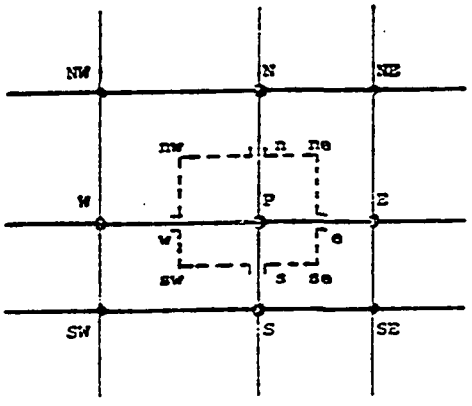

For convenience, we define the following coefficients:

$$A_E = a_p\{(\psi_{SE}+\psi_S-\psi_{NE}-\psi_N)+|\psi_{SE}+\psi_S-\psi_{NE}-\psi_N|\}/8$$

$$A_W = a_p\{(\psi_{NW}+\psi_N-\psi_{SW}-\psi_S)+|\psi_{NW}+\psi_N-\psi_{SW}-\psi_S|\}/8$$

$$A_N = a_p\{(\psi_{NE}+\psi_E-\psi_{NW}-\psi_W)+|\psi_{NE}+\psi_E-\psi_{NW}-\psi_W|\}/8$$

$$A_S = a_p\{(\psi_{SW}+\psi_W-\psi_{SE}-\psi_E)+|\psi_{SW}+\psi_W-\psi_{SE}-\psi_E|\}/8$$

$$B_E = \{(b_E+b_p)/4\}\{(z_N-z_S)/(x_E-x_p)\}$$

$$B_W = \{(b_W+b_p)/4\}\{(z_N-z_S)/(x_p-x_W)\}$$

$$B_N = \{(b_N+b_p)/4\}\{(z_E-z_W)/(x_N-x_p)\}$$

$$B_S = \{(b_S+b_p)/4\}\{(z_E-z_W)/(x_p-x_S)\}$$

and

$$V_p = \{(x_E-x_W)/2\}\{(z_N-z_S)/2\}$$

In the Cartesian coordinate system, the finite-difference equation is derived to be

$$\Phi_p = C_E\Phi_E + C_W\Phi_W + C_N\Phi_N + C_S\Phi_S + D$$

where

$$C_E = (A_E + B_E c_E)/\Sigma\ AB$$

$$C_W = (A_W + B_W c_W)/\Sigma\ AB$$

$$C_N = (A_N + B_N c_N)/\Sigma\ AB$$

$$C_S = (A_S + B_S c_S)/\Sigma\ AB$$

$$D = - d_p V_p/\Sigma\ AB$$

and

$$\Sigma\ AB = A_E + A_W + A_N + A_S + c_p(B_E + B_W + B_N + B_S)$$

For programming purposes, we can reexpress the formula in the form

$$\Phi_p = \frac{ANUM - d_p}{ADNM}$$

where

$$ANUM = \sum_j \{A_j' + c_j(b_j+b_p)B_j'\}\Phi_j$$

and

$$ADNM = \sum_j \{A_j' + c_p(b_j+b_p)B_j'\}$$

with j = N, S, E, and W, and A_j' and B_j' are defined by

$$A_j' = A_j/V_p$$

and

$$B_j' = B_j/V_p(b_j+b_p)$$